AD-A174 914   PASSIVELY DAMPED JOINTS FOR ADVANCED SPACE STRUCTURES   1/2
(U) MCDONNELL DOUGLAS ASTRONAUTICS CO HUNTINGTON BEACH
CA J H PEEBLES ET AL. 28 MAR 86 MDC-H2334
UNCLASSIFIED   AFOSR-TR-86-2075 F49620-83-C-0117   F/G 22/2   NL

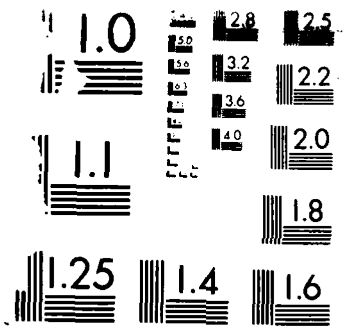

RESOLUTION TEST CHART

AD-A174 914

AFOSR-TR- 86-2075

PASSIVELY DAMPED JOINTS FOR ADVANCED SPACE STRUCTURES

JAMES H. PEEBLES
RICHARD W. TRUDELL
CREED E. BLEVINS
MCDONNELL DOUGLAS ASTRONAUTICS COMPANY
5301 BOLSA AVENUE
HUNTINGTON BEACH, CA 92647

JACKY C. PRUCZ
GEORGIA INSTITUTE OF TECHNOLOGY
225 NORTH STREET N.W.
ATLANTA, GA 30332

28 MARCH 1986

FINAL REPORT
For period 15 May 1983 – 15 January 1986

Approved for public release; unlimited distribution

PREPARED FOR
AIR FORCE OFFICE OF SCIENTIFIC RESEARCH
BOLLING AFB
WASHINGTON, DC 20332

86 12 09 032

UNCLASSIFIED
SECURITY CLASSIFICATION OF THIS PAGE

REPORT DOCUMENTATION PAGE

1a. REPORT SECURITY CLASSIFICATION: UNCLASSIFIED	1b. RESTRICTIVE MARKINGS: None
2a. SECURITY CLASSIFICATION AUTHORITY	3. DISTRIBUTION/AVAILABILITY OF REPORT: Approved for public release; distribution unlimited.
2b. DECLASSIFICATION/DOWNGRADING SCHEDULE: N/A	
4. PERFORMING ORGANIZATION REPORT NUMBER(S): MDC H1334	5. MONITORING ORGANIZATION REPORT NUMBER(S): **AFOSR-TR- 86-2075**
6a. NAME OF PERFORMING ORGANIZATION: McDonnell Douglas Astronautics Co. — 6b. OFFICE SYMBOL (If applicable)	7a. NAME OF MONITORING ORGANIZATION: Air Force Office of Scientific Research AFOSR
6c. ADDRESS (City, State, and ZIP Code): 5301 Bolsa Ave, Huntington Beach, CA 92647	7b. ADDRESS (City, State, and ZIP Code): Bolling AFB, Washington, DC 20332-6448
8a. NAME OF FUNDING/SPONSORING ORGANIZATION: AFOSR — 8b. OFFICE SYMBOL (If applicable): NA	9. PROCUREMENT INSTRUMENT IDENTIFICATION NUMBER: F49620-83-C-0107
8c. ADDRESS (City, State, and ZIP Code): Bolling AFB, Washington, DC 20332-6448	10. SOURCE OF FUNDING NUMBERS: PROGRAM ELEMENT NO. 61102F; PROJECT NO. 2302; TASK NO. N1; WORK UNIT ACCESSION NO.

11. TITLE (Include Security Classification): PASSIVELY DAMPED JOINTS FOR ADVANCED SPACE STRUCTURES (U)

12. PERSONAL AUTHOR(S): Peebles, James H.; Blevins, Creed E.; Trudell, Richard W.; Prucz, Jacky

13a. TYPE OF REPORT	13b. TIME COVERED	14. DATE OF REPORT (Year, Month, Day)	15. PAGE COUNT
Final	FROM 5/15/83 TO 1/15/86	1986 March [illegible]	[illegible]

16. SUPPLEMENTARY NOTATION

17. COSATI CODES			18. SUBJECT TERMS (Continue on reverse if necessary and identify by block number)
FIELD	GROUP	SUB-GROUP	Passive, Damping, Joints, Space, Structures

19. ABSTRACT (Continue on reverse if necessary and identify by block number)

This final report contains a description of the significant technical accomplishments of the subject research during its two-year duration. These include: (1) the development of a viscoelastic materials selection guide for this research activity; (2) the development of an analytic statics model of the joint specimens; (3) the design, fabrication and testing of 21 viscoelastic joint specimens, including the development of a new material; (4) the procurement, fabrication and assembly of test equipment for the test program at the Georgia Institute of Technology, as well as the development of data reduction software; (5) the development and successful demonstration of transient decay and sinusoidal steady state methods for evaluating energy losses in joints; and (6) the performance of outgassing tests on several viscoelastic materials.

20. DISTRIBUTION/AVAILABILITY OF ABSTRACT: ☐ UNCLASSIFIED/UNLIMITED ☐ SAME AS RPT ☐ DTIC USERS	21. ABSTRACT SECURITY CLASSIFICATION: UNCLASSIFIED
22a. NAME OF RESPONSIBLE INDIVIDUAL: [illegible]	22b. TELEPHONE (Include Area Code): [illegible] — 22c. OFFICE SYMBOL: [illegible]

DD FORM 1473, 84 MAR — 83 APR edition may be used until exhausted. All other editions are obsolete. — SECURITY CLASSIFICATION OF THIS PAGE

PREFACE

The work reported herein was performed under Air Force Office of Scientific Research contract number F49620-83-C-0117. This report documents the accomplishments of this two year program and was prepared in satisfaction of Contract Data Requirements List Item 0002AA. The Air Force Project Manager for this effort is Dr. Anthony Amos. The research is supported by technical specialists (see Section 3) at McDonnell Douglas Astronautics Co. and Georgia Institute of Technology.

CONTENTS

FIGURES

TABLES

Section 1
INTRODUCTION AND SCOPE

Many of the future space structures currently being proposed will be extremely large with basic dimensions on the order of hundreds of meters. Mission requirements for these large structures raise fundamental questions concerning controllability and general vibration control. Many missions contain optical payloads that require extremely accurate pointing and jitter control; others involve material manufacturing in space and must be maintained at low vibration levels. A key element of any vibration control approach is passive damping. The enhancement of structural damping results in improved vibration isolator performance and more robust control systems (Ref. 1).

Until now the application of damping to structures has been limited to add-on approaches intended to fix a vibration problem that emerges after the structure has already been designed and built. These fixes were usually in the form of constrained-layer viscoelastic damping treatments applied over large areas or viscous dampers applied to problem components. Though generally successful, penalties such as poor damping efficiency and excessive added weight are to be expected due to the add-on nature of the approach. The primary goal of this research is to minimize these penalties by developing a designed-in approach to damping that takes maximum advantage of the basic characteristics of the structure to be controlled. In the case of a large space experiment platform like Space Station and laser optical systems like ACOSS (Active Control of Space Structures), whose primary structural support is provided by trusswork, a simple extensional damper spliced into each strut (see Fig. 1) may be very effective for controlling unwanted vibrations and constitutes a well integrated approach to damping enhancement (Refs. 2 and 3).

The hypothesis that a favorable tradeoff results when a small portion of structural stiffness is exchanged for increased structural damping forms the basis for incorporating damped joints directly into the members of the truss. The need to accept reduced structural stiffness arises from the requirement to make the joints somewhat flexible so that a reasonable portion of the total

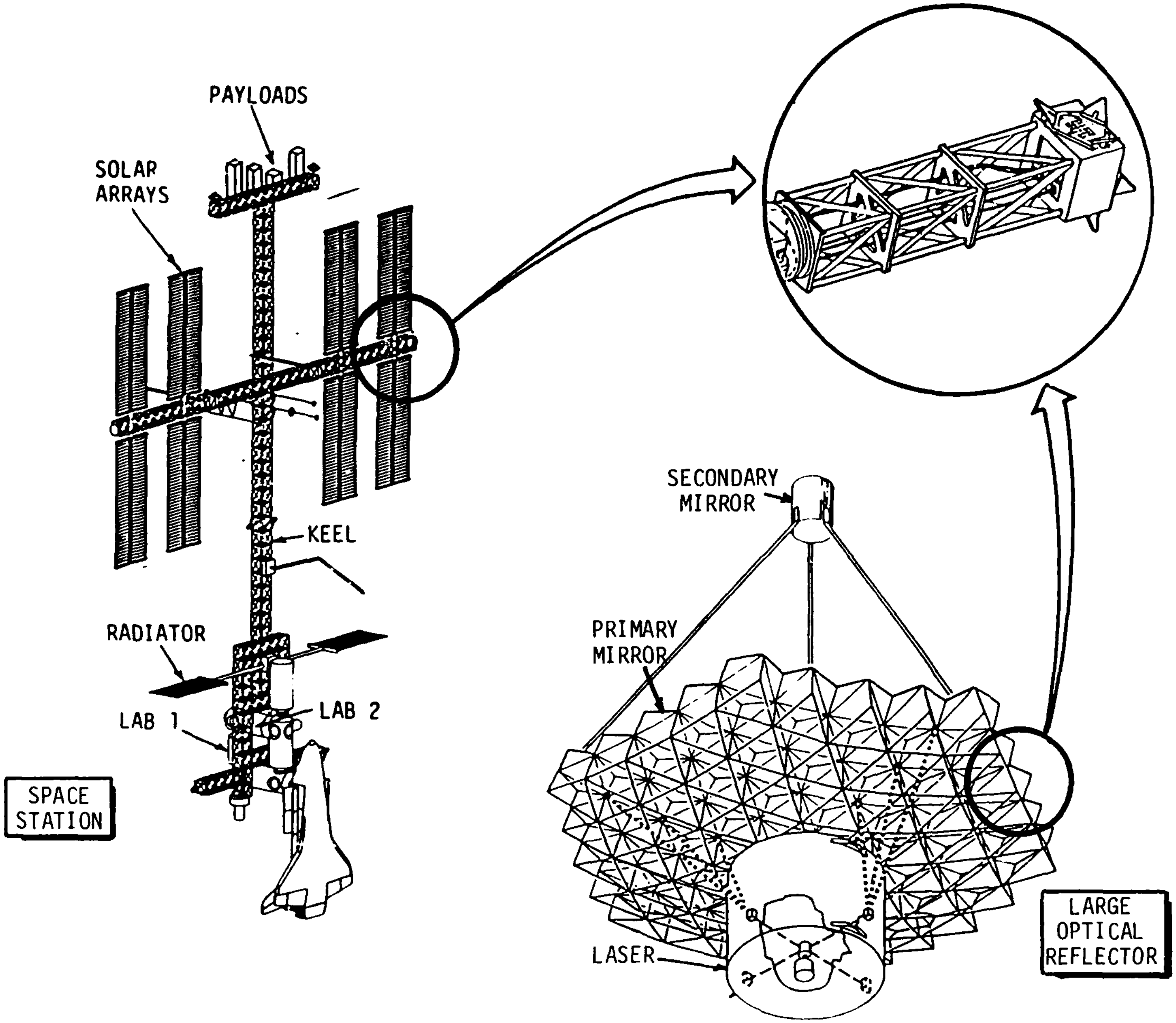

Figure 1. Viscoelastic Damper Built Into Each Strut

strain energy in the structure is resident in the joints. This strain energy is then available for dissipation in the high loss joint materials selected expressly for this purpose. This approach seems particularly useful for increasing the damping of low loss factor structures (on the order of 0.005 or less) to the order of 0.1 as is illustrated in Fig. 2. The reduction in stiffness is only on the order of 10%, which reduces the platform frequencies by only 5%.

Figs. 3 and 4 illustrate the effects of a uniformly distributed damping change on the Space Station configuration shown in Fig. 1. These figures show the benefits to be gained in payload pointing performance by adding damping uniformly to the structure. In this case, the disturbance is a unity weight unbalance in a large Specimen Research Centrifuge located in Lab 1. This disturbance is transmitted along the keel truss structure, producing undesirable base motion at the stellar-viewing payload platform. The magnitude of the response, as shown in Fig. 3, is a function of forcing frequency (or centrifuge spin rate). The reduction in the magnitude of the dynamic response with damping is significant. An additional benefit is realized in that the rate of change of the phase versus frequency (Fig. 4) has been significantly reduced. This characteristic is a key element to increasing control system robustness by reducing sensitivity to plant estimation errors.

In the Space Station case illustrated, the assumption of uniform damping may not be reasonable since the dampers were only considered for placement within the truss members and not for the attached payloads and solar arrays. A common approach to approximate the nonproportional damping conditions inherent in most large space structures is to compute a modal damping factor based on the product of an estimated damping factor for each member and the modal strain energy in the member divided by the total strain energy in the structure. This modal strain energy approach is based, however, on the assumption that the damped modes of the structure are not significantly different from the undamped modes. This approach has been applied to the ACOSS laser optical system shown in Fig. 1. Fig. 5 shows the strain energy distribution and the modal density of the unforced structure. Examination of Fig. 6 reveals that damping devices selectively placed in the high strain members of the secondary mirror support struts can substantially reduce the forced response of the

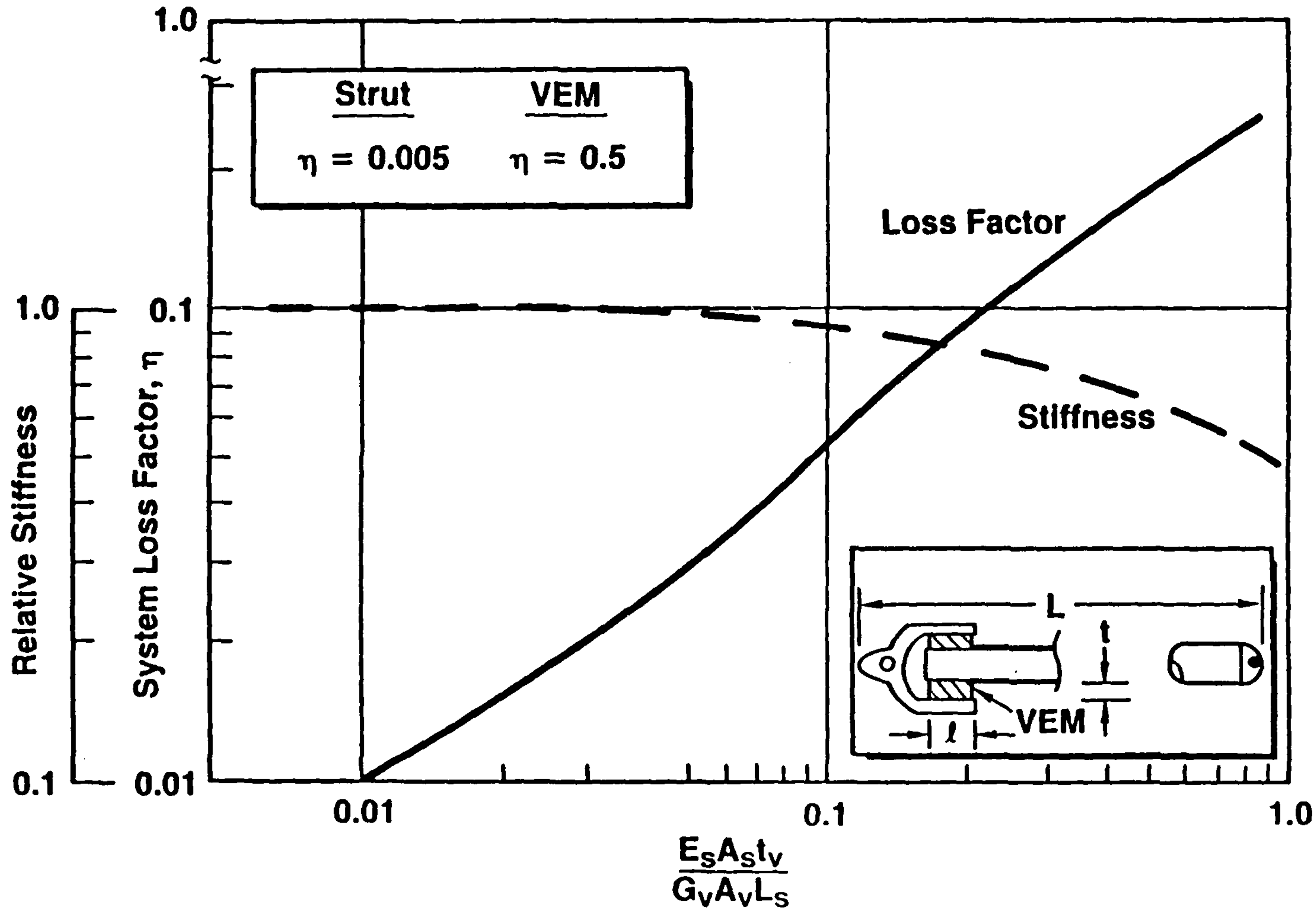

Figure 2. Viscoelastic Materials Effectiveness of Damping Treatment on Strut Extensional Damping

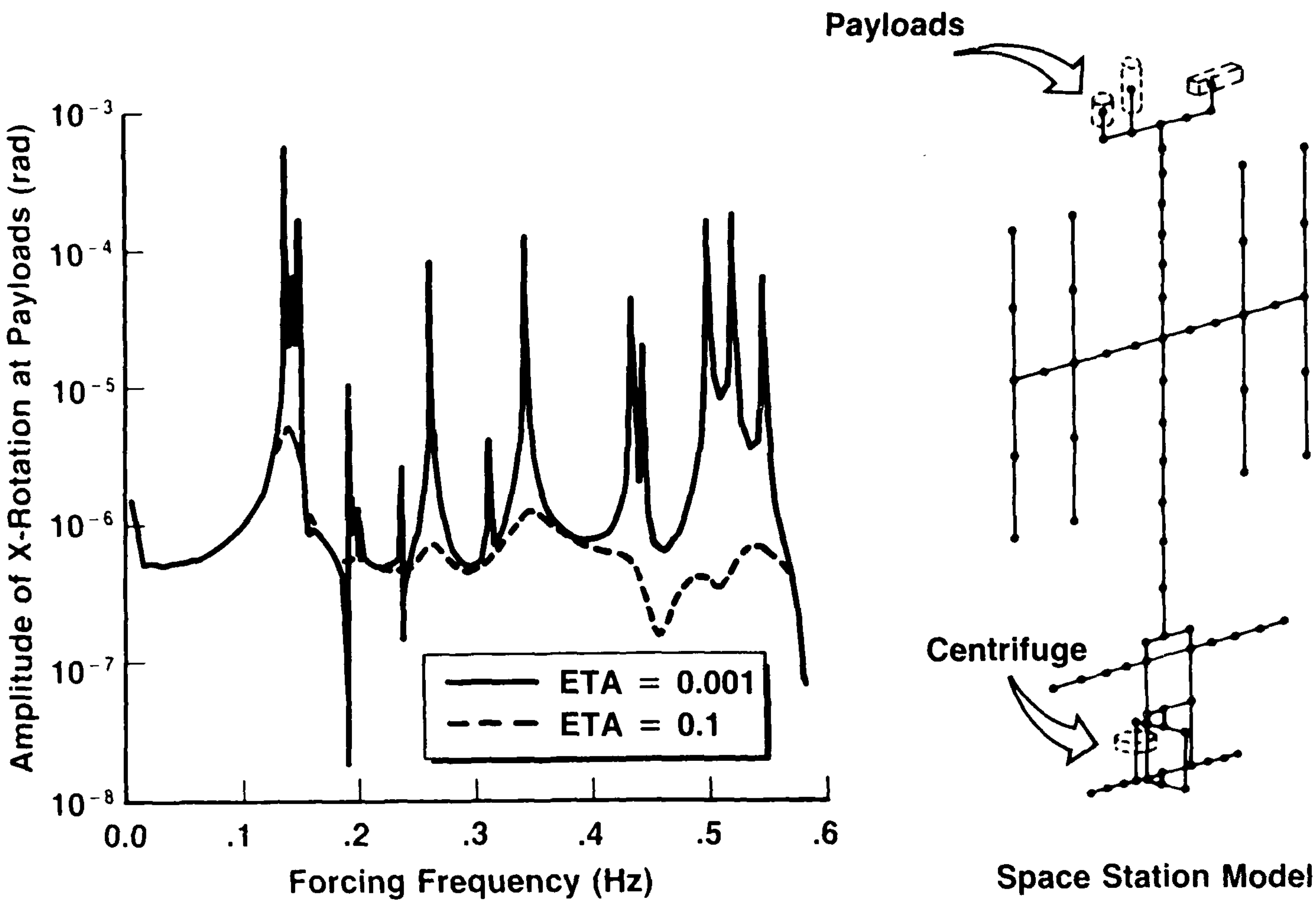

Figure 3. Space Station Amplitude Response of Payload Platform From a Unity Centrifuge Mass Unbalance

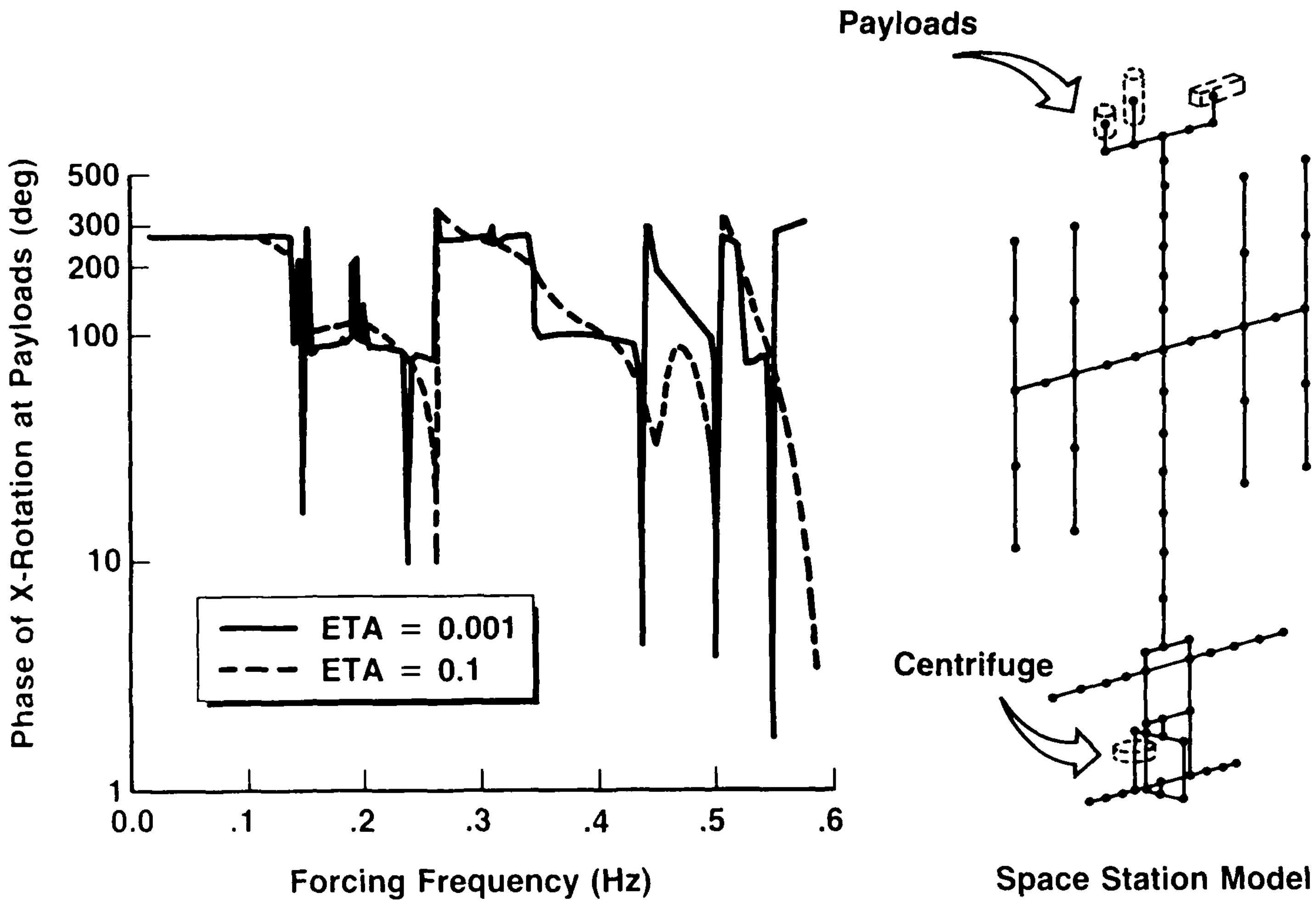

Figure 4. Space Station Phase Response of Payload Platform From a Unity Centrifuge Mass Unbalance

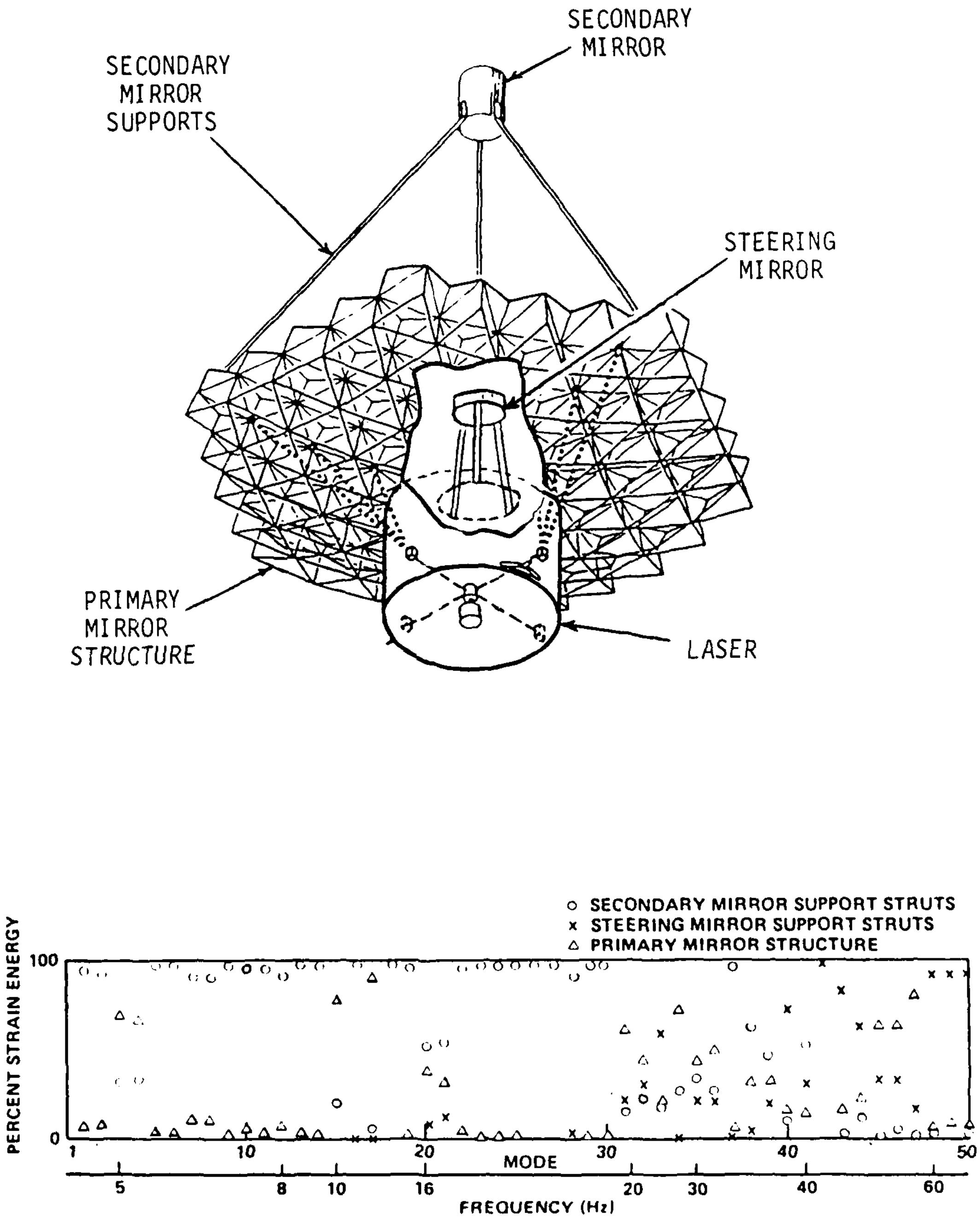

Figure 5. Large Optical Reflector Strain Energy Distribution

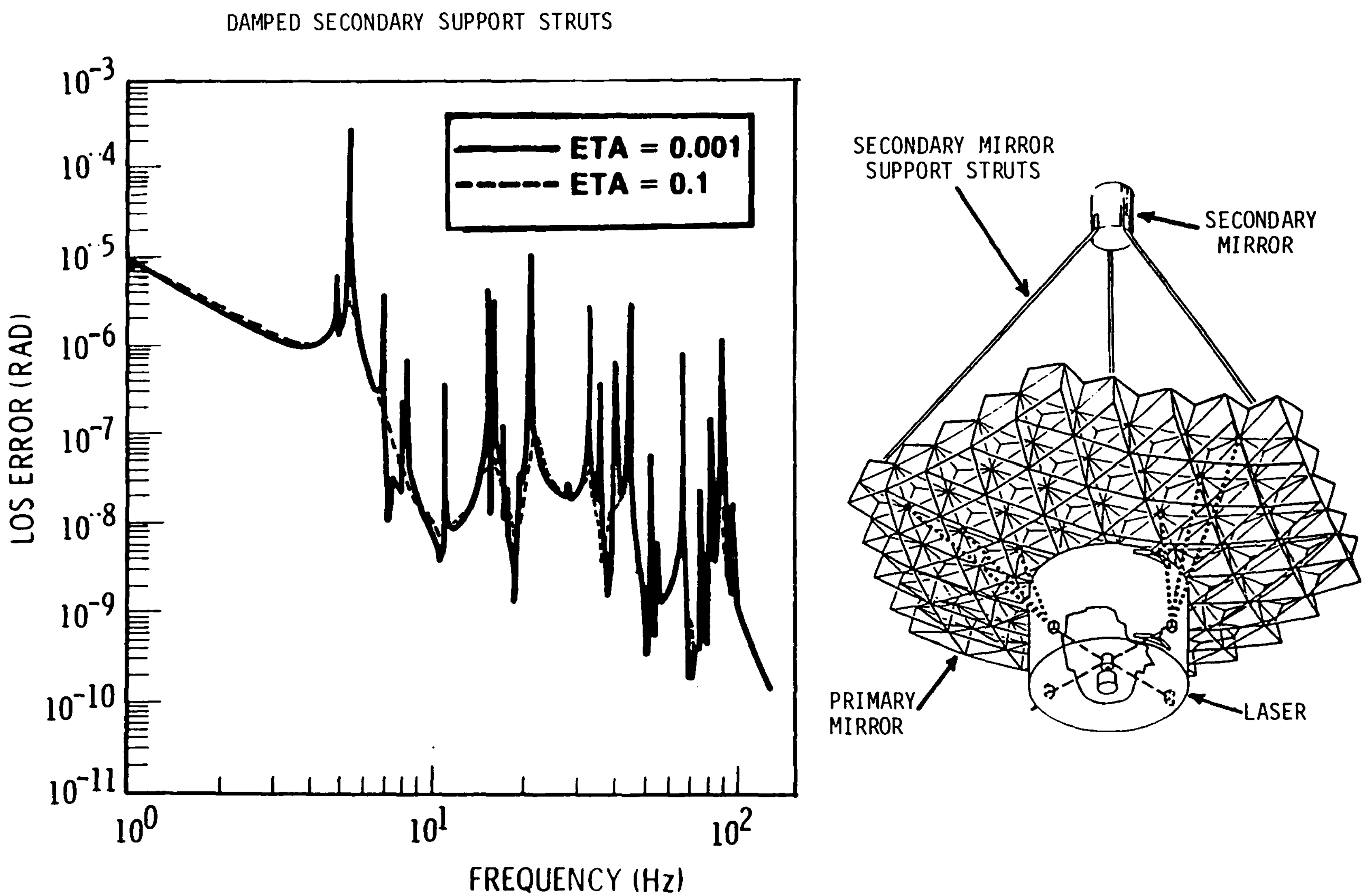

Figure 6. Large Optical Reflector Amplitude Response with Nonproportional Damping

structure, especially improving the performance in the lower frequency modes that were dominated by these members. The figure shows that many modes have the low damping associated with the untreated portions of the structure. These examples serve to show that locally placed damping in the struts of a platform truss or mirror backup truss will achieve practical and useful results.

The purpose of this research program was to characterize and model the structural and damping performance of generic bonded joint concepts so that a technology base would be available for future Air Force programs. The new analytical models and dynamic test methods developed, as well as the new viscoelastic material damping, stiffness, and outgassing data obtained during this program, have contributed substantially to this technology base. The output from this program has demonstrated that the concept of bonding high loss viscoelastic materials between composite layers of truss members is a viable, space-practical approach for reducing unwanted vibrations in high performance space structures.

Section 2
TECHNICAL PROGRESS SUMMARY

The Air Force Office of Scientific Research contracted with the McDonnell Douglas Astronautics Company (MDAC) to perform research on generic damped joints for the purpose of improving the damping, and therefore the performance, of large advanced space structures.

MDAC executed a subcontract with the Georgia Institute of Technology (GIT) to test and evaluate the joints developed at MDAC. Under the terms of the prime contract, the MDAC/GIT team were to perform the following tasks over a two-year period:

a. Development of structural joint concepts which incorporate viscoelastic materials as vibration energy dissipation media.

b. Analytical modeling and assessment of the performance characteristics of such concepts.

c. Validation of analytical methods developed and joint performance predictions through a carefully planned and executed experimental program.

d. Iteration on joint designs for enhanced damping characteristics.

e. Experimental evaluation of final joint designs.

The main thrust of this research has been the characterization, modeling, and test of generic space-practical damped joints for large truss structures. Several types of joints were considered, two of which are shown in Fig. 7. These joints are symmetric lap joints, one of which incorporates a return-to-zero feature (elastic elements). The damping is achieved by the shearing of

NOTES

1 DIMENSIONS GIVEN IN INCHES

2 ABBREVIATIONS: VEM - VISCOELASTIC MATERIAL

GR/EP - GRAPHITE EPOXY

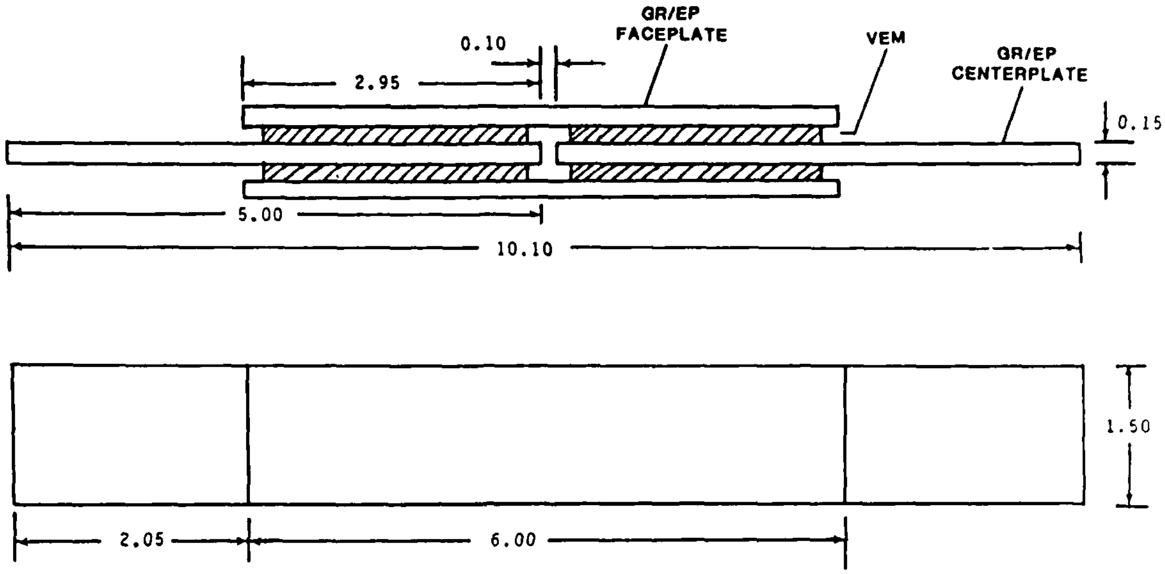

Figure 7a. Passively Damped Joint Specimen Without Elastic Link Between Members

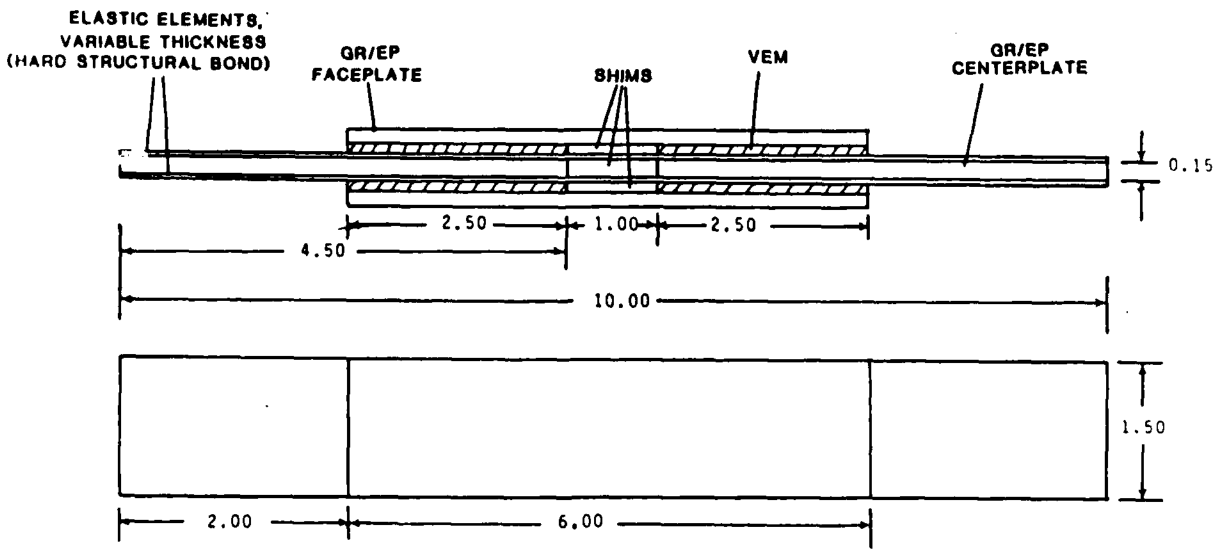

Figure 7b. Passively Damped Joint Specimen With Elastic Elements

the viscoelastic material that results when an axial force is applied to the joint. The unidirectional glass shown limits the maximum flexibility of the joint at elevated temperatures and also results in a restoring force to provide the return-to-zero function. Test specimens have been fabricated for evaluation of both the concept and suitable materials.

The major accomplishments of the program are:

1. Development of joint concepts for damping.

   - Two double lap shear joint concepts were developed: one with a return-to-zero feature, and the other without.

2. Evaluation and development of damping materials.

   - A viscoelastic material selection guide was compiled evaluating 38 candidate damping materials.

   - A new rubber/plastic alloy material was developed.

3. Development of an analytical model for predicting axial behavior.

   - Double lap joint analysis of L. J. Hart-Smith was extended to include a return-to-zero feature and the viscoelastic properties of damping materials.

   - Three different models were employed and compared in analytical studies.

     o Approximate design formula
     o Fully elastic model
     o Viscoelastic model

   - Models demonstrated that joint characteristics are predictable from component properties.

   - Established parametric trends useful for designing space-practical damped joints.

4. Development of two new test methods for measuring axial stiffness and damping.

   - Successfully developed and implemented the steady state and sine pulse propagation test methods.

   - Fabricated a special piezoelectric displacement transducer and test fixture.

- Demonstrated the usefulness of these new test methods for characterizing the damping behavior of materials and built-up joints.

5. Evaluation of samples and validation of joint models over a wide temperature and frequency range.

   - Obtained the damping and stiffness characteristics of 21 joint specimens using 7 viscoelastic materials.

   - Test results validated the analytical joint models.

   - New outgassing results were acquired for five previously untested viscoelastic materials.

6. Definition of payoffs of developed concepts in large space structures.

As stated previously, the objectives of this research were to design, fabricate, analytically characterize, and test generic passive damping joints that could significantly improve the performance of large space truss structures. Once the basic concepts of Fig. 7 were selected for evaluation, the tasks of selecting or developing appropriate viscoelastic materials (VEM) and the actual sizing and fabrication of the test specimens could begin.

Selection of appropriate viscoelastic materials were based on their anticipated performance in the environment which they are expected to withstand. Many of the intended uses of Large Space Structures (LSS) involve precision optics or radar whose performance is subject to many sources of vibration such as coolant mass shifts, appendage slewing, station-keeping thrusters, etc. It is anticipated that most of these vibrations will be in a very low frequency range (0.1-100 Hz). Viscoelastic joint damping is a very promising concept for controlling these low frequency LSS vibrations, provided that the material loss factor remains high over a broad temperature range (typically -270 to 200°F) and structural stiffness is not substantially degraded by the presence of the joints. With this in mind, some basic goals were established for guiding the viscoelastic material selection process:

1. The VEM loss factor (η) should be over 0.50 over a frequency range of 0.1-100 Hz at 21°C. If the VEM provides damping over a very broad temperature range, a lower loss factor is acceptable.

2. The VEM shear storage modulus (G') should not change by more than an order of magnitude when the temperature changes approximately 20°C.

Table 1 lists all the VEMs initially considered for selection along with their material properties. A new rubber/plastic alloy material not listed in this table was developed later as described in Appendix A. The source of the data for this initial survey and a detailed description of the structural and environmental behavior of these materials has been previously reported in Ref. 4, Appendix I, Annex C.

Some important environmental effects to be considered when selecting a VEM for space applications are temperature and frequency dependence, creep due to imposed loads, outgassing due to high vacuum, and degradation due to UV exposure. The use of VEMs for passive damping is a design challenge because of their sensitivity to these conditions. Both the loss factor and shear storage modulus are functions of temperature and frequency, with temperature changes having a larger effect than frequency changes. Since most VEMs are soft, lossy materials, they generally have poor creep resistance and structural redundancy is needed. The high vacuum of space could cause outgassing and loss of low molecular weight components of the VEM, such as plasticizers or absorbed water. High temperatures (200°F) caused by solar heating aggravate the outgassing problem. The UV exposure that would normally degrade the material properties of VEMs probably has no significant influence on the characteristics of lap joints because of the protection afforded the VEM by the faceplates; only the edges of the VEM would be exposed. If additional UV resistance is required, carbon black or other additives could be mixed with the VEM or encapsulation of the joint with an opaque low-outgassing sealant could be used.

After considering the design objectives, the environmental factors stated above, and other processing considerations, seven VEM materials were selected for use in the prototype joint development (see Table 2). Additional material properties are given in Table 3. The rationale for selecting each of these VEMs is described in more detail in Appendix I of Ref. 4.

Table 1. VEM Candidates and Material Properties

Material	Temperature Range for $\eta > 0.5$, °C 0.1 Hz	1 Hz	100 Hz	T_G at 5 Hz °C	G' at T_G N/m^2, (psi)	Maximum G' Slope °C/Decade G'
EAR C2003	-2 to 38	4 to 50	21 to 75	30	6.3×10^7 (9,140)[1]	20
EAR C1002	-	-16 to 14	-4 to 31	4	4.0×10^7 (5,800)[1]	14
MACBOND IB1120	-	-43 to 5	-16 to 48	-10	2.8×10^6 (406)	20
" IB1160	-	-50 to -2	-20 to 42	-16	8.5×10^5 (123)	14
" IB1200	-	-56 to -16	-30 to 25	-26	6.0×10^6 (870)	14
" IB1220	-	-40 to 0	-10 to 42	- 8	1.7×10^6 (246)	14
" IB1248	-	-62 to -26	-35 to 14	-40	5.0×10^6 (725)	15
" IB1320	-	-43 to 7	-15 to 51	- 9	4.5×10^6 (653)	16
" IB1400	-	-51 to -13	-21 to 27	-21	4.0×10^6 (580)	17
" IB1401	-	-61 to -15	-31 to 29	-28	4.5×10^6 (653)	17
" IB1622	-	-62 to -31	-34 to 7	-37	5.0×10^6 (725)	15
" IB2101	-	-57 to 8	-31 to 56	-29	1.3×10^7 (1,890)	21
" IB2107	-54 to 3	-43 to 21	-17 to 67	-13	6.0×10^6 (870)	24
" IB2130	-	-58 to -2	-32 to 42	-31	7.5×10^6 (1,090)	19
SOUNDCOAT D	-12 to 53	0 to 75	31 to 134	52	7.5×10^5 (109)	46
SOUNDCOAT M	-	-78 to -27	-47 to 25	-26	4.3×10^6 (624)	18
SOUNDCOAT N	-	-43 to 14	-24 to 49	- 8	4.0×10^6 (580)	20
SOUNDCOAT R	-	-67 to -16	-40 to 30	-35	3.0×10^6 (435)	15
" DYAD 601	-	-43 to 4	-15 to 46	-12	7.0×10^6 (1,020)	19
" DYAD 606	-24 to24	-14 to 40	11 to 83	17	1.2×10^7 (1,740)	26
" DYAD 609	-19 to 7	-7 to 23	23 to 60	18	1.5×10^7 (2,180)	26
SOUNDFOIL LT-12	-	-101 to -63	-70 to -18	-74	1.0×10^7 (1,450)	19

Table 1. VEM Candidates and Material Properties (Cont'd)

Material	Temperature Range for $\eta > 0.5$, °C 0.1 Hz	1 Hz	100 Hz	T_G at 5 Hz °C	G' at T_G N/M^2, (psi)	Maximum G' Slope °C/Decade G'
3M ISD 110	-32 to 34	-21 to 55	6 to 105	21	1.0×10^6 (145)	25
" 112	-	-49 to 10	-23 to 55	-14	1.6×10^6 (232)	25
" 113	-	-72 to -17	-43 to 29	-36	2.0×10^6 (290)	16
" 113M	-	-71 to -25	-42 to 19	-44	3.0×10^6 (435)	19
" 830	-	-97 to -60	-67 to -19	-74	9.0×10^6 (1,300)	16
ENJAY BUTYL 268	-	-78 to -28	-52 to 15	-45	1.6×10^7 (2,320)	18
3M 467	-53 to 21	-45 to 43	-23 to 98	-2	1.2×10^6 (174)[1]	22
SYLGARD 188	-	-38 to 33[2]	-27 to 74[2]	-6	2.8×10^6 (406)[1]	76
LD 400	-16 to 16	- 4 to 31	18 to 71	17	1.3×10^8 (18,900)[1]	16
PARACRIL BJ NITRILE	-	-28 to 9	-19 to 13	-18	8.3×10^7 (12,000)[1]	7
3M 428	-	-107[3] to -23	-77[3] to 18	-59	1.2×10^7 (1,740)[1]	17

NOTES:

1. Estimated from E' using G' = 1/3 E'
2. $\eta > 0.3$
3. Extrapolated

Table 2. Selected VEMs and Material Properties

Material	Type	0.1 Hz		1 Hz		10 Hz		100 Hz		Maximum G' Slope	Estimated Creep	Meets JSC	Estimated UV	Processing
		η	G', psi	η	G', psi	η	G', psi	η	G', psi	°C/Decade G'	Resistance	Outgassing	Resistance	Ease
3M ISD 110	Acrylic	0.77	23	1.2	58	1.2	203	0.95	798	25	Poor	Yes	Good	Good
3M EC 2216	Epoxy	--	--	0.14	21,000	0.14	100,000	--	--	31	Good	Yes	Good	Good
Soundcoat Dyad 606	Polyurethane	0.55	145	0.85	435	1.05	1,590	0.8	8,700	26	Good	Yes	Good	Good
Hysol EA 9326	Polyurethane	(Estimated values: η = 0.1-0.3, G' = 1500 psi)								--	Good	No	Good	Good
GE SMRD 100F90	Epoxy-based	0.012*	1200	0.07	1,600	0.39	2,200	1.00*	3,200*	25	Fair	Yes	Good	Good
GE RTV 630	Silicone	(Estimated values: η = 0.1-0.3, G' = 130 psi)								--	Good	No	Good	Good
Rubber/Plastic Alloy	Rubber/Plastic	(Estimated values: η = 0.1-0.7, G' = 5000 psi)								--	Fair-Good	No	Good	Good

*Extrapolated

Table 3. Additional VEM Material Properties

Material	Type	Contains Fillers	Estimated Coefficient of Thermal Expansion (in/in°F x 10^{-5})	Density (gm/cc)
3M ISD 110	Acrylic	No	--	0.965
3M EC 2216	Epoxy	Yes[1]	1.1-2.8	1.29
Soundcoat Dyad 606	Polyurethane	No	5-25	0.965
Hysol EA 9326	Polyurethane	No	5-25	1.08
GE SMRD 100F90	Epoxy-based	Yes[2]	0.6-1.9	0.75-0.82
GE RTV 630	Silicone	Yes[3]	45	1.28
Rubber/Plastic Alloy	Rubber/Plastic	Yes[4]	5-25	1.0-1.1

NOTES:

1. Mineral Fillers
2. Microballoons
3. Fumed Silica, etc.
4. Carbon Black

The selected VEMs were incorporated into the joint designs shown in Fig. 7. To optimize the conversion of mechanical energy to thermal energy in the LSS joints, it is necessary to maximize both the VEM strain energy and the VEM loss factor. To obtain a given spring rate, the shear area A, VEM thickness t, and elastic element stiffness K_{EL} can be varied.

The design of the MDAC-HB LSS test specimens has been guided by two major criteria:

1. The ultimate strength of the joint should be at least 1/10 that of a longeron in a space truss.

2. When elastic elements are included in the joint, the equivalent shear stiffness of the VEM layers should be equal to the axial stiffness of the elastic elements in order to provide the maximum damping for the minimum stiffness loss.

Preliminary calculations made it clear that elastic elements would generally be required to accomplish the first objective. Elastic elements would also eliminate creep. During this program, several joint specimens were developed that include an elastic return-to-zero feature designed to carry the static loads the joints are expected to experience on orbit. The design of these elastic elements is discussed in detail in Appendix B to this report, which also presents previously unreported fabrication information and test results on specimens 18 and 19. The test results for some initial specimens (15, 16 and 17) have been reported previously in Annex A to Appendix I of Ref. 4.

Graphite/epoxy was selected for the basic joint construction due to its high strength- and stiffness-to-weight ratios, low coefficient of thermal expansion, and low outgassing. The layup consisted of 22 unidirectional plies of prepreg tape with a ±45° ply used on each face, resulting in a total thickness of approximately 0.15 inch.

Considering the first design objective above, a typical joint similar to the one shown in Fig. 7 would have an overall spring rate of 118,800 lb/in. Using this number as a guide, the optimized K_{VEM} for each joint end had to be

twice that amount (237,600 lb/in.) since the joint ends act as springs in series. The VEM thickness can be readily calculated from the formula

$$t_V = \frac{G_M A}{K_{VEM}}$$

where

G_M = magnitude of VEM shear modulus = $[(G')^2 + (G'')^2]^{0.5}$

where G' = shear storage modulus

G'' = shear loss modulus

A = shear area of joint end

K_{VEM} = VEM stiffness

Using this formula, test specimens were designed and fabricated for each of the seven VEM candidates.

A complete list of the test specimens that includes their viscoelastic layer thickness and the tests each was subjected to is given in Table 4. A pair of specimens was constructed for each VEM selected. Specimens 13 and 14 represent graphite/epoxy control specimens, where specimen 13 is a solid bar cut from the same laminate as the joint plates and specimen 14 uses double lap construction bonded with a thin layer of highly rigid epoxy. Specimens 15-19 all incorporate fiberglass strips in their design to provide structural redundancy and enhance creep resistance. Specimens 20 and 21 were fabricated using a new rubber/plastic alloy VEM of our own design. The development of joint specimens 20 and 21 is described in Appendix A.

During and immediately following completion of the joint fabrication process, an analytical effort was carried out to model the quasi-static axial behavior of the joints. A description of these modeling methods, correlations with the test data, and some parametric study results are included in Appendix C. The modeling methods used are based on the work of L. J. Hart-Smith (Ref. 5) and have been extended to include the effect of structural bypasses (elastic elements). The models developed are useful for evaluating joints that contain a nontrivial amount of strain in the adherends compared to the strain in the viscoelastic materials. These models have been used in this research to establish parametric trends that can be used to design a better joint, and to

Table 4. Joint Test Specimens

Specimen Number	Viscoelastic Material Manufact.	Name	Chemical Base	Thickness of Adhesive Layer (in.)	Testing Performed[1] Room Temp. HL	SSS	SPP	Environmental SSS
1	3M	ISD 110	Acrylic	0.0062	X	X		X
2	3M	ISD 110	Acrylic	0.0051	X			
3	3M	EC 246	Epoxy	0.1260	X	X	X	X
4	3M	EC 246	Epoxy	0.1270	X			
5	Soundcoat	DYAD 606	Polyurethane	0.0515	X	X		X
6	Soundcoat	DYAD 606	Polyurethane	0.0515	X			
7	Hysol	EA 9326	Polyurethane	0.0480	X	X		
8	Hysol	EA 9326	Polyurethane	0.0505	X			
9	GE	SMRD 100F90	Epoxy	0.0580	X	X		X
10	GE	SMRD 100F90	Epoxy	0.0580	X			
11	GE	RTV 630	Silicone	0.0073	X	X		X
12	GE	RTV 630	Silicone	0.0063	X			
13[2]	---	GR/EP Bar, Solid		---	X	X		X
14[3]	---	EA956	Epoxy	0.0220		X		
15[4]	3M	EC 2216	Epoxy	0.0573	X	X	X	X
16[4]	3M	EC 2216	Epoxy	0.0582	X	X		
17[4]	3M	EC 2216	Epoxy	0.0615	X			
18[4]	Soundcoat	DYAD 606	Polyurethane	0.0249	X	X		X
19[4]	Soundcoat	DYAD 606	Polyurethane	0.0249	X			
20	MDAC	Rubber/Plastic Alloy		0.0504	X			
21	MDAC	Rubber/Plastic Alloy		0.0499	X	X		X

NOTES

(1) HL = Hysteresis Loop
SSS = Simplified Steady State
SPP = Sine Pulse Propagation

(2) Reference GR/EP Laminate

(3) Standard Bonded Joint with Elastic Adhesive

(4) Includes Fiberglass Strips for Elastic Elements

correlate experimental results with predictions where the simplified GA/t shear stiffness model commonly used for joint design might not provide adequate agreement. Good correlation was achieved between the analytical model and experimental data, thus indicating that the dynamic behavior of complex built-up joints can be accurately predicted from the structural properties of its components. The good correlation also serves to validate the analytical model as a damped joint design tool.

Dynamic testing of selected joint specimens was performed to determine their stiffness and damping characteristics. The data generated was used to validate the analytical models and define the sensitivity of generic joints to varying temperature and frequency conditions. Three different test methods and a new data reduction procedure were used in the experimental program. The first test method was a standard hysteresis-loop approach employed for preliminary testing at low frequencies. Two new methods not limited to low frequencies, a simplified steady state technique and a sine-pulse propagation approach, have been developed and applied in this research. The simplified steady state method is, like the hysteresis loop approach, another nonresonant test technique that is not restricted to linear or homogeneous systems. Its advantage over conventional nonresonant techniques is that a relative displacement measurement across the joint is not required; only vectors of the applied voltage to the piezoelectric motion transducer and the measured output force from a load cell are required. The major disadvantage is that to get good generic data the overall stiffness of the test fixture (including the transducer and load cell) must be precisely determined a priori. The sine pulse propagation technique does not have this limitation. With this method, generic joint damping and stiffness data free of specimen/fixture interaction effects is obtained by measuring the changes that occur in certain characteristics of a stress wave as it passes through the joint. The stress wave is initiated by applying a gated sine-pulse of a prescribed frequency at one end of the joint test specimen.

All three test methods were used to gather damping and stiffness data at room temperature and varying frequency for the selected specimens indicated in Table 4. Data at low and elevated temperatures (-50°F to 200°F) was acquired using only the steady state method because it employs a more conventional measure of damping and the test fixture fit within the environmental chamber.

The experimental results confirm the trends predicted by the analytical models and demonstrate that the design goals established for the joints were generally met. Typically, joints that contain elastic elements or relatively stiff viscoelastic materials seem to offer the best damping/stiffness tradeoffs, and those tested over a wide range of temperature display characteristics similar to the raw viscoelastic materials from which they are made. Particularly notable was the performance of the new rubber/plastic alloy material developed by MDAC to provide moderate damping over a broad temperature range. As designed, this new material showed little sensitivity to temperature variations over the 250°F range tested. The data acquired by the various test methods show, in general, good agreement and low scatter within each method. The low scatter is particularly remarkable compared with existing damping properties data. A detailed description of each test method along with summaries of the resulting data are presented in Appendix D. Additionally, the data reduction process is described in Appendix E, the tabulated joint data is presented in Appendix F, and a history of the development of the piezoelectric transducer built specifically for the simplified steady state technique is provided in Appendix G.

Of the seven candidate damping materials (see Table 2) selected for study by MDAC in this research program, only two had been tested and shown to meet standard JSC outgassing requirements: 3M ISD 110, and GE SMRD 100 F90. Therefore, samples of the remaining five candidate materials in their raw sheet form were sent to NASA/White Sands Missile Base for outgassing evaluation. A definition of the JSC requirements, a description of the samples, and existing and new outgassing test results are presented in Appendix H. The tests indicated that Soundcoat Dyad 606 and 3M EC 2216 are also at acceptable levels. However, the GE RTV 630, HYSOL EA 9326, and rubber/plastic alloy showed unacceptable performance. This does not eliminate them from consideration as viable damping materials, however, since in an actual constrained layer or lap shear configuration the VEM sheet has only its edges exposed, thus significantly reducing the emission of volatile materials. In particular, the rubber/plastic alloy is a new material, the outgassing properties of which might be improved with further processing.

Section 3
PERSONNEL, PUBLICATIONS, AND INTERACTIONS

3.1 PERSONNEL

The following individuals were active contributors to the research effort:

Name	Title	Function
MDAC		
R. W. Trudell	Principal Engineer Scientist	Principal Investigator
C. E. Blevins	Sr. Engineer - Technology	Materials Engineer
J. H. Peebles	Sr. Engineer Scientist	Structural Dynamics Analyst
B. E. Hom	Engineer Scientist	Structural Statics Analyst
Georgia Tech		
Dr. L. H. Rehfield	Professor of Aerospace Eng'g	Task Leader
Ambur D. Reddy	Sr. Research Engineer	Investigator
Jacky C. Prucz	Graduate Student	Investigator
Phil C. Smith	Graduate Student	Investigator

The research was also supported by other technical specialists in the laboratories of both MDAC and Georgia Tech.

3.2 PUBLICATIONS AND PATENTS

The principal publication for this past year was AIAA paper 85-0756-CP, Experimental Characterization of Passively Damped Joints for Space Structures, which was contributed to the AIAA 26th Structures, Structural Dynamics and Materials Conference.

A patent disclosure detailing the simplified steady state testing methodology was filed during this research program, but a patent was not granted.

3.3 INTERACTIONS

The following meetings and conferences were supported during the program:

- First Forum on Space Structures - September 1983 - MIT. Sponsored by AFOSR - J. H. Peebles of MDAC attended and participated in forum discussions.

- AFWAL Vibration Damping Workshop - February 1984 - Long Beach, CA. Paper entitled Passively Damped Joints for Advanced Space Structures was orally presented by R. W. Trudell and L. H. Rehfield.

- 25th Structures, Structural Dynamics and Materials Conference - May 1984 - Palm Springs, CA. Two papers presented at Work-In-Progress sessions:
  - MDAC paper G9059, Designed-in Damping Joints for Advanced Space Structures, by R. W. Trudell, MDAC; L. W. Rehfield, GIT
  - MDAC paper G9061, A New Approach to Dynamic Characterization of Structural Joints, by J. Prucz, A. D. Reddy, L. W. Rehfield, GIT

- Second Forum on Space Structures - June 1984 - Tyson's Corners, VA. Sponsored by AFOSR - R. W. Trudell of MDAC participated in Passive Control Committee proceedings and GIT participated in the Hardware Issues Committee proceedings. Written inputs were provided to the committee chairmen.

- 26th Structures, Structural Dynamics and Materials Conference - April 1985 - Orlando, FL. Two papers presented and recently accepted for publication in the Journal of Spacecraft and Rockets:
  - AIAA Paper 85-0756-CP, Experimental Characterization of Passively Damped Joints for Space Structures, by J. Prucz, A. D. Reddy, L. W. Rehfield, GIT; R. W. Trudell, MDAC.
  - AIAA Paper 85-0780-CP, Analysis of Design Trade-offs for Passively Damped Structural Joints, by J. Prucz, GIT.

- Third Forum on Space Structures - July 1985 - College Station, TX. Sponsored by AFOSR - J. H. Peebles of MDAC and L. W. Rehfield, J. Prucz of GIT participated. Written inputs were provided at the forum's conclusion.

o Vibration Damping Workshop II - March 1986 - Las Vegas, NV. Paper entitled Influence of Temperature on Structural Joints with Designed-in Damping will be presented.

Section 4

ACCOMPLISHMENTS, CONCLUSIONS AND RECOMMENDATIONS

4.1 ACCOMPLISHMENTS

The activities and major accomplishments of the program are as follows:

- A viscoelastic materials selection guide was compiled that includes design and fabrication information on 38 candidate materials applicable for use in space.

- A new rubber/plastic alloy damping material was developed that provided moderate damping over a broad temperature range.

- Several generic damped joint concepts (double lap shear) were conceived and 21 test specimens using 7 viscoelastic materials were fabricated.

- An existing analytical model of a lap shear joint was extended to include a return-to-zero feature for structural redundancy and improved creep resistance. A complex modulus representation of the viscoelastic materials used in the joint was also included in the analytical model.

- The successful correlation of existing and acquired test data with the analytical models proves that the overall joint dynamic behavior can now be accurately predicted using the structural properties of the joint's components.

- The analytical models developed have demonstrated their usefulness as a design tool for generic lap shear joints.

- Two new test methods, the steady state and sine pulse propagation methods, were developed and implemented to provide improved means of acquiring generic damping and material qualification data over broad frequency and temperature conditions.

- New outgassing results were obtained for five previously untested materials.

- Performance payoffs were defined resulting from the inclusion of damped joints into representative large truss space structures.

The primary goal of this research program has been accomplished - the advancement of the state of the art in analysis and test of generic passive damping joints for large space structures. The viscoelastic material survey, joint development activities, and the generated test data all contribute to the existing data base for viscoelastic materials application.

Most of the technical problems encountered with the experimental facilities have been resolved. The testing apparatus and data reduction procedures are well established and understood and the nonlinearities generated by the mechanical construction of the piezoelectric transducer have been explained and adequately accounted for in evaluating the experimental data. Room temperature results using all test methods correlate well with the analyses but persistent problems still plague the data gathering process in the high/low temperature regimes. These problems are probably caused by a temperature dependency of the mechanical features of the piezoelectric transducer used to conduct the environmental testing. To resolve the problems, the transducer has been calibrated for each temperature condition being considered and the resulting joint test data appear to follow the same trends displayed by the viscoelastic material from which the joints are made. Additionally, the "zero crossings" technique used to determine the phase shift for the steady state method is not very accurate. Since the results are so sensitive to error in the computed phase shift, other means of obtaining it should be considered. Harmonic or other curve fitting methods that statistically estimate the phase shift using many cycles of data may provide more accurate results.

4.2 CONCLUSIONS

Based on the analysis and test results obtained during this research program, the following conclusions have been drawn:

- The amount of damping loss in the joint is dependent on the amount of strain energy resident in the viscoelastic layer.

- The viscoelastic layer's share of strain energy decreases (therefore, the damping loss decreases) as the VEM's shear modulus G increases, since more of the extensional deformation is transmitted through the VEM layers to the adherends.

- Better trade-offs between the overall damping and stiffness performance of the joint result when stiffer VEM's are selected, provided that the loss factor of the stiff material is not much lower than that of the softer material.

- A thinner viscoelastic layer enhances overall joint stiffness and results in improved bondline strength without significantly altering the achievable damping.

- When a return-to-zero element is included, good joint performance relies on having an appropriate matching between the stiffness of the viscoelastic layer and the return-to-zero element.

- Although the simple $K = GA/t$ formula is adequate for preliminary design, a more complex analytical model, like the modified Hart-Smith model, is required when a stiff VEM or elastic elements are used, since a significant percentage of the strain energy resides in the joint's adherends; a characteristic ignored by the approproximate formula, which assumes that all strain energy is resident in the VEM.

- Both the sine pulse and steady state test methods offer a viable means of collecting reliable joint and material damping data and have demonstrated the feasibility of using a piezoelectric motion transducer for dynamic testing over broad ranges of frequency and temperature.

- The frequency and temperature dependence of the joints mimics that of the viscoelastic materials from which the joints are made.

- The new rubber/plastic alloy VEM developed by MDAC demonstrated remarkable insensitivity to temperature variation.

- Outgassing test results for the seven selected viscoelastic materials indicate that four meet JSC requirements; the remaining three may also eventually meet the requirements with further processing of the raw material or by virtue of the fact that emissions are substantially reduced by the presence of the joint faceplate adherends.

- Incorporating viscoelastic materials into a double lap shear joint configuration can enhance the damping in the joint by an order of magnitude.

- A double lap shear configuration is a viable concept for incorporating damping into the members of a truss supported space structure. Favorable tradeoffs between damping benefit and stiffness penalty have been established by this research program and serve to demonstrate the validity of the damping design approach.

4.3 RECOMMENDATIONS

The work accomplished during this research program involved the development and demonstration of analytical and experimental methods useful for evaluating the damping of viscoelastic double lap shear joints subjected to loading in the axial direction. Potentially beneficial improvements and extensions of this work are as listed below.

- The reliability and accuracy of the gathered dynamic data might be improved by employing statistical averaging and ensembling or Fourier fitting techniques.

- Creep testing of the joints at elevated temperatures should be conducted to verify their strength and suitability for the space environment.

- Methods to perform the analytical modeling and testing of the joints in the transverse directions should be developed and implemented to complete our understanding of how the joints behave under arbitrary loading conditions.

- Multiple joints should be incorporated into a synthetic truss structure to demonstrate the damping benefits and define propagation characteristics at the system level.

- Other joint concepts should be studied, especially those that take optimum advantage of deformations that occur in multiple directions.

- The use of finite element techniques should be evaluated as a means of providing completely general analytical modeling capability for arbitrary damped joint concepts.

- The influence of passive damping devices on the requirements of active control systems should be better defined and the interaction and possible marriage of these two distinctly different vibration control techniques should be more rigorously investigated.

Section 5
REFERENCES

1. R. W. Trudell, R. C. Curley, and L. C. Rogers. Passive Damping in Large Precision Space STructures. AIAA paper 80-0677-CP, May 1980.

2. McDonnell Douglas funded work in support of Space Station studies.

3. McDonnell Douglas funded work in support of ACOSS studies.

4. R. W. Trudell. Passively Damped Joints for Advanced Space Structures - Annual Technical Report. McDonnell Douglas Astronautics Co. report MDC H1178, June 1984.

5. L. J. Hart-Smith. Adhesive-Bonded Double-Lap Joints. NASA CR-112235, January 1973.

Appendix A

RUBBER/PLASTIC ALLOY DEVELOPMENT

Introduction

The AFML issued a technical report on the use of rubber/plastic alloys for broad temperature range damping (AFML-TR-70-242, Dec. 1970). A pure damping material has only one damping peak over a narrow temperature range, centered at its T_G. AFML found that by blending several selected damping materials having different glass transition points, the damping peaks could be made to overlap. This resulted in moderate damping over a broad temperature range.

The AFML alloys were designed for free layer damping, not constrained layer damping. In free layer damping, the damping effectiveness increases as the stiffness of the damping material increases. For most of the AFML alloys, G' was 40,000 psi at 70°F, 100 Hz. This high stiffness was obtained by adding polystyrene to a vinyl (polyvinyl butyral)/acrylonitrile (Paracril-D) mixture. By substituting butyl rubber for the polystyrene, MDAC hoped to obtain a VEM suitable for constrained layer damping with a G' of about 1250 psi. The strain energy is higher than for the stiffer material. However, by eliminating the polystyrene, some of the damping above 150°F is lost. The three-component alloy listed in Table A-1 was anticipated to have a loss factor of 0.1 to 0.7 from -75 to +150°F.

The following topics concerning the develoment of this new material will be discussed in this appendix:

a) Joint Sizing

b) Joint Fabrication Method

c) Test Method

d) Results, Discussion

Joint Sizing

The damping material thickness needed was readily calculated. The desired spring rate for each end of the specimen was 237,600 lb/in. An overlap of about 2.7 inches was assumed, giving an end area of 8 in^2. This gave an overall spring rate of 118,800 lb/in.

$$t = \frac{GA}{K} = \frac{(1250\ \text{lb/in}^2)(8\ \text{in}^2)}{237{,}600\ \text{lb/in.}} = 0.042\ \text{in.}$$

Table A-1. Composition of MDAC-HB Rubber/Plastic Alloy (Specimens 20, 21)

Material	Manufacturer	Purpose	Weight (gm)	T_G (°F)
Butyl (Enjay 268)	Exxon	Elastomer	100	-50
Paracril-D	Uniroyal	Elastomer	100	60
Polyvinyl Butyral	Monsanto	Polymer	50	130
TP-95	Thiokol	Plasticizer	45	
SAF Carbon Black	Various	Reinforcement	50	
ZnO	Various	Promotes Cure	10	
Antioxidant 2246	Vanderbilt	Antioxidant	1	
Dicumyl Peroxide	Hercules	Catalyst	7	

Joint Fabrication Method

The rubber/plastic alloy described in Table A-1 was mixed on a heated rubber mill. The higher melting point polymers were added first. The carbon black and plasticizer were then added. The curing agents were added last. The uncured mixture was then calendered out to a 0.080-0.100 in. thickness.

The graphite/epoxy joint plates were lightly scuff sanded and solvent wiped before priming with Chemlok 205 primer. The rubber/plastic alloy was then vulcanized in place to the plates using a press cure. Stops were used to limit the damping material thickness to 0.05 in.. Locating pins (later removed) were used to prevent lateral movement of the plates during vulcanization. Approximately 2.75 in. of overlap existed at the ends of the specimens.

Test Method

A load/deflection test was performed at 75°F on each joint in an Instron test machine. The joints were deflected ±0.002 in. at about 0.1 Hz for 10-12 cycles (Figs. A-1 and A-2). The extensometer was attached near the grips so the deflection measured was the sum of the damping material and centerplate strains.

Results, Discussion

The joint dimensions and spring rates are listed in Table A-2. The actual overall spring rates were 23-44,000 lb/in. instead of the 118/800 lb/in. predicted. The shear modulus was apparently overestimated during specimen design. G_M was closer to 284-536 psi than to 1250 psi. This is not too surprising, since the MDAC-HB formula was a novel one and G_M could not be easily estimated for it. The variation in K and G_M between specimens 20 and 21 was high. Calculations indicated that specimen 20 had as much as 6% air voids in it, while the void content of specimen 21 was closer to 1%. This may explain some of the variation. Gross examination of the specimen edges also showed that more voids were present in specimen 20. The data for specimen 21 is therefore judged more reliable.

Hysteresis loops were obtained for each joint during the deflection testing (Figs. A-3 and A-4). The hysteresis loop area, measured in in-lbs of work, was used to calculate the joint loss factors.

Values for the loss factor, G', G" and G_M were calculated. Their values are shown in Tables A-2 and A-3. The loss factors are close for the two joints, but the shear moduli show the same variation discussed above. Significant damping is shown at room temperature (η = 0.284-0.342).

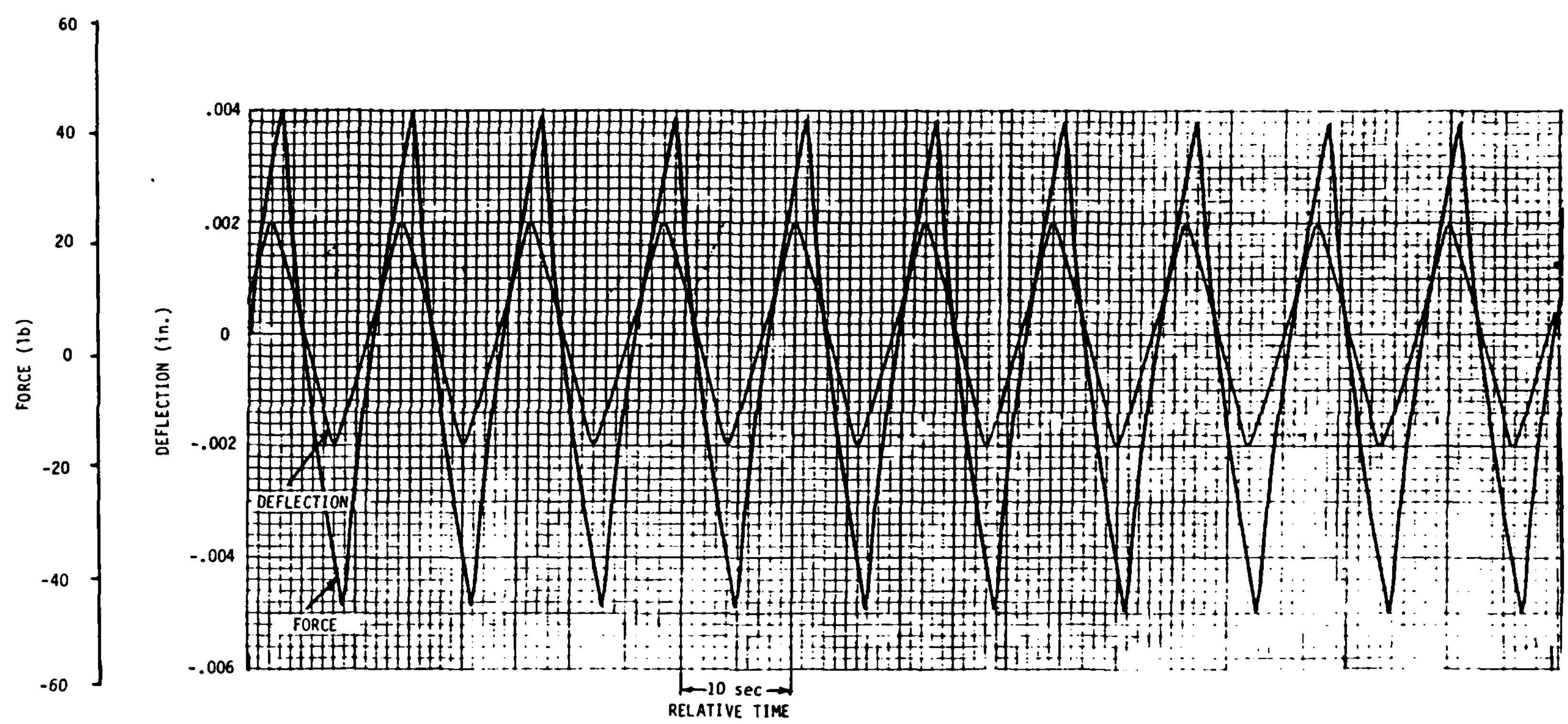

Figure A-1. Load/Deflection Results for Specimen No. 20

Figure A-2. Load/Deflection Results for Specimen No. 21

Table A-2. Low Frequency Spring Rate

Damping Material	Rubber/Plastic Alloy	Rubber/Plastic Alloy
Specimen No.	20	21
Frequency (Hz)	0.0844	0.0739
Max. Load (lbs)	43.99	81.21
Avg. Deflection (± in.)	0.00198	0.00192
Area, End (in^2)	8.183	8.243
VEM Thickness (in.)	0.0504	0.0499
Results - Spring Rate (lb/in)		
Overall	22,200	42,300
Overall*	23,030	44,240
End	44,400	82,600
End*	46,050	88,480
G_M (psi)	273	497
G_M* (psi)	284	536

*Corrected for graphite/epoxy centerplate spring rate

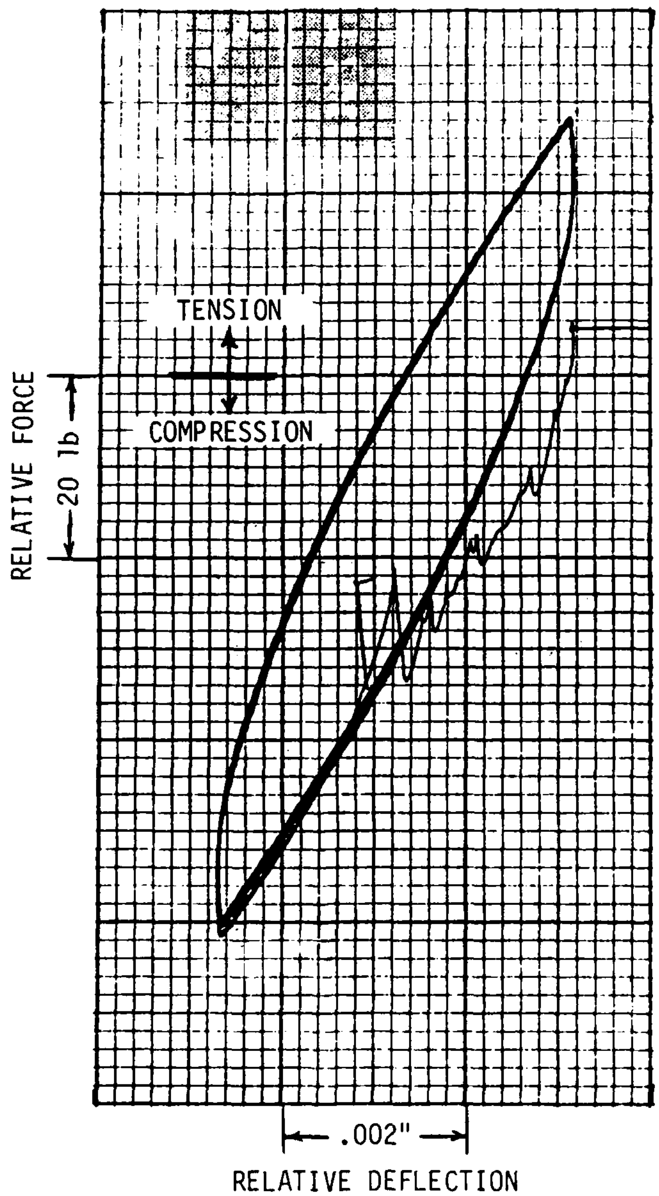

Figure A-3. Hysteresis Loop for Specimen No. 20

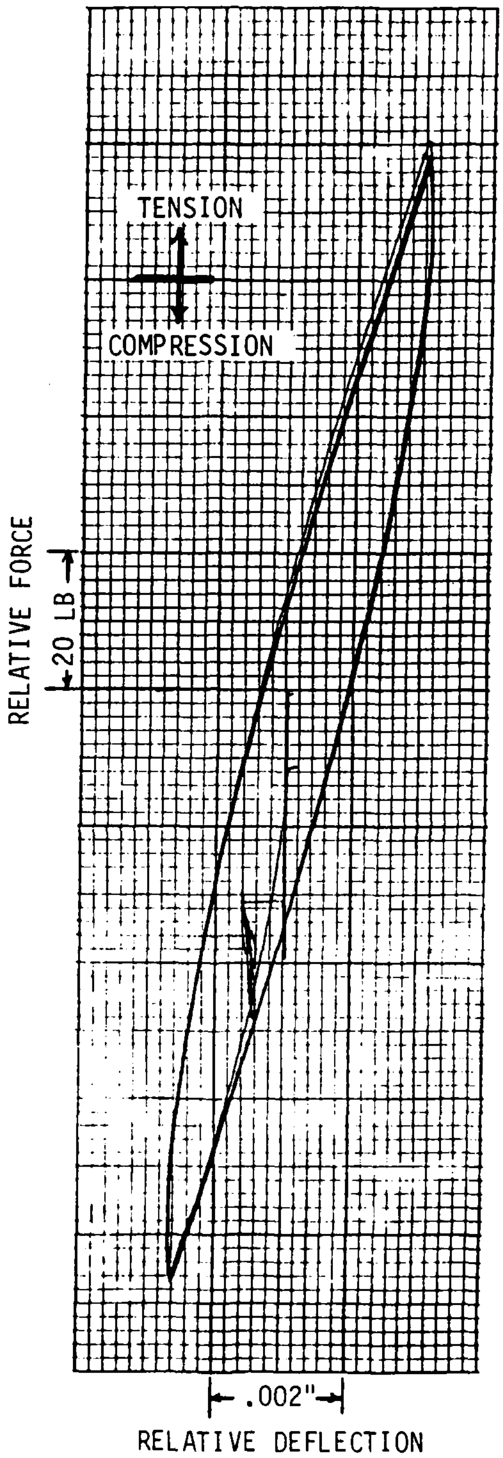

Figure A-4. Hysteresis Loop for Specimen 21

Table A-3. Low Frequency Damping Results

Damping Material	Specimen No.	Frequency (Hz)	Loss Factor* (η)	G' (psi), Actual	G" (psi), Actual
Rubber/Plastic Alloy	20	0.0844	0.342	269	91.9
	21	0.0739	0.284	515	146.0

*Calculated using $\eta = \dfrac{\text{Work}}{2\pi(\text{Stiffness})\left(\dfrac{\text{Total Deflection}}{2}\right)^2}$

Appendix B

ELASTIC ELEMENT DEVELOPMENT

Introduction

Since most VEMs are soft materials they generally have poor creep resistance, and structural redundancy is needed. MDAC-HB has designed, built and tested five prototype joints specimens (15-19) which have redundant, elastic elements. These joints were sent to GIT for testing. Joints 1-14 and 20-21 did not contain elastic elements.

The following topics will be discussed in this appendix:

a) Elastic Element Joint Design

b) Elastic Element Joint Fabrication

c) MDAC-HB Testing and Results

Elastic Element Joint Design

MDAC-HB decided to implement the elastic restoring elements in the form of two fiberglass strips running the length of each specimen.

The fiberglass strips were made using epoxy/fiberglass (DPM 4700, STM0043-03, American Cyanamid). The properties of this material are listed in Table B-1. The fiberglass strips used in joints 15-17 were 0.0235 inch thick, 1.5 inches wide, and ran the length of each specimen. The same type of fiberglass was used for specimens 18-19 but the strips were thinner (0.01088 inch). The fiberglass was rigidly bonded to the graphite/epoxy centerplates except for a 1-inch section in the center. This 1-inch section acted as the elastic element.

Nonadhering shims were placed on both sides of the elastic elements to prevent buckling of the elements under compression.

For joints 15-17, the combined spring rate for the two pieces of fiberglass is readily calculated:

$$K_{EL} = \frac{EA}{\ell} = \frac{(3 \times 10^6)(2)(1.5)(0.0235)}{1} = 211{,}500 \text{ lb/in.}$$

Table B-1. Fiberglass Elastic Element Properties

Glass Fabric:	MIL-C-9084, TY VIII B (#181 Cloth)
Epoxy Resin:	MIL-R-9300
Ult. Tensile Strength:	50,000 psi
Tensile Modulus:	3.0×10^6 psi
Ult. Flexural Strength:	55,000 psi
Flexural Modulus	3.2×10^6 psi
Ult. Compressive Strength, Edgewise:	50,000 psi
Interlaminar Shear Strength	3,000 psi
Density	1.72 gm/cc

To optimize the strain energy, K_{VEM} (overall) must equal K_{EL}. Therefore, K_{VEM} at each end of the joint must be 2(211,500) = 423,000 lb/in. Using EC 2216 for a VEM (G_M = 2600 lb/in. at 0.1 Hz, 22°C), and assuming that each VEM layer measures 2.5 inches long and 1.5 inches wide, the required VEM thickness to obtain K_{VEM} = 423,000 lb/in. can be readily calculated:

$$t = \frac{G_M A}{K} = \frac{2600\ (1.5)(2.5)(2)}{423{,}000} = 0.0460 \text{ inch}$$

The elastic element stiffness K_{EL} and the required VEM layer thickness for specimens 18-19 can be calculated in a similar fashion. Both of these joints employ Soundcoat Dyad 606 as the VEM. Using $K_{EL} = EA/\ell$, the spring rate of the elastic elements was calculated to be about 99,000 lb/in. To optimize strain energy, K_{VEM} must equal K_{EL}. Therefore, K_{VEM} for each joint end mustAppen(99,000) = 198,000 lb/in.

From studies of joints 5 and 6, G_M for Dyad 606 (at 25°C and 0.1 Hz) was known to be about 685 psi. If each VEM pad is 2.5 inches long and 1.5 inches wide, the required thickness can be calculated:

$$t = \frac{G_M A}{K} = \frac{(685)(1.5)(2.5)(2)}{198{,}000} = 0.0258 \text{ inch}$$

Elastic Element Joint Fabrication

All bonding surfaces of the graphite/epoxy plates and elastic elements were lightly scuff sanded with 400 grit paper and lightly solvent wiped with MEK. No primers were used. The two centerplates were first bonded to the elastic element strips with EA 956 epoxy. A 4 mil glass scrim cloth was used for bondline control. A nonadhering shim was inserted between the elastic elements in the 1-inch elastic center section before bonding. Two specimens (15 and 16) were made with silicone rubber shims. Three specimens (17-19) were made with graphite/ epoxy and aluminum shims, to offer even more support against buckling. A small elastic pad was placed at the end of each rigid shim so that axial movement (±0.007") would be possible. The adhesive was allowed to cure before proceeding to the next step.

The sideplates were then clamped to the bonded assembly with shims. The VEM layer dimensions actually achieved were close to the target dimensions. For specimens 15-17, the degassed EC 2216 was injected using a Semco gun and a VEM thickness of 0.0573-0.0615 inch was achieved (target value = 0.0460 inch) as shown in Table B-2. For specimens 18-19, some 25 mil sheets of Dyad 606 were in stock and were used (target value = 0.0258 inch).

<u>MDAC-HB Testing and Results</u>

A cyclic load/deflection test was performed at 75°F on each joint in an Instron test machine. The joints were deflected ±2 mils. This cyclic loading was repeated about 10 times with a target test frequency of 0.1 Hz. The actual test frequency varied from 0.0881 to 0.144. Hysteresis loops were also generated.

Fig. B-1 shows that the extensometer was attached to the centerplates near where the grip area started, 2 inches from the end. The deflection measured was, therefore, the sum of the centerplate and elastic element strains. Typical force and delection time histories for specimens 18 and 19 are shown in Figs. B-2 and B-3.

The overall joint spring rates measured for our specimens are listed in Table B-2. The overall joint K_{VEM} is also listed. K_{VEM} is obtained by subtracting the centerplate and elastic element spring rate contribution from the overall spring rate. Data for specimens 5 and 6 (no elastic element) are included in the table to allow a more direct stiffness comparison between joints that contain elastic elements and those that do not. The overall joint spring rates, determined by test, for specimens 16 and 17 agree very closely with the targeted value. However, the stiffness of specimen 15 is much higher, possibly due to variations in fabrication or testing. The actual spring rates for joints 18 and 19 were significantly higher than the targeted value. This may have been caused, in part, by lot-to-lot variations in the VEM.

G_M was calculated for each specimen once K_{VEM} was known; η was obtained from hysteresis loop areas using:

Table B-2. VEM Joint Dimensions and Spring Rates

VEM Material	Specimen	Frequency Hz	Maximum Load, lbs	Deflection ±in.	Area End, in²	VEM Thickness in.	Spring Rate, lb/in. Overall	Overall*	End	End*
EC 2216	15	0.116	925	0.00179	6.95	0.0573	516,800	354,200	1,033,500	708,500
EC 2216	16	0.141	780	0.00199	6.86	0.0582	392,000	229,400	783,900	458,900
EC 2216	17	0.144	750	0.00195	6.88	0.0615	384,600	222,100	769,200	444,200
DYAD 606	18	0.0881	580	0.00200	7.48	0.0249	290,200	204,200	580,400	408,500
DYAD 606	19	0.0959	561	0.00184	7.404	0.0249	305,400	221,300	610,900	442,700
DYAD 606	5	0.0795	72	0.00210	5.87	0.0515	34,300	36,800	68,600	73,600
DYAD 606	6	0.0740	78.9	0.00208	5.89	0.0515	38,000	41,000	75,900	82,100

*Elastic element spring rate (corrected for centerplate contribution) subtracted out to leave only K_{VEM}

$$K_{VEM} = K_{OVERALL} - \frac{K_{CP}\,K_{EL}}{K_{CP} + K_{EL}}$$

where K_{CP} = GR/EP Centerplate Spring Rate = 702,000 lb/in.

$K_{EL}^{15,16,17}$ = 211,500 lb/in.

K_{EL}^{18} = 97,970 lb/in.

K_{EL}^{19} = 95,560 lb/in.

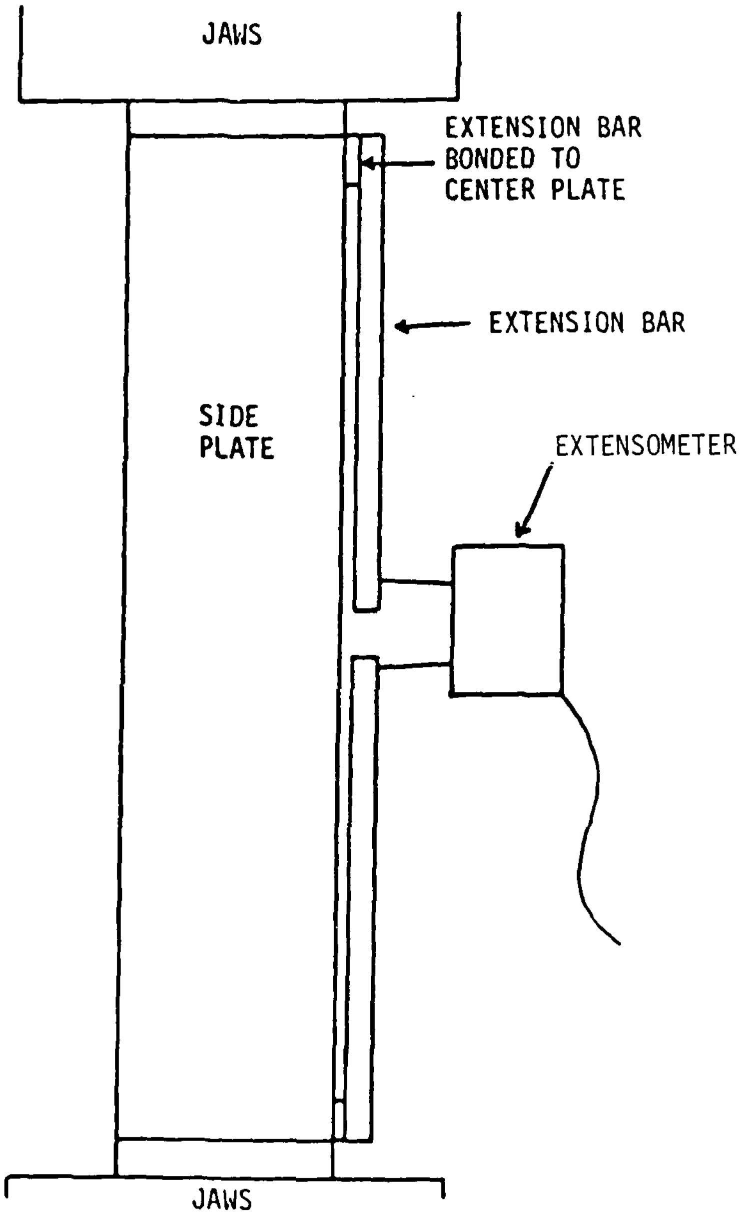

Figure B-1. Method Used to Attach Extensometer to Joint

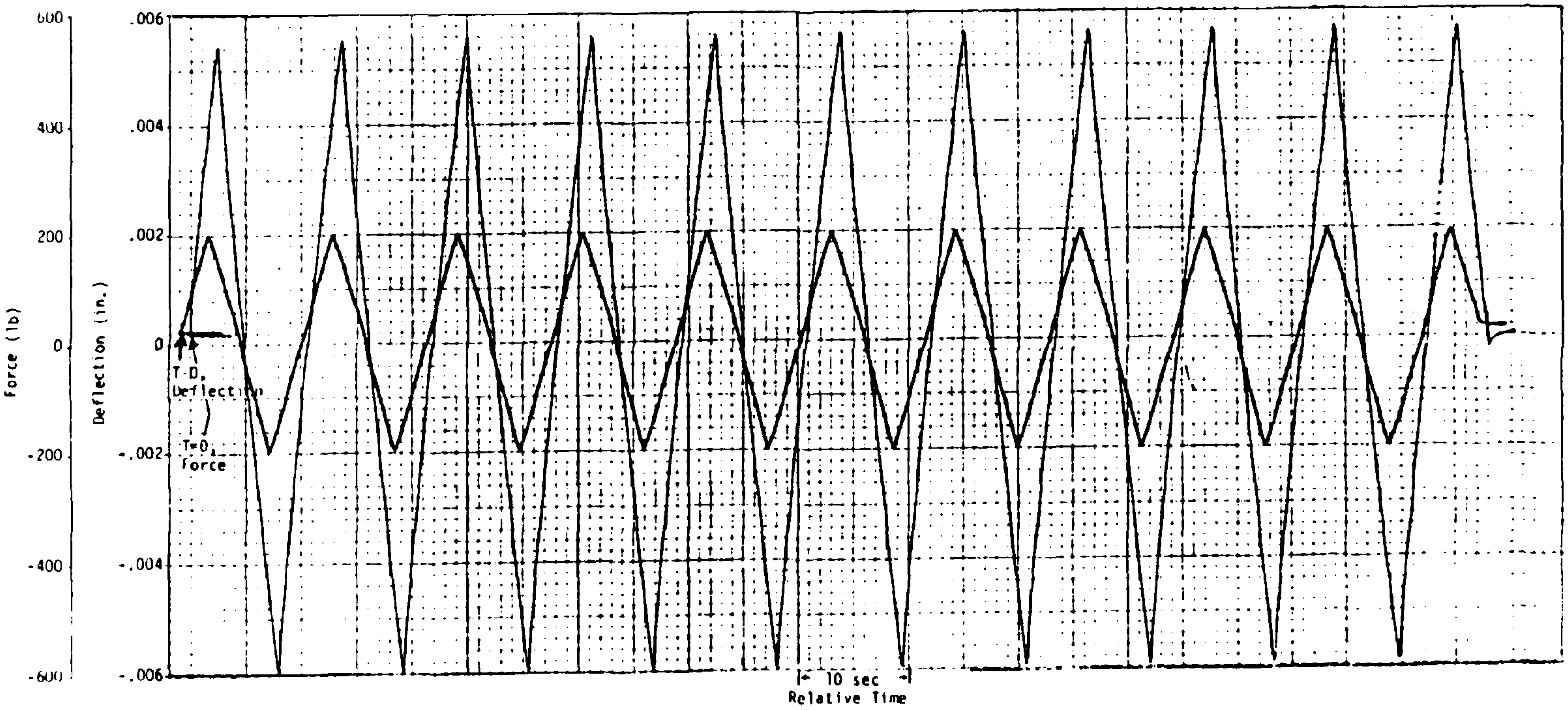

Figure B-2. Force/Deflection Chart for Specimen 18

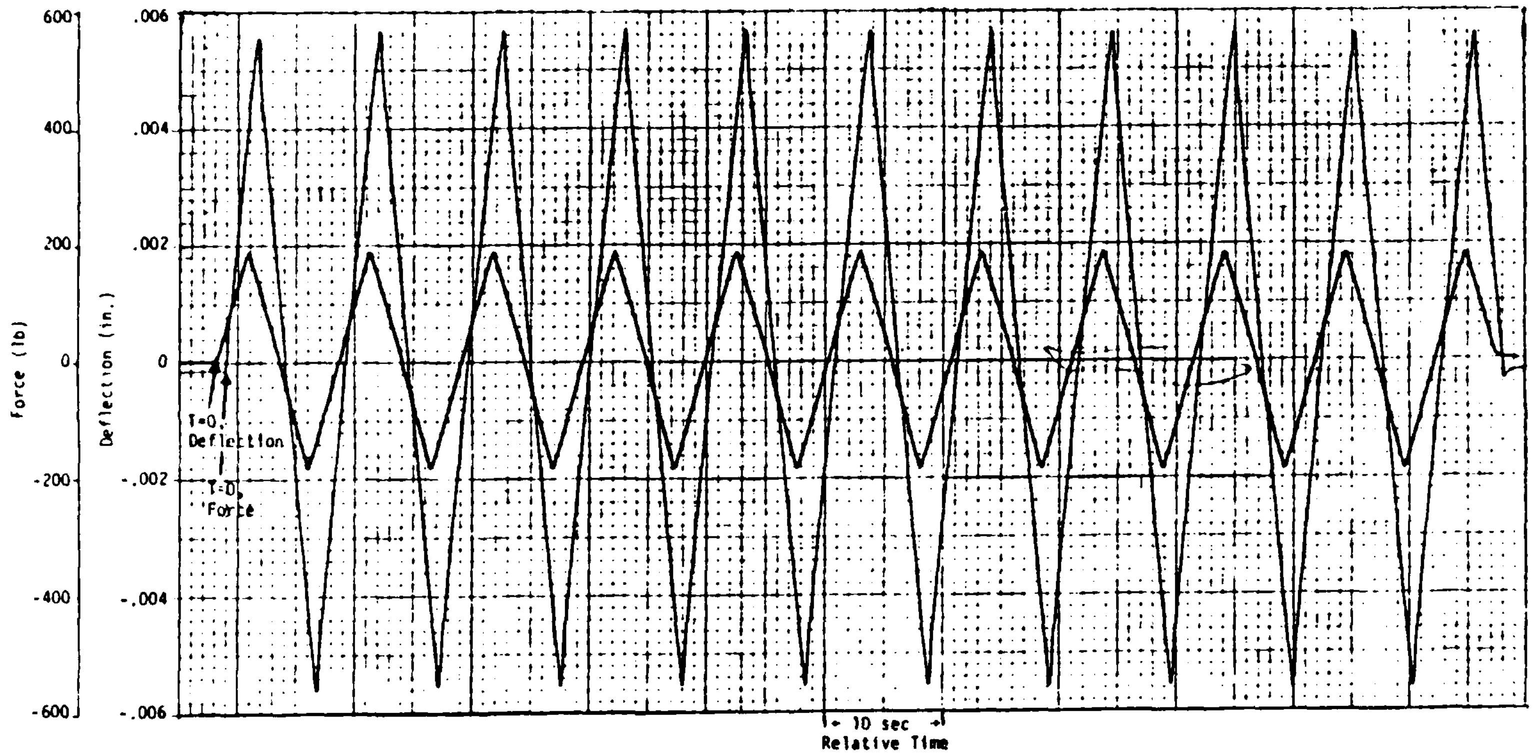

Figure B-3. Force/Deflection Chart for Specimen 19

$$\eta = \frac{\text{Work}}{2\pi(\text{Stiffness})\left(\frac{\text{Total Deflection}}{2}\right)^2}$$

where stiffness = max. load/max. deflection
work = hysteresis loop area, in-lbs

The hysteresis loops for specimens 15-17 were presented in Ref. 4 of the main report. The hysteresis loops for specimens 18 and 19 are shown in Figs. B-4 and B-5, respectively. The hysteresis loop area can be measured as in-lb of work and was used to calculate the joint loss factors.

G_M and η are listed in Table B-3. Once G_M and η were known, G' and G" were calculated using the following equations:

$$\eta = G''/G'$$

$$G_M = [(G')^2 + (G'')^2]^{0.5}$$

G' and G" are also listed in Table B-3, along with extrapolated values for G_M, G', G" and η from some Anatrol and UDRI data. The test values for G_M, G' and η agree well with the Anatrol data. G" for specimens 16 and 17 is low. The close agreement between specimens 16 and 17 indicates that shim type did not have any apparent effect on damping or moduli. The shear moduli of specimens 18 and 19 are higher than those of specimens 5 and 6, probably due to the difference in their VEM layer thickness. Specimens 5 and 6 had VEM layers twice as thick as those used in 18 and 19. The degree of shear strain can influence shear moduli. Since all four specimens were deflected 2 mils, specimens 18 and 19 experienced twice as much shear strain as 5 and 6, thus offering an explanation for the higher shear moduli. Since the overall spring rate was higher than predicted, the G_M and G' values for specimens 18 and 19 are higher than those obtained for 5 and 6. The G" values for these four specimens agree. The UDRI predictions for Dyad 606 shear moduli appear to be low. The Anatrol values for G' are closer to the experimental results. The actual loss factors for all specimens are lower than those predicted by UDRI. This may be because the UDRI data had to be extrapolated so far. Specimens 18 and 19 have lower loss factors than 5 and 6 because they contain elastic elements. The addition of an elastic element to a joint will always lower the VEM strain energy.

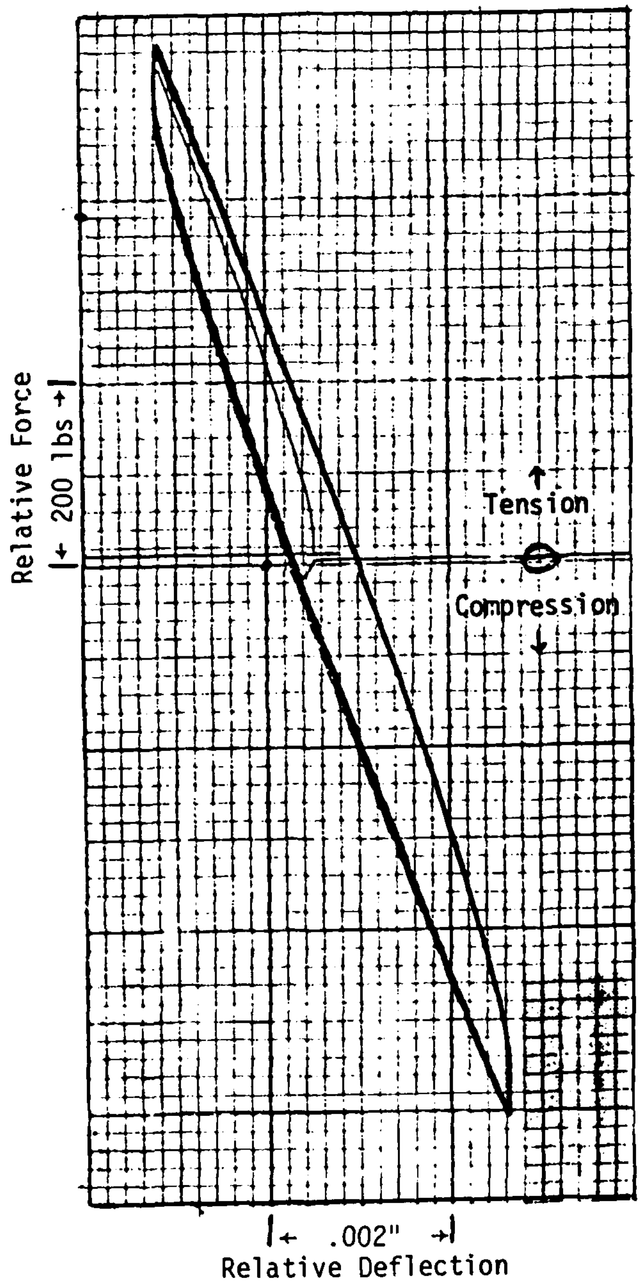

Figure B-4. Hysteresis Loop for Specimen 18

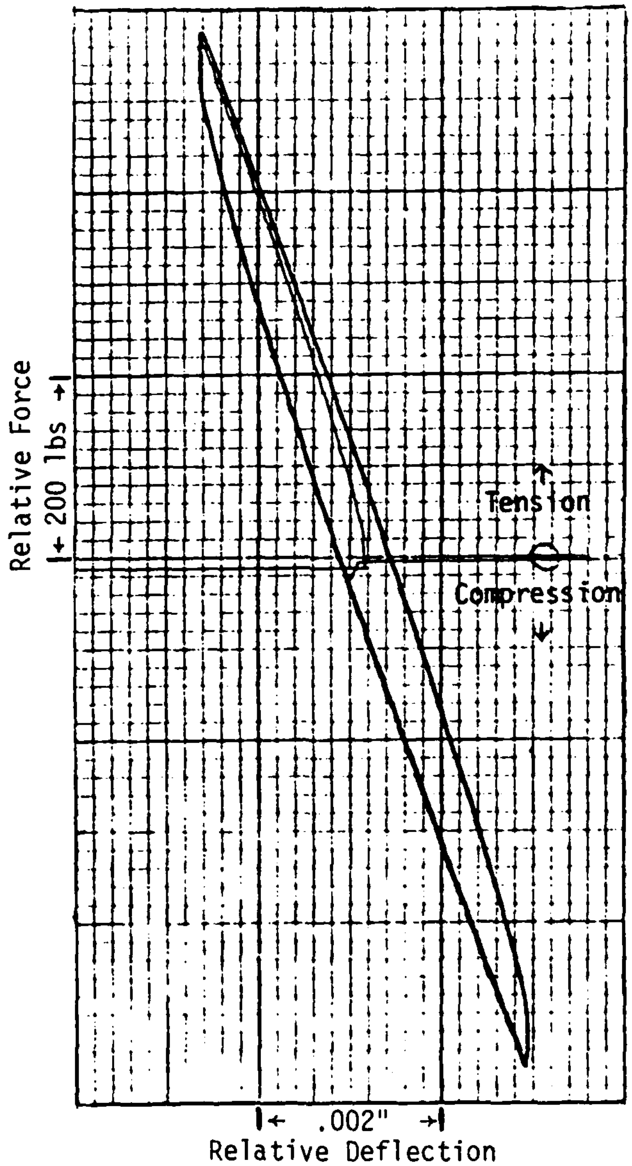

Figure B-5. Hysteresis Loop for Specimen 19

Table B-3. VEM Joint Damping Properties

Material	Specimen	Frequency, Hz	Loss Factor			G', psi			G", psi			G_M, psi		
			Actual	UDRI	Anatrol	Actual	UDRI	Anatrol	Actual	UDRI	Anatrol	Actual	UDRI	Anatrol
EC 2216	15	0.116	0.165	--	0.140*	5762	--	5000*	950	--	950*	5840	--	5090*
EC 2216	16	0.141	0.125	--	0.140*	3863	--	5000*	483	--	950*	3893	--	5090*
EC 2216	17	0.144	0.120	--	0.140*	3942	--	5000*	473	--	950*	3970	--	5090*
DYAD 606	18	0.0881	0.09115	0.52**	--	1352	145**	450**	123	75.4**	--	1358	163**	--
DYAD 606	19	0.0959	0.0765	0.53**	--	1483	147**	450**	114	77.9**	--	1488	166**	--
DYAD 606	5	0.0795	0.249	0.52**	--	627	143**	450**	156	75.0**	--	602	161**	--
DYAD 606	6	0.0740	0.249	0.51**	--	697	138**	450**	173	70.3**	--	664	155**	--

*Extrapolated for 0.1 Hz, 75°F
**Extrapolated

Appendix C

ANALYTICAL MODELING

Introduction

An essential step toward implementing the designed-in approach to passive damping enhancement is the development of useful analytical models. The underlying guidelines for the development of these models are simplicity and a realistic representation of the actual physical behavior.

The modeling process begins by defining a realistic joint concept that clearly will provide enhanced performance of the structure for the anticipated disturbances and environmental factors. The symmetric, double-lap configuration shown in Fig. C-1 is particularly well suited for space truss structures where the main loading direction of the members is the axial one. In this configuration the axial load is transferred through the joint from one member to the other by shear stresses in the viscoelastic (VEM) adhesive layers. The high damping produced by the shearing of viscoelastic materials is a well known phenomenon.

Following the joint configuration definition, mathematical relationships are defined that accurately represent the actual physical characteristics of the joint system and its components. The resulting mathematical model permits parametric design studies that enhance the analyst's understanding of the joint component interactions leading to a better design of the joint system.

The following topics will be discussed in this appendix:

a) Comparison of Modeling Methods

b) Model Correlations

c) Evaluation of Parametric Trends

d) Damped Joint Design

Comparison of Modeling Methods

In this research program three analytical models were used to represent the damped joint behavior - a simple GA/t representation, a fully elastic model, and a viscoelastic model. In this section these models will be compared with respect to their limitations, relative advantages, and potential uses. For all these modeling methods the only external load acting on the joint is

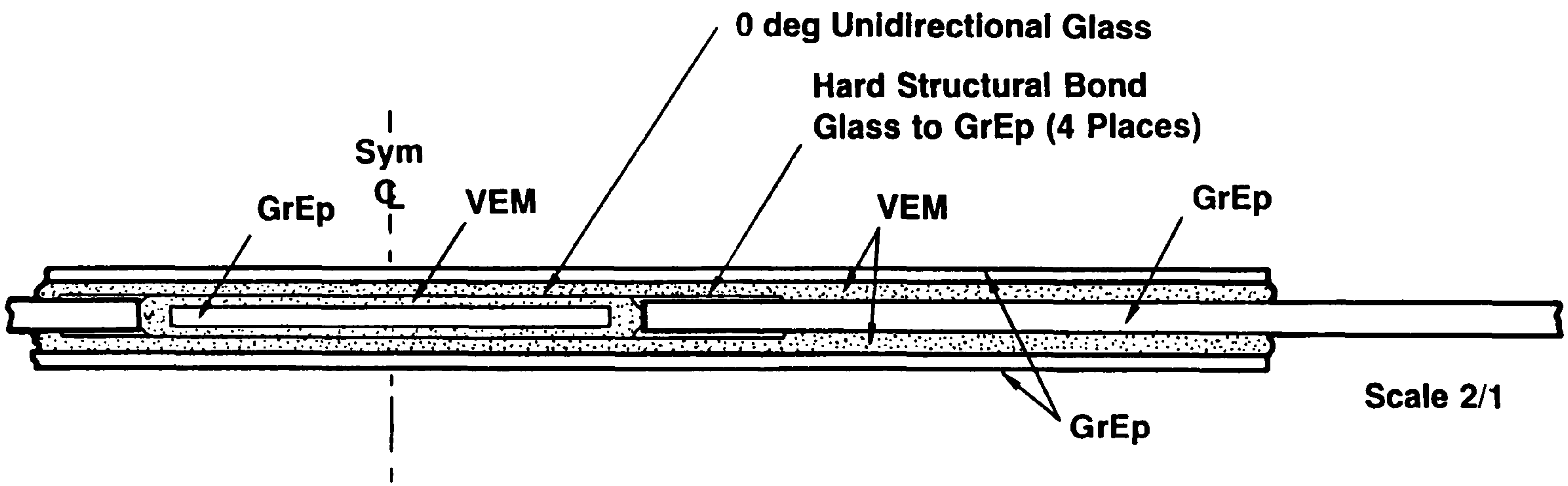

Figure C-1. Structural Damping Joint Configuration

assumed to be a fluctuating axial force applied on one member, which is transferred through the joint to the other member. Therefore, the present analyses are confined to a uniaxial response which can be described by a single coordinate. This configuration permits the evaluation of damping and stiffness properties associated with the primary, axial loading direction only.

The axial load is assumed to be purely static for the GA/t and fully elastic approaches, whereas the viscoelastic approach allows quasi-static motion. The assumption of static or quasi-static motion preserves the simplicity of the analysis by neglecting inertia, frequency, and other time-dependent effects.

The formula K = GA/t, which was briefly described in Section 2 of the main report, is the simplest representation of the stiffness in a lap shear joint. The corresponding expression for the elastic displacement at the external end of the inner adherend is u = Pt/bG, where P is the applied load and b is the specimen width. This model assumes that the adherends are infinitely rigid and therefore all of the strain energy is resident in the VEM layers. This is a reasonable assumption when the VEM is very soft relative to the adherends and no elastic element has been provided. Therefore, this simple model serves as a good tool for the initial design work of sizing the joint components. For stiffer VEMs or when an elastic element is incorporated, one of the other more sophisticated models should be used.

The fully elastic model and the viscoelastic model are very similar, both being derived from the well known Hart-Smith analysis of double-lap bonded joints (Ref. C-1). The models have been modified to include a direct elastic connection between the inner adherends. The only significant difference between the two models is that the latter used a viscoelastic representation of the adhesive layer which essentially means that a complex value of the shear modulus G is used. The governing differential equation is as follows:

$$\frac{d^2\tau}{dx^2} - \lambda^2\tau = 0$$

where

$$\lambda^2 = \frac{G}{t_v}\left(\frac{1}{E_0 t_0} + \frac{2}{E_1 t_1}\right)$$

A complete description and computer code listing for the fully elastic model, shown in Fig. C-2, is given in Refs. C-2 and C-3. A complete description of the development of the viscoelastic model also shown in Fig. C-2 is given in Ref. C-4. Note that two differences exist between these two models - the origin of the coordinate axis and the assumed form of the elastic connection. The fully elastic model uses a spring, whereas the viscoelastic model uses a linearly elastic strip. These models have been used to study the influence of elastic strips and adherend elasticity on the damping and stiffness behavior of joints. Parametric studies were conducted to establish trends useful for the purpose of designing joints with a good balance between damping capacity and stiffness. The static and quasi-static analysis methods on which these models are based are particularly well suited to space structures where low vibration frequencies are expected to be dominant and inertia effects may be neglected without serious errors.

Model Correlations

The models described in the previous section have been numerically exercised to satisfy two major objectives: (1) assess the validity of the models with regard to their ability to predict the correct physical behavior, and (2) illustrate potential applications of the model in the areas of preliminary design and test data correlations. The results of this numerical study have been reported in Ref. C-4 and are repeated here for completeness and to illustrate the correlation that can be expected from the various models.

To achieve the objectives stated above, the VEM layer strain energy U_{tv} (related to damping) and the deflection at the external end of the inner adherend $u_{i1}(\ell)$ (related to stiffness) have been plotted as a function of several important parameters for the simple design formula K = GA/t, the fully elastic model, and the viscoelastic model. The joint properties selected for these correlation studies are

$$P = 1 \text{ lb}$$
$$E_i = E_o = 8.5 \times 10^6 \text{ psi}$$
$$t_i = 0.2 \text{ in.}$$
$$t_o = 0.1 \text{ in.}$$
$$t_s = 0.047 \text{ in.}$$
$$b = 1.0 \text{ in.}$$
$$\ell_s = 0.5 \text{ in.}$$

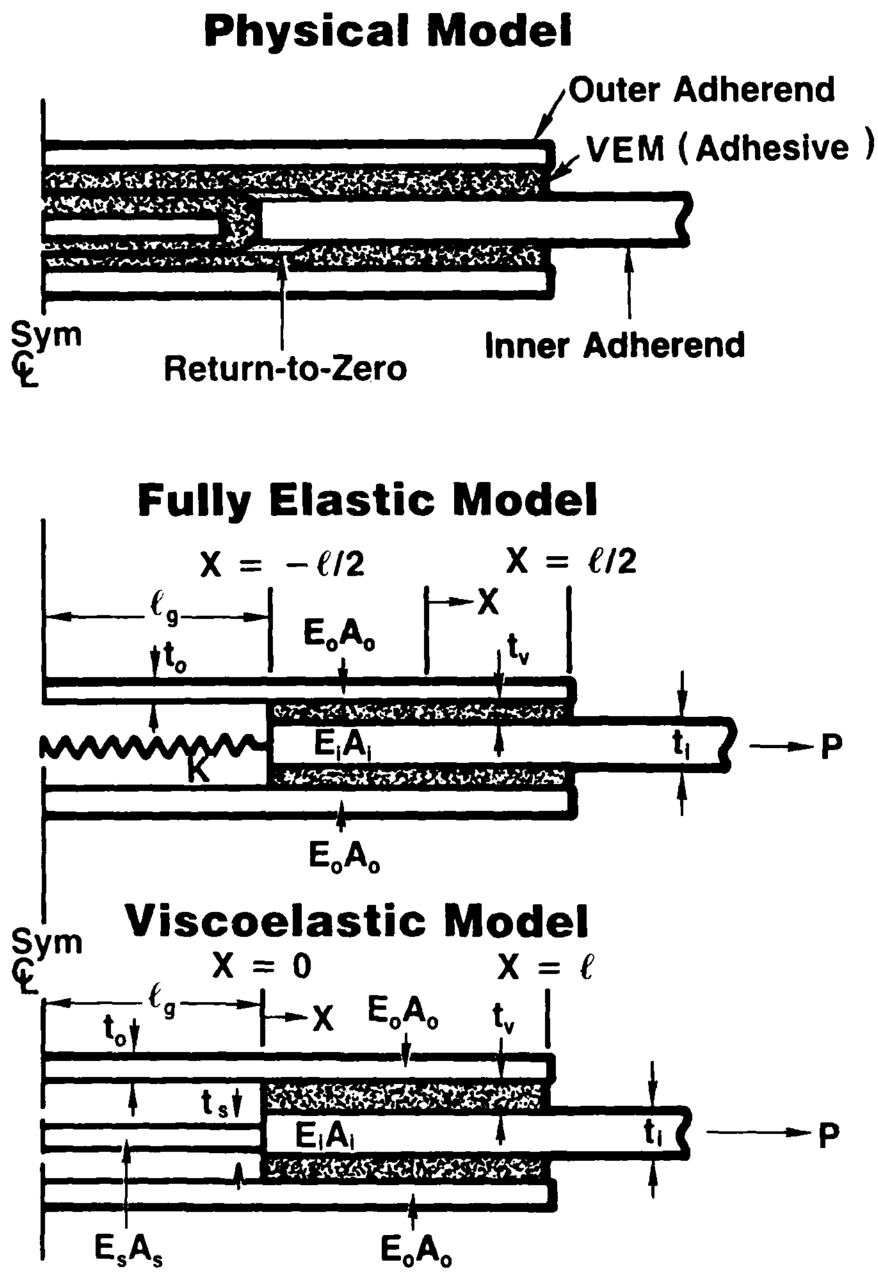

Structural Parameters

G' = VEM Shear Storage Modulus
G'' = VEM Shear Loss Modulus
G_M = VEM Shear Modulus (Magnitude)
t_v = VEM Layer Thickness
E_o = Outer Adherend Young's Modulus
E_i = Inner Adherend Young's Modulus
A_o = Outer Adherend Area
A_i = Inner Adherend Area
t_o = Outer Adherend Thickness
t_i = Inner Adherend Thickness
ℓ_g = Gap Length
ℓ = Overlap Length
K = EA_{Spring}/ℓ_g
E_s = Elastic Strip Young's Modulus
A_s = Elastic Strip Area
t_s = Elastic Strip Thickness
P = Applied Load

Figure C-2. Double-Lap Joint Models

To get a direct comparison of the models, the structural properties of the elastic strip used in the viscoelastic model were selected to produce the equivalent spring stiffness K_s used by the fully elastic model.

All three methods compared in Figs. C-3 and C-4 predict the same physical behavior associated with the increase of the overlap length. Due to the corresponding increase in the total stiffness of the VEM layers, both the strain energy and the deflection parameters decrease asymptotically to zero and to a finite value determined by the adherend's stiffness, respectively. A comparison between Figs. C-3 and C-4 shows, as expected, that a stiffer return-to-zero element reduces both the strain energy stored in the VEM layers and the end deflection. This is especially true for short overlaps where the strain energy share of the VEM layers is higher due to their lower stiffness. Also, examination of these plots reveals that the approximate equation generates higher deflection values than the more accurate analytical models which produce essentially identical results. This is because it assumes that all the strain energy of the joint is stored in the VEM layers so that it yields lower predictions for the overall joint stiffness than the actual values. The difference is more pronounced when the strain energy share of the VEM layers is lower, like in the case of stiff return-to-zero elements. The results generated by the formula $K = GA/t$ approach the predictions of the analytical models for longer overlaps since the assumption of averaged uniform shear stress distribution is more suitable to these cases.

Similar conclusions can be drawn from Figs. C-5 and C-6 which display the VEM thickness effect on the same parameters for a soft and a stiff return-to- zero element, respectively. In the first case, most of the total joint strain energy is stored in the VEM layers. Since their stiffness is reduced when their thickness increases, both the VEM strain energy and the end deflection increase almost linearly as t_v becomes larger. In the case of a stiff elastic strip, the VEM stiffness is less dominant since a greater share of strain energy is stored in the elastic strip and inner adherend. As a result, the VEM strain energy and the end deflection are less than in the previous case. They do not increase linearly with the VEM thickness but become asymptotic to finite values determined by the stiffness of the joint elastic elements. Again, all the methods predict the same physical behavior and numerical differences still exist between the predictions of the approximate equation and those of the other analytical models.

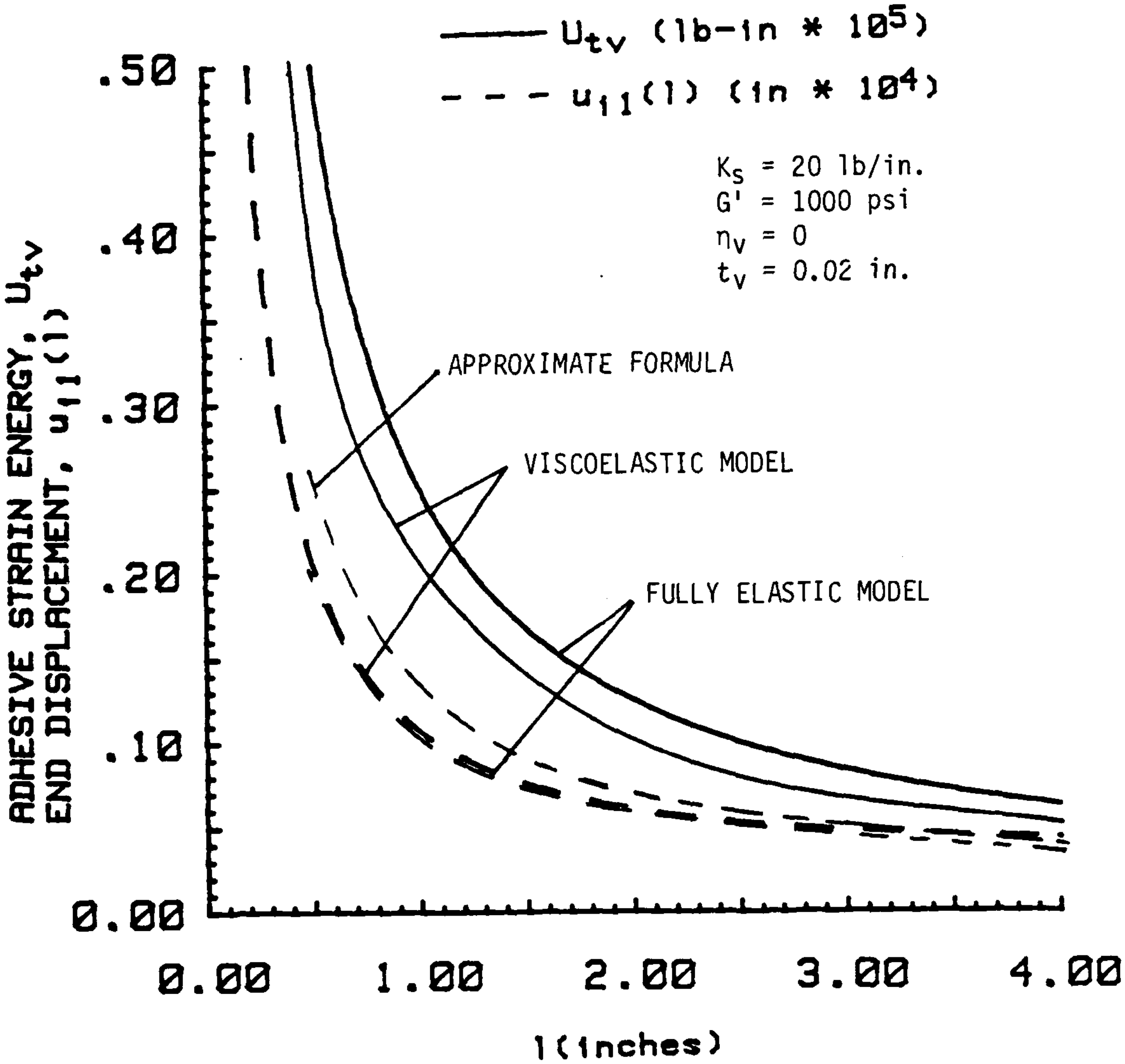

Figure C-3. Model Correlation of Overlap Length Effect - Soft Elastic Strip

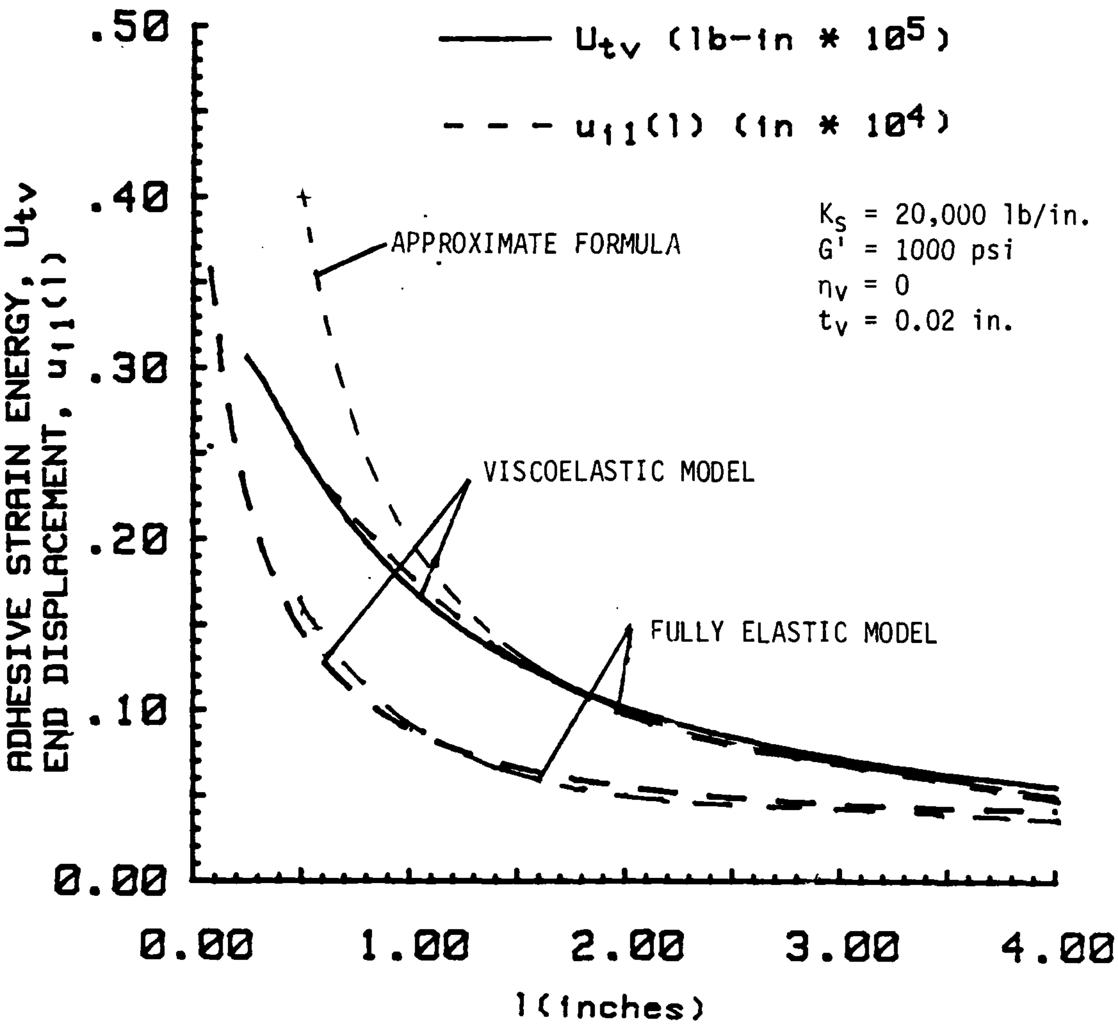

Figure C-4. Model Correlation of Overlap Length Effect - Sti·· Elastic Strip

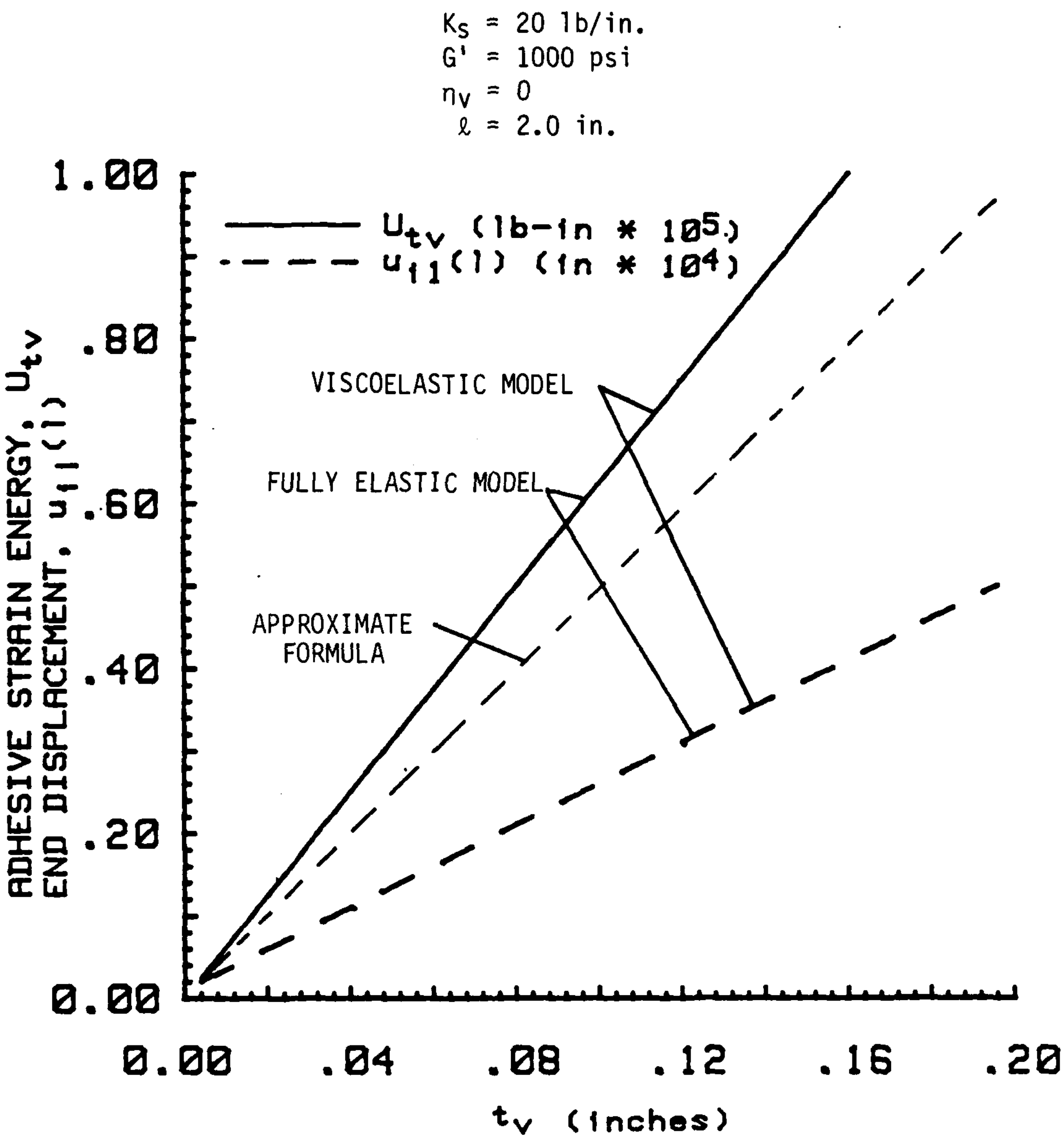

Figure C-5. Model Correlation of VEM Thickness Effect - Soft Elastic Strip

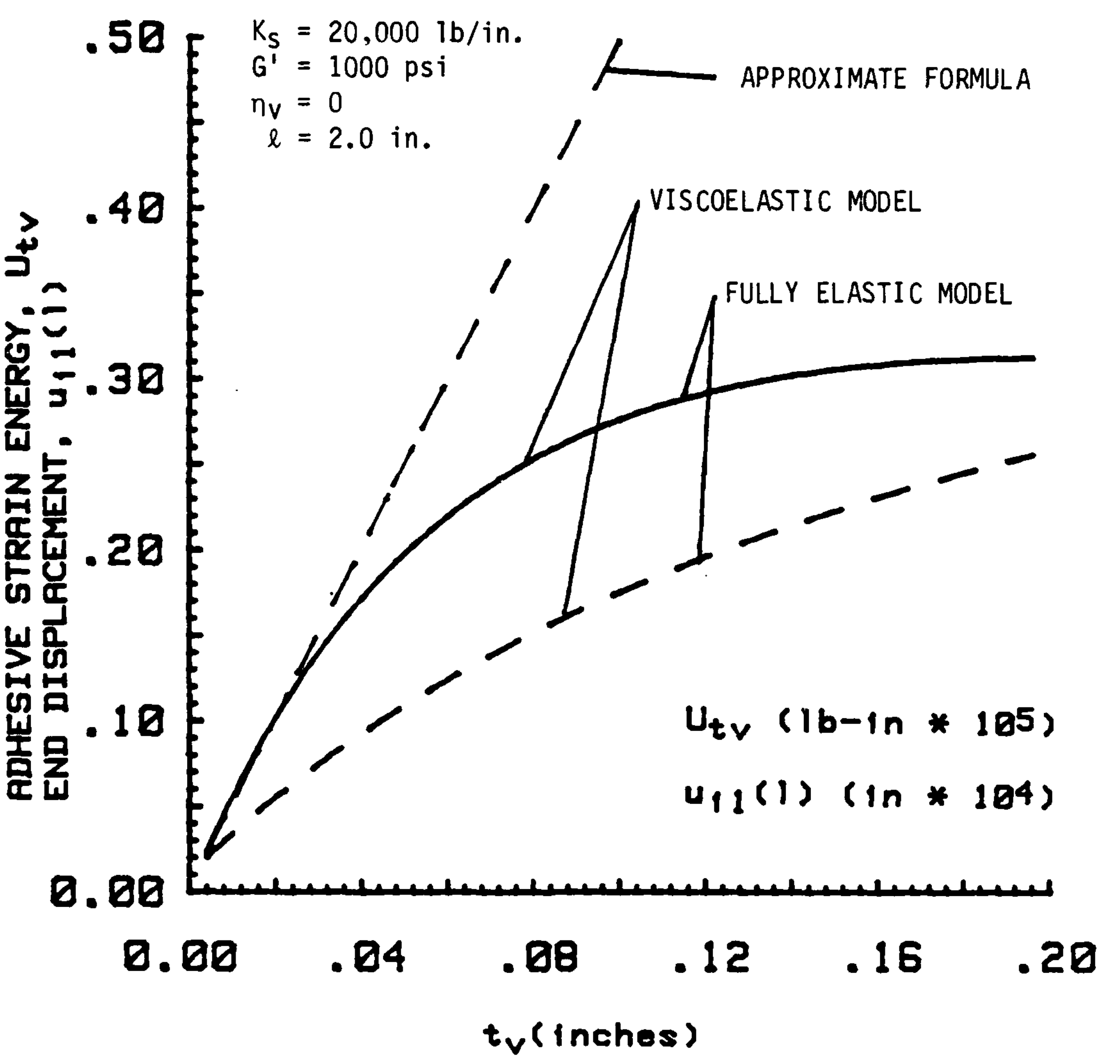

Figure C-6. Model Correlation of VEM Thickness Effect - Stiff Elastic Strip

The effect of the VEM shear modulus on its strain energy and the inner adherend end deflection is shown in Figs. C-7 and C-8 for a soft and a stiff elastic strip, respectively. As the VEM layers become stiffer, their strain energy decreases asymptotically to zero. At the same time, the end deflection decreases asymptotically to a finite value determined mainly by the stiffness of the inner adherend. The influence of the elastic strip stiffness is visible only at low values of G'. Again, previous conclusions about the good model correlation are confirmed.

The analytical models developed can be readily used to correlate the experimental data with the analysis results. Curves like that shown in Figs. C-9 and C-10 demonstrate how the joint axial stiffness and loss factor can be determined from the elastic shear modulus and loss factor of the VEM used in the joint. Conversely, using the same curves, the VEM properties can be extracted from measured joint data. These curves were generated using the quasi-static (viscoelastic) analytical model and the actual test specimen properties listed below:

$$P = 1 \text{ lb}$$

$$E_i = E_o = 15.6 \times 10^6 \text{ psi}$$

$$t_i = t_o = 0.15 \text{ in.}$$

$$t_s = 0.047 \text{ in.}$$

$$\ell = 3.0 \text{ in.}$$

$$\ell_s = 0.5 \text{ in.}$$

$$b = 1.5 \text{ in.}$$

Fig. C-9 illustrates the relationship between the predicted joint stiffness (normalized by K_r) and the shear modulus and thickness of the VEM. Fig. C-10 shows the relationship between the predicted joint loss factor and the shear modulus and loss factor of the VEM.

Correlation of these predicted results with available material data and hysteresis-loop test results for three specimens is given in Table C-1. The good correlation achieved between the analytic predictions and the measured test results is very significant because it proves that the analytical models developed can be used to predict overall joint behavior from the properties of the joint's components. The specimens included in this comparison were

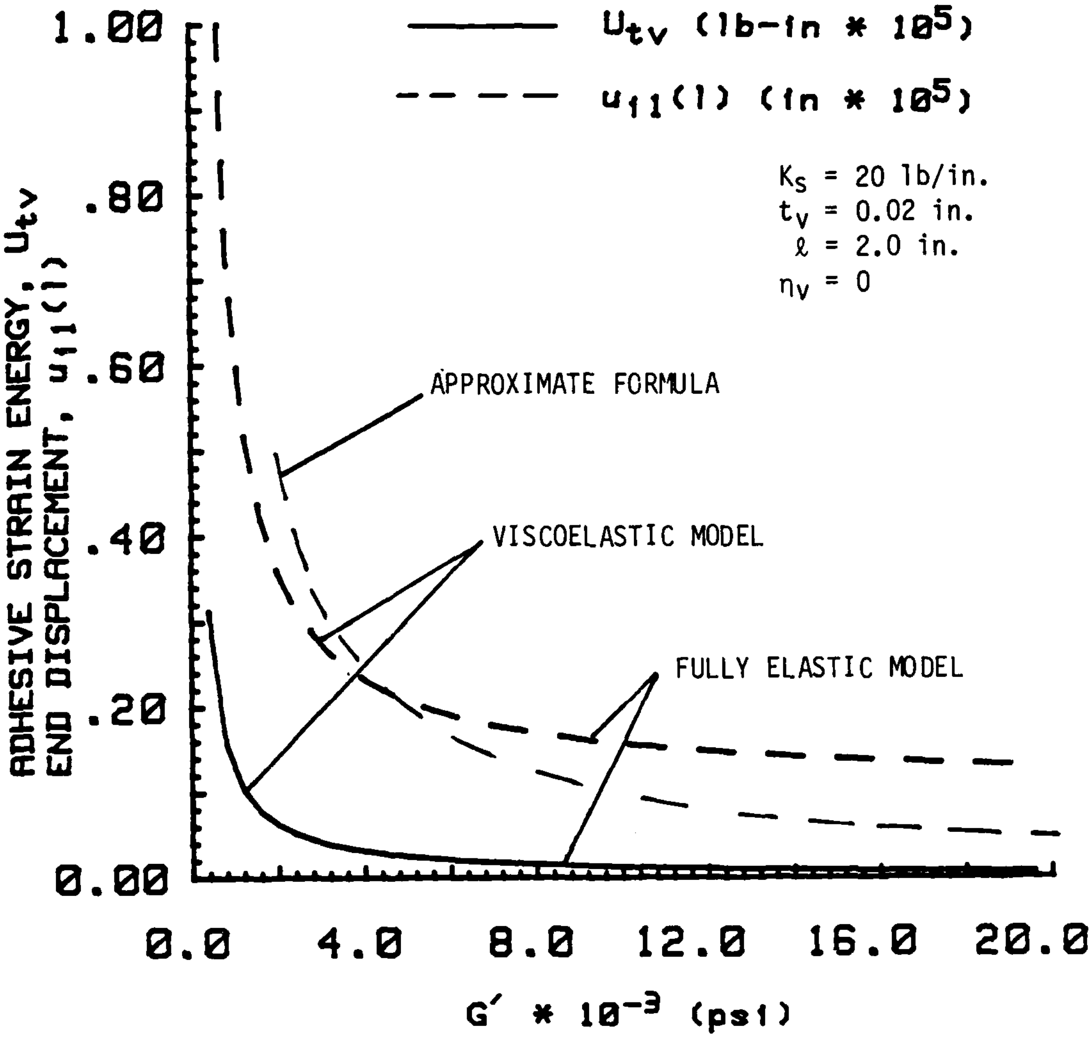

Figure C-7. Model Correlation of VEM Stiffness Effect - Soft Elastic Strip

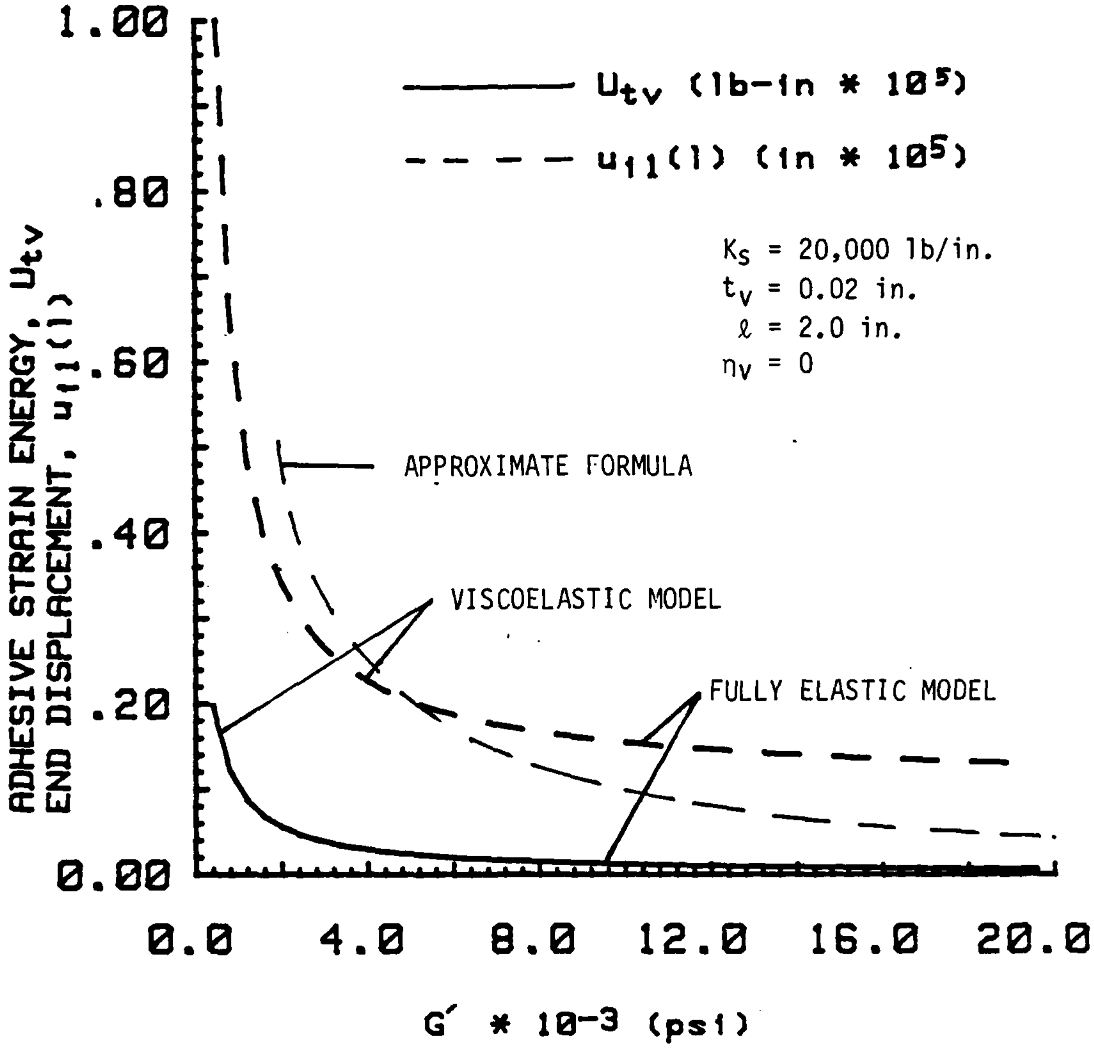

Figure C-8. Model Correlation of VEM Stiffness Effect - Stiff Elastic Strip

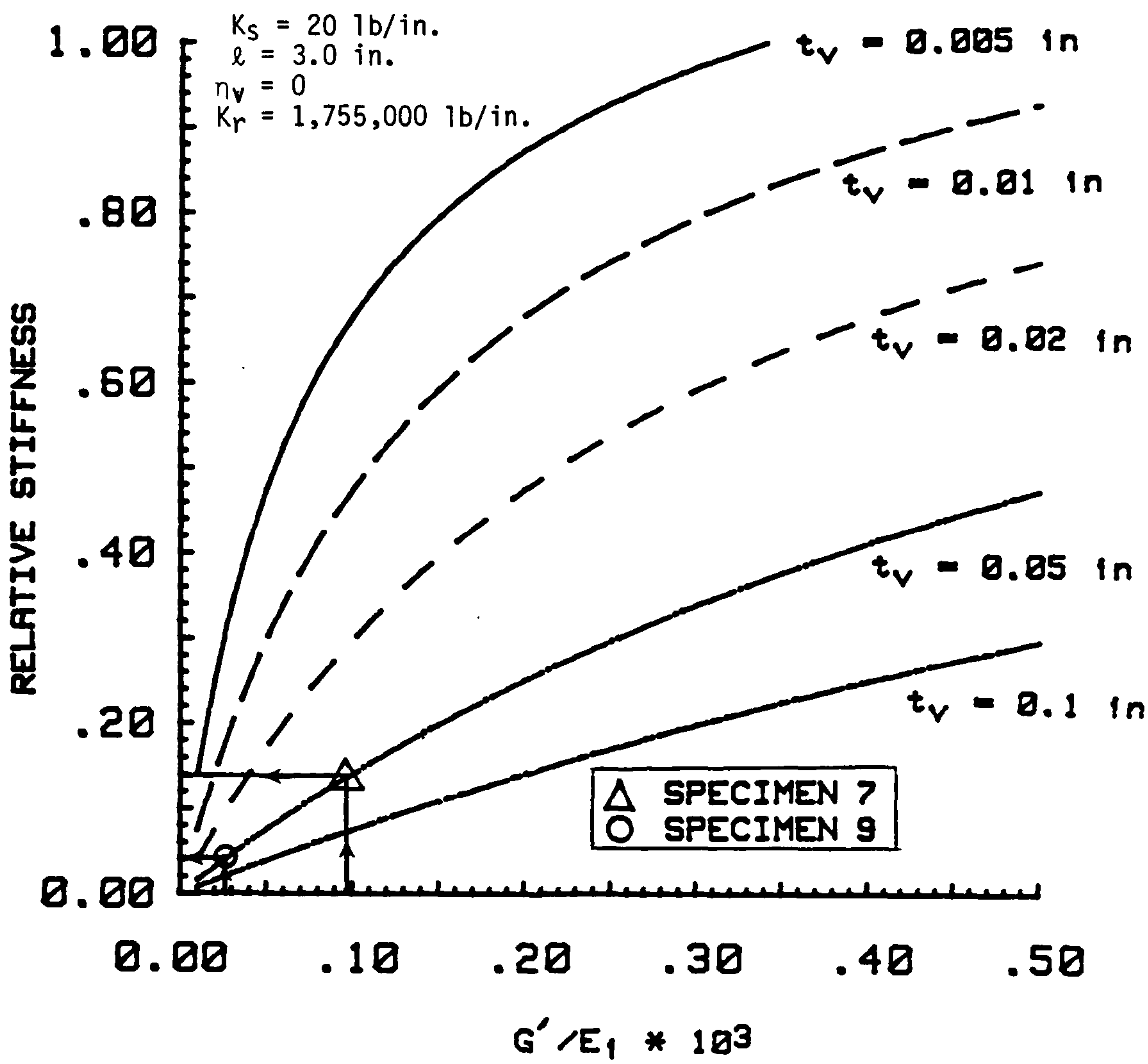

Figure C-9. Prediction of Joint Stiffness Test Data

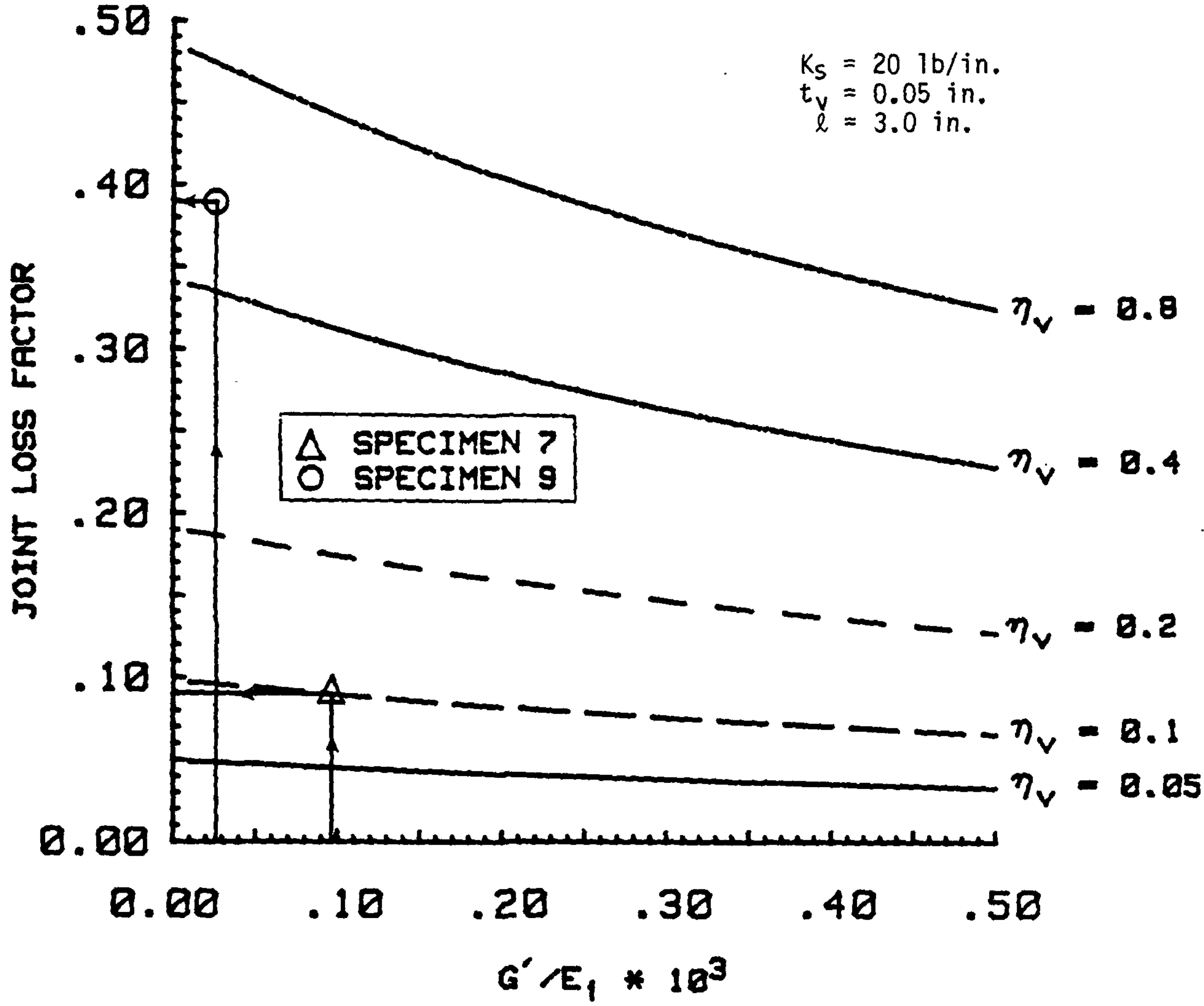

Figure C-10. Prediction of Joint Damping Test Data

Table C-1. Prediction of Joint Properties from Material Data

Specimen Number	Viscoelastic Material	Available Material Data [1]			Joint Stiffness (lb/in)		Joint Loss Factor	
		Source	G' (psi)	η_v	Predicted	Measured	Predicted	Measured
5	DYAD 606 Polyurethane	UDRI[2]	143	0.53	26,325	28,688	0.385	0.47
7	EA 9326 Polyurethane		1500	0.1-0.3	236,925	191,102	0.09	0.11
9	SMRD 100 F90 Epoxy	GE	399	0.57	70,200	77,908	0.39	0.31

(1) Based on information given in Ref. C-4

(2) University of Dayton Research Institute

identical in geometry and construction and essentially only differed in the material properties of their VEM adhesive layers. Each specimen had a VEM layer thickness of about 0.05 inch and none included a return-to-zero element in its configuration. These results illustrate how the analytical model can be used as a tool either in material qualification tests or correlation studies between data measured on joints and previously known properties of the corresponding viscoelastic materials.

Evaluation of Parametric Trends

The fully elastic model and the viscoelastic model have been exercised extensively to determine the basic component interrelationships that govern the behavior of the joint system. For the fully elastic model, parametric studies have been performed and reported previously in Appendix II of Ref. C-2. These results plotted the strain energy in the VEM layer and the deflection at the end of the inner adherend as a function of overlap length, VEM thickness, and VEM shear modulus for both stiff and soft return-to-zero elements. Similar trade studies were performed for the viscoelastic model and are reported in Ref. C-4. Those results plotted the relative stiffness and loss factor of the joint as a function of overlap length, VEM thickness, VEM shear modulus, VEM loss factor, and elastic element modulus. Also studied was the relative strain energy resident in the various components of the joint as a function of the above parameters.

The subsequent statements summarize the results of those trade studies.

- Since the VEM layers are the softest element of the joint, they usually contain most of its strain energy.

- The amount of damping loss in the joint is dependent on the amount of strain energy resident in the VEM layer.

- The VEM layer's share of strain energy decreases as the VEM shear modulus G increases, since more of the extensional deformation is transmitted through the VEM layers to the adherends.

- With a stiff return-to-zero elastic strip, most of the strain energy is in the strip when a soft VEM is used. The VEM's share of the strain energy increases as G increases to a certain optimum value, after which it decreases as the VEM becomes stiffer.

- The axial stiffness of the joint is greatly enhanced by selecting stiffer viscoelastic materials regardless of the stiffness of the return-to-zero element.

- The stiffness enhancement achieved by increasing G is greater than the associated reduction in the damping benefits.

- An increase in the VEM loss factor η_v yields a pronounced increase in the total damping performance and a reduction in the total elastic stiffness of the joint.

- Better trade-offs between the overall damping and stiffness performance of the joint result when stiffer VEMs are selected, provided that the loss factor of the stiff material is not much lower than that of the softer material.

- Good joint performance relies on having an appropriate matching between the stiffness levels of the VEM layer and the return-to-zero elastic strip.

- An increase of elastic element stiffness is associated with a strain energy transfer from the VEM layers to the elastic element. The rate of this transfer is higher for the softer viscoelastic materials.

- The increase of elastic element stiffness is associated with an overall stiffness enhancement and a reduction in the overall damping performance.

- For a constant width specimen, the overlap length is directly proportional to shear area and, therefore, associated with VEM stiffness. Increasing overlap length produces higher joint stiffness and slightly lower damping performance due to less deformation in the viscoelastic material.

- Thicker VEM layers have lower shear stiffness, and therefore yield lower joint stiffnesses. Total loss factor is unaffected by the VEM layer thickness t_v in the case of a soft return-to-zero element. It decreases asymptotically to zero as t_v increases in the case of a stiff return-to-zero element, since the VEM layers become insignificant in the load transfer process through the joint.

The numerical results that support the above statements have been plotted and more fully evaluated in Ref. C-4.

Damped Joint Design

The analytical models provide a relationship among the overall characteristics of a passively damped joint and the mechanical and geometrical properties of its individual components. This relationship may be represented in the form of design graphs, as shown previously in Figs. C-9 and C-10. By using such graphs, the designer can select quickly a basic joint configuration which fulfills his overall performance requirements. The two performance parameters considered in these figures are the overall axial stiffness for Fig. C-9 and the overall loss factor for Fig. C-10. The elastic shear modulus of the viscoelastic material has been selected as the abscissa. Fig. C-9 shows how the total axial stiffness of the joint can be predicted for various combinations of the shear modulus of the VEM layers and their dimensions. Since the material loss factor of the VEM does not affect the elastic stiffness of the joint, it is sufficient to draw such graphs only for $\eta_v=0$. Prediction of the total loss factor of the joint for various combinations of the VEM stiffness and loss factor is exemplified in Fig. C-10. Similar graphs can be drawn for different values of overlap length, VEM thickness, elastic element stiffness, and other parameters.

Other design graphs like those shown in Figs. C-11 and C-12 can be postulated to better display the relationships a particular designer is most interested in. Fig. C-11 demonstrates the joint stiffness enhancement that is achievable with only a minor reduction in the loss factor when a stiff VEM is selected. Fig. C-12 clearly shows the influence of an elastic element on the same performance parameters. The elastic element further enhances the stiffness but at the expense of the joint loss factor since the strain energy that would normally be carried by the VEM is now resident in the elastic strip. Similar

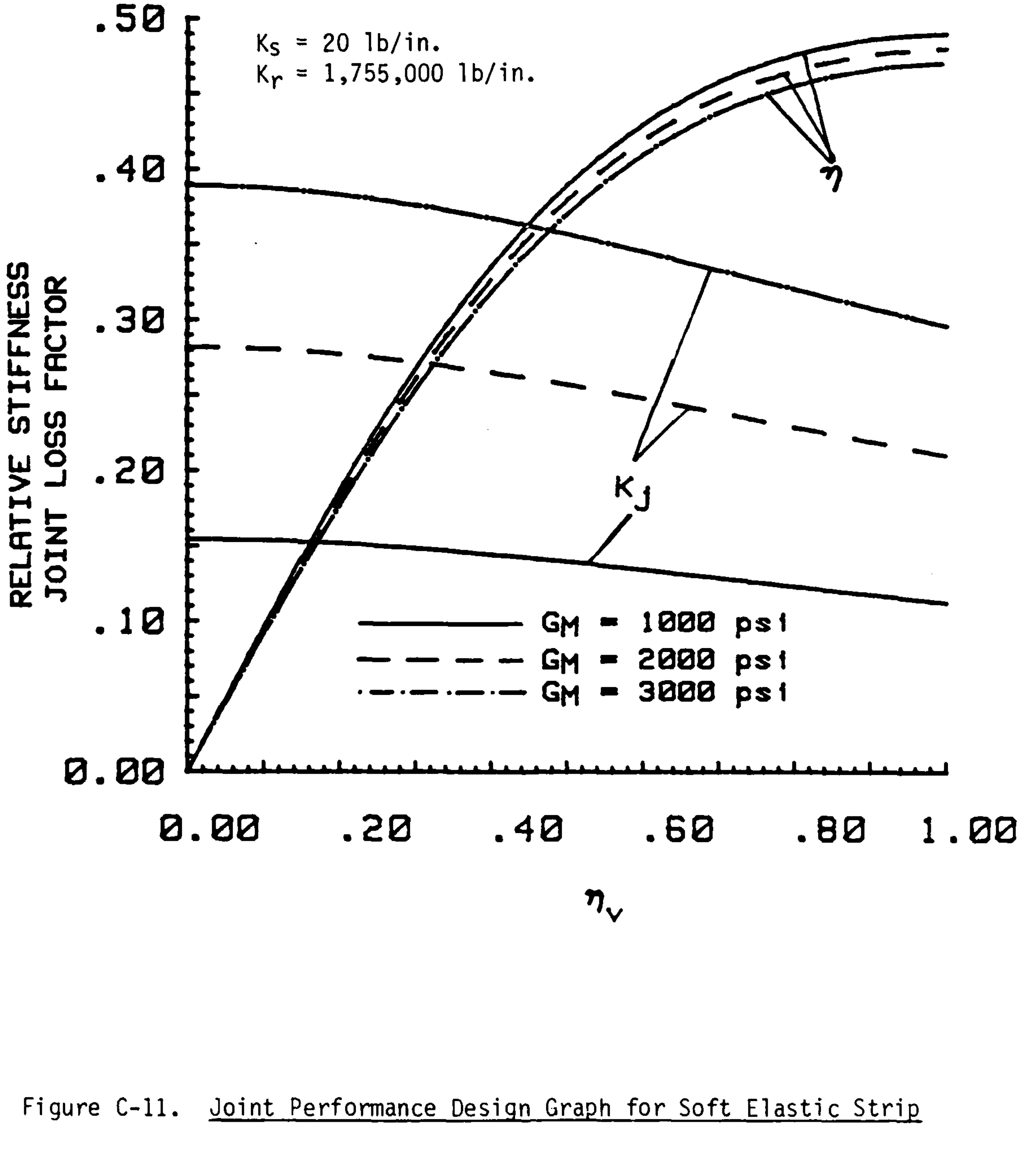

Figure C-11. Joint Performance Design Graph for Soft Elastic Strip

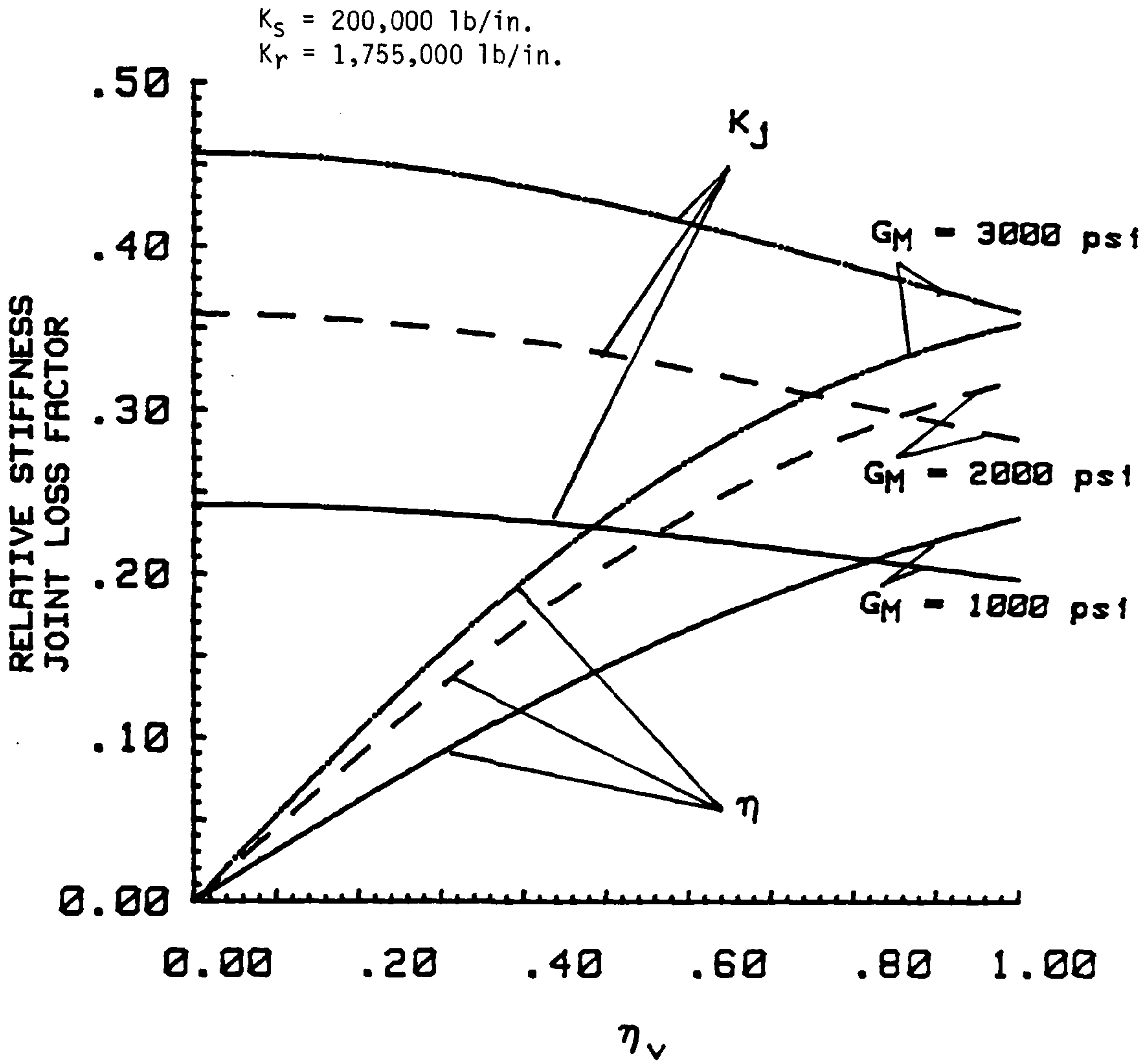

Figure C-12. Joint Performance Design Graph for Stiff Elastic Strip

curves plotted as a function of VEM thickness t_v rather than loss factor η_v indicate that the VEM layers should be as thin as possible, especially when return-to-zero elements are included in the joint.

In conclusion, the total stiffness of the joint system is determined by the stiffness and thickness of the VEM layers and the other structural components. The total loss factor of the joint is determined both by the material loss factor of the VEM and its share of the total strain energy. Good damping performance of a joint requires, therefore, not only the use of high loss factor viscoelastic materials but also proper structural design for effective interactions among its individual components.

References

C-1. L. J. Hart-Smith. Adhesive-Bonded Double-Lap Joints. NASA CR-112235, January 1973.

C-2. R. W. Trudell. Passively Damped Joints for Advanced Space Structures - Annual Technical Report. McDonnell Douglas AStronautics Co. report MDC H1178, June 1984.

C-3. R. W. Trudell, et al. Passively Damped Joints for Advanced Space Structures. Presented at the Vibration Damping Workshop, sponsored by AFFDL, February 1984, and published in the proceedings.

C-4. J. C. Prucz. Analytical and Experimental Methodology for Evaluating Passively Damped Structural Joints. Ph.D. Thesis submitted to Georgia Institute of Technology, May 1985.

Appendix D

EXPERIMENTAL PROGRAM

Introduction

Certain features of passively damped joints, like large vs. small motion effects, nonhomogeneity, significant frequency and temperature dependence of mechanical properties, impose an unusual variety of requirements on their experimental evaluation. Generic and accurate test results acquired over a wide and continuous range of expected frequencies and ambient temperatures are required when the properties of the overall structure are synthesized from those of its components.

Many experimental techniques have been developed in the past for the dynamic characterization of structural materials and components. However, none of the conventional approaches seem to fulfill all the test data requirements imposed by the various modeling approaches for passively damped joints. Therefore, two new test methods have been developed and demonstrated - a simplified, non-resonant forced vibration approach, and a stress pulse propagation approach. Additionally, a conventional hysteresis loop approach has been employed for comparative purposes. Each method has been presented previously in Refs. D-1 and D-2 and is briefly described here. The simplicity and reliability of the two new methods make them attractive for extended applications in the areas of material qualifications and structural characterizations. This multiple method approach not only enhances the statistical confidence in the results, but also provides a reliable data base for correlation between the various testing techniques. New and innovative data acquisition and reduction procedures, based on advanced digital instrumentation, have been utilized in this experimental program.

Since the primary candidates for large space structures are repetitive lattice trusses, the main loading direction considered in the design and testing of the passively damped joint specimens, shown in Fig. D-1, is the axial one. The tests are limited to the 0.1-100 Hz frequency range and low strain levels, which are expected to be dominant in these structures. Both room temperature and environmental testing over a temperature range of -50°F to 200°F were included in the program.

NOTES

1 DIMENSIONS GIVEN IN INCHES

2 ABBREVIATIONS: VEM - VISCOELASTIC MATERIAL

GR/EP - GRAPHITE EPOXY

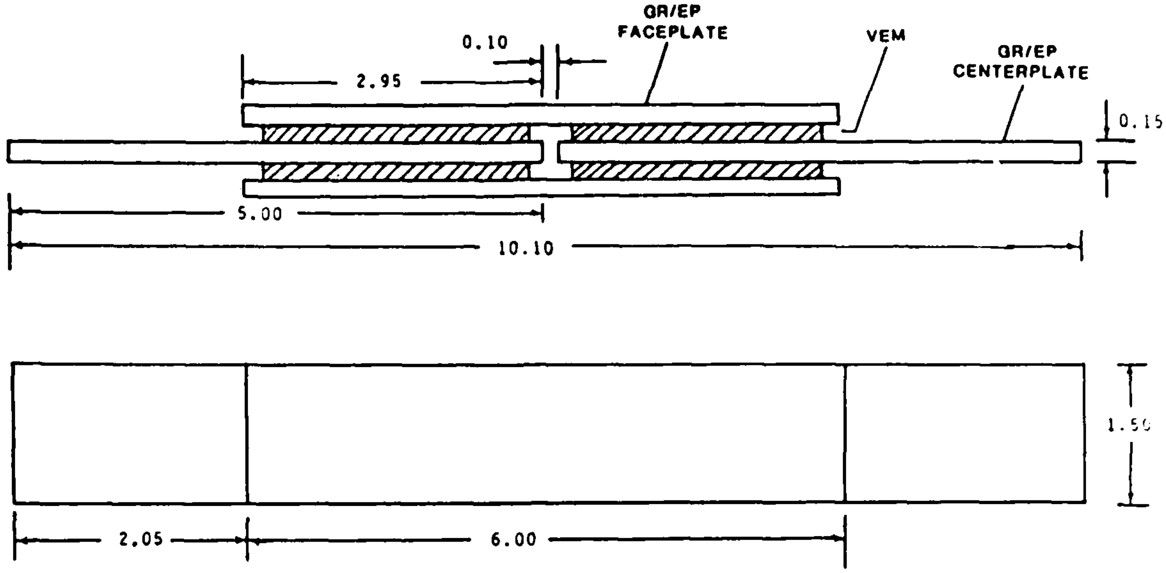

Figure D-1a. Passively Damped Joint Specimen Without Elastic Link Between Members

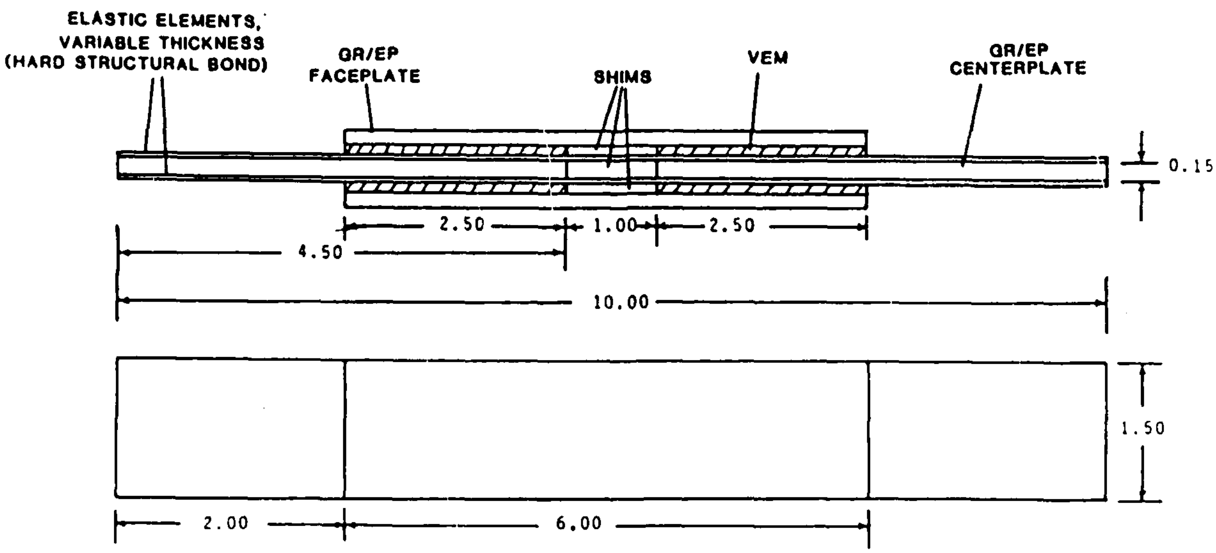

Figure D-1b. Passively Damped Joint Specimen With Elastic Elements

The following topics will be discussed in this appendix:

a) Comparison of Experimental Methods

b) Transducer and Facility Development Problems

c) Room Temperature Results

d) High and Low Temperature Results

Comparison of Experimental Methods

The experimental setup used for the hysteresis-loop technique is shown in Fig. D-2. The specimen is mounted vertically in an Instron Universal Testing Machine and a cyclic axial load is applied to it by the moving crosshead of the machine. A strain gage load cell built into the opposing crosshead measures the resultant load on the specimen. The relative axial displacement between the edges of the joint section of the specimen is measured by a linear variable differential transformer (LVDT) extensometer. The stiffness and damping characteristics of the joint can be extracted from the resulting force vs. deflection curve.

The advantages of the hysteresis loop approach are that it is very simple to implement using commonly available physical testing machines, it is not restricted to linear or homogeneous systems, and it is capable of measuring very low levels of material damping as would be expected from metals. The disadvantages of the method are that it is limited to very low loading frequencies and great care must be taken to properly include specimen/fixture interaction effects in the analysis if generic test data is to be obtained.

The experimental setup used for the simplified steady state method is shown in Fig. D-3. A special test fixture and piezoelectric displacement transducer have been developed to implement this approach. Since the fixture was used for the low temperature testing, where corrosive liquid nitrogen was employed as a cryogenic agent, it was made of AISI 304 stainless steel. Three major considerations guided the design of the fixture:

1. Geometric compatibility with the BLUE M environmental chamber, Model No. LN-270C-1, whose inside dimensions are 25 x 20 x 20 inches.

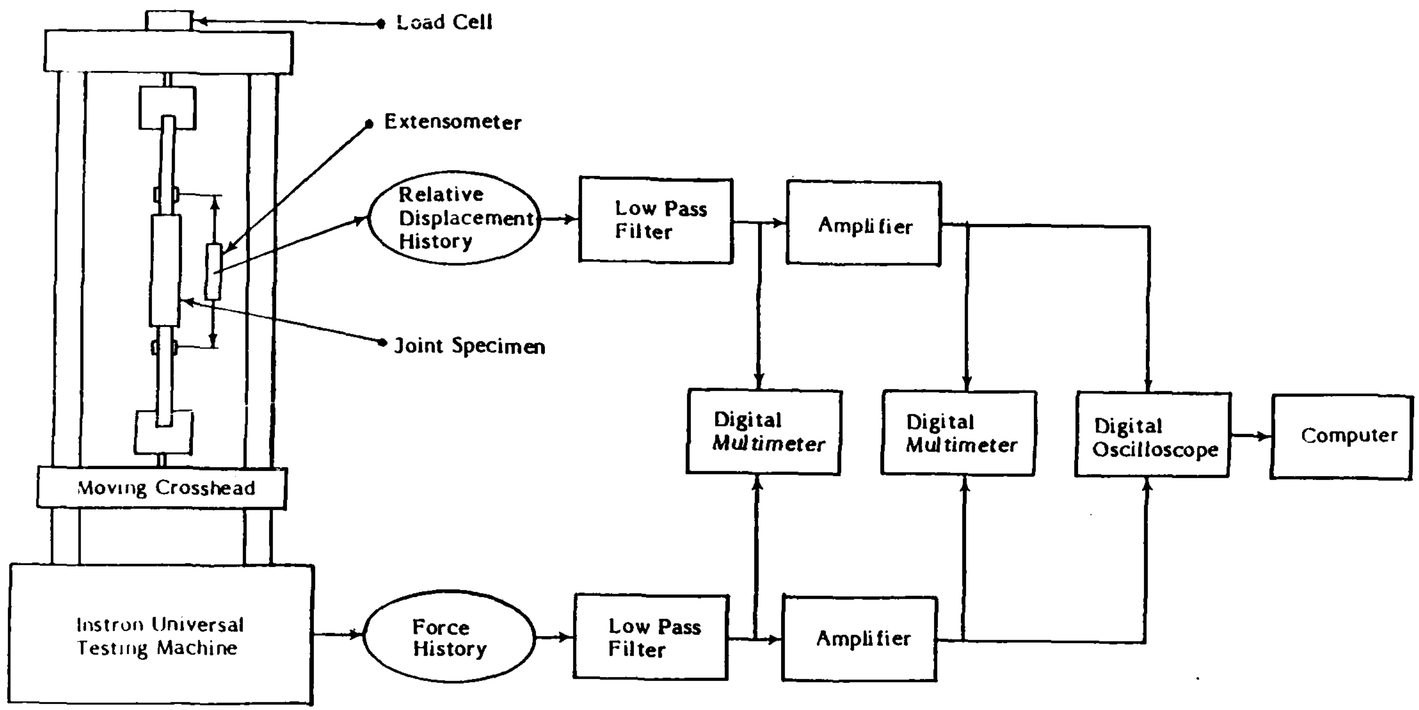

Figure D-2. Experimental Setup for the Hysteresis Loop Approach

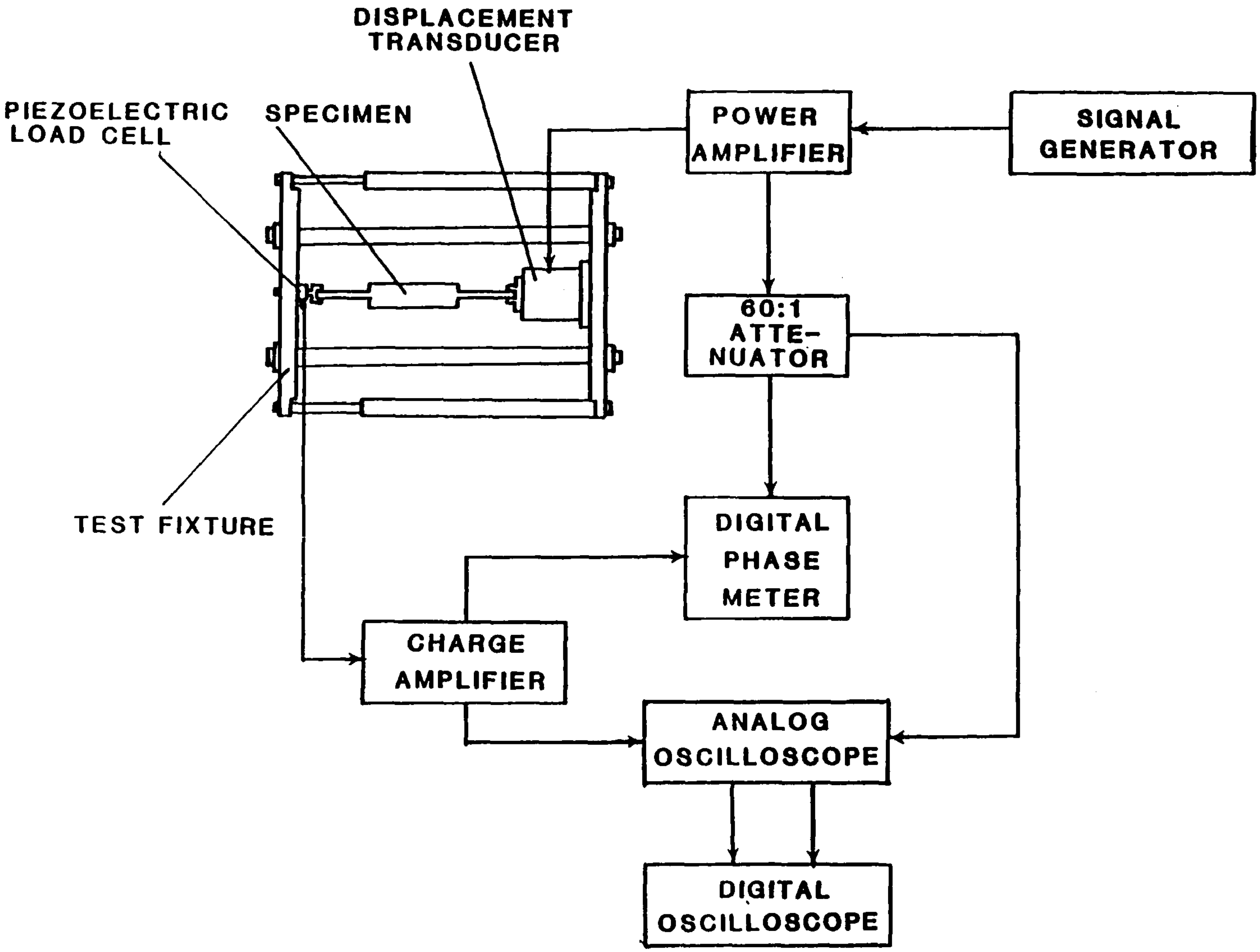

Figure D-3. Experimental Setup for the Simplified Steady State Approach

2. Maximum versatility, such that the fixture can accommodate specimens of different lengths and can be used without major changes for the two primary testing techniques: the pulse propagation approach and the simplified steady state approach.

3. Maximum possible stiffness within reasonable weight limits. The upper weight limit has been chosen to be about 80-85 lbs, so that two people can handle the assembled fixture.

The major requirement of the piezoelectric transducer, developed by Wilcoxon Research, Inc., was to provide a displacement output proportional to a voltage input for dynamic excitation of specimens from 0.1 to 100 Hz. Problems encountered with the design of this transducer are discussed in the next section.

The simplified steady state method is, like the hysteresis loop approach, another nonresonant test technique. The advantage of this method over resonant techniques is that it provides data over the continuous frequency spectrum, not just at a few specific frequencies. Its advantage over the hysteresis loop approach is that it is not limited to the low frequencies usually associated with physical test machines. The primary advantage of this method over conventional nonresonant techniques is that a relative displacement measurement across the joint is not required; only vectors of the applied voltage and the measured force are required. This is a very attractive feature considering the inherent high stiffness, low displacement of joints envisioned for large space structures. Again, the major disadvantage is that to get good generic data the specimen/fixture interactions must be accounted for precisely.

A new sine pulse propagation technique has been developed to provide generic joint damping and stiffness data free of specimen/fixture interaction effects. A sine-pulse of the desired frequency is applied at one end of the specimen and the corresponding longitudinal response is measured at two fixed locations, before and after the joint section. The damping information is extracted from the changes that occur in certain characteristics of this stress wave as a result of its passage through the joint.

No custom-built test fixture or exciter are needed for application of the sine-pulse propagation method. Nevertheless, the facilities developed for the

simplified steady state technique have been used also for the transient tests in order to facilitate data correlation between the two methods. The corresponding experimental setup is shown in Fig. D-4. The voltage signal applied to the piezoelectric exciter is supplied and amplified by the same equipment as in the simplified steady state tests, but the continuous sine wave generated by the function generator is now gated to the desired pulse length. All the excitation pulses used in the tests contain just one full cycle. The stiffness and damping properties of the test specimen are determined by comparing the response signals from two identical PCB piezoelectric load cells mounted at its ends.

The sine-pulse method, like the hysteresis loop and steady state methods, does not require the specimen to be linear and homogeneous. Its major advantage over these methods is that it does not require any knowledge of the fixture's characteristics. Its advantage over other pulse propagation methods is that it is not restricted to the high rates of loading that result from the axial impact type of excitation usually associated with these methods - the frequency of the input sine wave can be precisely prescribed.

A detailed discussion of the data reduction procedures that accompany the hysteresis loop, simplified steady state, and sine pulse methods is presented in Appendix E.

Transducer and Facility Development Problems

The design requirements set forth to Wilcoxon Research for development of the piezoelectric motion transducer are listed in Table D-1. The transducer, as initially delivered in the Fall of 1983, did not meet the linearity criterion by a substantial amount. An investigation revealed that the vendor had used a piezoelectric material with good temperature stability without regard to its voltage/ displacement characteristics. The transducer was reworked and the problem corrected by the vendor at his own expense. Wilcoxon shipped the reworked transducer to GIT in June 1984.

At GIT an accelerometer was cemented to the transducer face to conduct acceptance and calibration tests. Two problems were encountered during this checkout activity - distortion in the output signal and rising sensitivity at frequencies below 100 Hz. The transducer was returned to the manufacturer

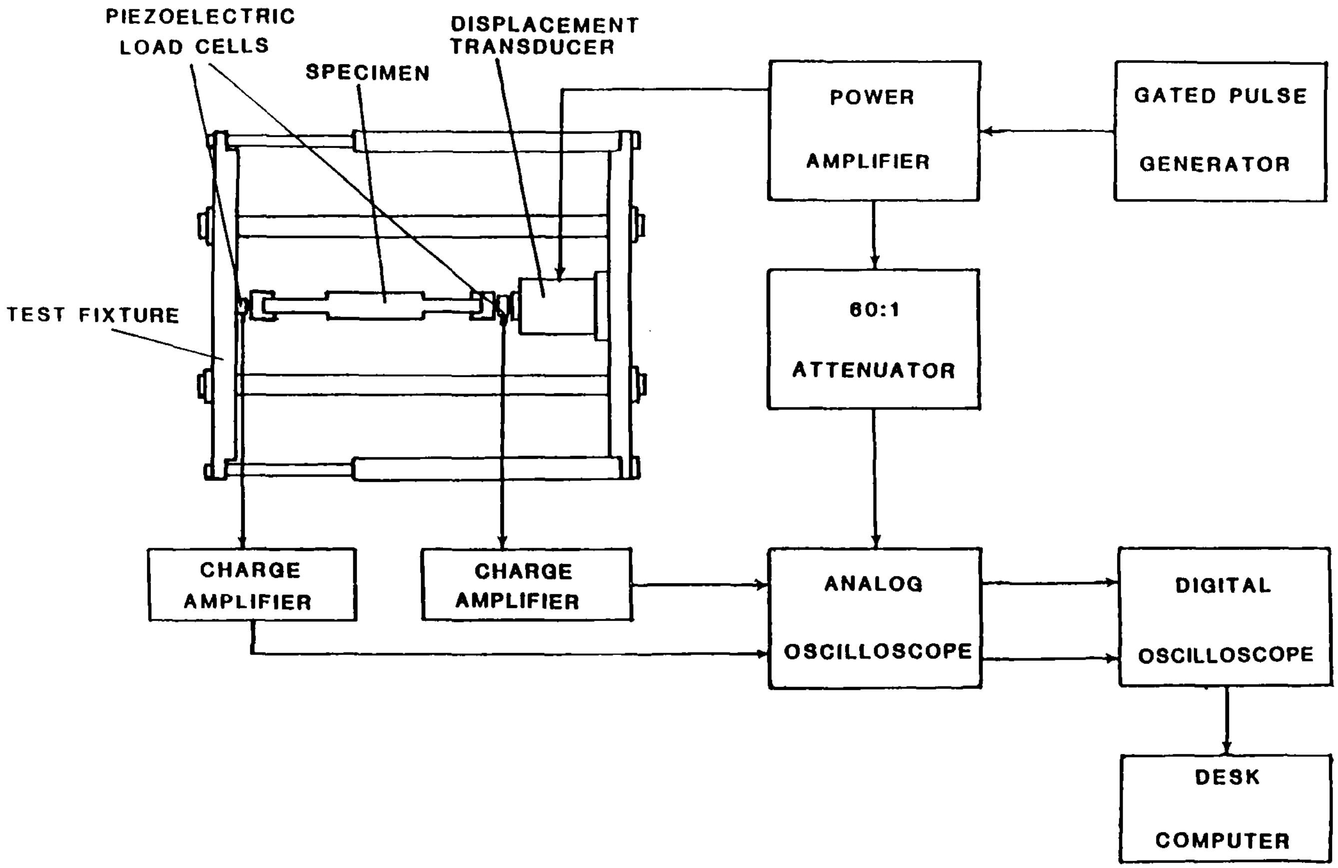

Figure D-4. Experimental Setup for the Sine-Pulse Propagation Approach

Table D-1. Piezoelectric Motion Transducer Requirements

Output motion	±100 μin. (minimum)
Sensitivity	>0.3 μin./volt (goal) at 20°C
Linearity	1% of B.S.L. (10-100 μin.)
Hysteresis	1% loss factor maximum at ≥1 μin.
Operating temperature range	-320 to +400°F
Stiffness	>2 x 10^6 lb/in. (>5 x 10^6 lb/in. desired)
Physical size limits	<3" diameter x 4" long
Operating frequency range	0.1 to 100 Hz

for evaluation. The first problem was largely caused by the digital function generator used by GIT to generate sine waves. The digital function generator numerically approximated a sine wave using a series of tiny "stairsteps." The effective double differentiation of this approximated output signal by the accelerometer resulted in the distortion. The second problem was caused by radial strain of the exciter crystal being transmitted to the accelerometer cemented to the transducer's face. The distorted output caused by induced case strain in the piezoelectric accelerometer erroneously suggested a transducer sensitivity variation where none really existed.

During room temperature testing of several joint specimens at GIT, a load dependency of the transducer's internal stiffness was discovered. Apparently some additional flexibility exists in the transducer's internal components, possibly caused by a warpage of the face due to single point preloading of the piezoelectric crystal stack. Subsequent testing of the transducer at MDAC-HB established the existence of some stiffness nonlinearity. The piezoelectric material itself is not suspect, but the mechanical construction of the transducer is believed to be the cause of the problem. Some degree of nonlinearity, by itself, is not particularly devastating. As long as the stiffness of the instrument at the given operating point of the experiment is known, the simplified steady state method will produce correct results. Details of how the piezoelectric displacement transducer functions, the physical laws that govern its behavior, and the results of initial calibration tests are given in Appendix G.

Testing was further delayed in the Spring of 1985 by facility modifications at GIT. These modifications were required to safely vent out of the laboratory area the nitrogen used to cool the environmental chamber during low temperature testing. Additional delays were encountered in the Fall of 1985 during the environmental testing when a temperature dependency of the transducer's stiffness was discovered. Again, the temperature dependency, like the load dependency, does not affect the reliability of the simplified steady state method as long as the transducer's stiffness at the operating point of the experiment is known.

Room Temperature Results

In all, 21 test specimens were made. A pair of specimens was fabricated for each of the seven selected VEMs (specimens 1-12 and 20-21). Five specimens (15-19) contained elastic elements and two specimens (13 and 14) were used to obtain reference data. Preliminary hysteresis testing indicated there were no significant differences between specimens of similar VEM and construction. Therefore, only about half of the specimens were rigorously tested, as indicated in Table D-2. For the room temperature tests, all three test methods were employed - hysteresis, steady state, and sine pulse. Detailed test results for each of these methods is provided in Appendix F in tabular form. Graphs summarizing the data are presented in this section.

The hysteresis test data provide a representative picture of the damping and stiffness properties of the passively damped joints at very low frequencies. They enable both a comparative evaluation between the different design configurations and an illustration of typical performance characteristics of passively damped joints as compared with a reference homogeneous specimen (Specimen 13 in Table D-2). The results presented in Appendix F correspond to three motion speeds of the Instron's crosshead - 0.05 in/sec, 0.1 in/sec and 0.2 in/sec. The interpretation of these results for practical applications is facilitated by considering their relative values with respect to the reference specimen, as shown in Table D-3. The "damping benefit" is the ratio between the loss factor of the joint and that of the reference specimen, whereas the "stiffness penalty" is calculated as the ratio between the stiffness of the reference specimen and that of the joint. A combined parameter, which is labeled "merit factor," can be defined as follows:

$$Mf = \frac{\eta_j K_j}{\eta_r K_r}$$

where η_j = loss factor of joint

K_j = stiffness of joint

η_r = loss factor of reference

K_r = stiffness of reference

Table D-2. Joint Test Specimens

Specimen Number	Viscoelastic Material Manufact.	Name	Chemical Base	Thickness of Adhesive Layer (in.)	Testing Performed[1] Room Temp. HL	SSS	SPP	Environmental SSS
1	3M	ISD 110	Acrylic	0.0062	X	X		X
2	3M	ISD 110	Acrylic	0.0051	X			
3	3M	EC 246	Epoxy	0.1260	X	X	X	X
4	3M	EC 246	Epoxy	0.1270	X			
5	Soundcoat	DYAD 606	Polyurethane	0.0515	X	X		X
6	Soundcoat	DYAD 606	Polyurethane	0.0515	X			
7	Hysol	EA 9326	Polyurethane	0.0480	X	X		
8	Hysol	EA 9326	Polyurethane	0.0505	X			
9	GE	SMRD 100F90	Epoxy	0.0580	X	X		X
10	GE	SMRD 100F90	Epoxy	0.0580	X			
11	GE	RTV 630	Silicone	0.0073	X	X		X
12	GE	RTV 630	Silicone	0.0063	X			
13[2]	---	GR/EP Bar, Solid		---	X	X		X
14[3]	---	EA956	Epoxy	0.0220		X		
15[4]	3M	EC 2216	Epoxy	0.0573	X	X	X	X
16[4]	3M	EC 2216	Epoxy	0.0582	X	X		
17[4]	3M	EC 2216	Epoxy	0.0615	X			
18[4]	Soundcoat	DYAD 606	Polyurethane	0.0249	X	X		X
19[4]	Soundcoat	DYAD 606	Polyurethane	0.0249	X			
20	MDAC	Rubber/Plastic Alloy		0.0504	X			
21	MDAC	Rubber/Plastic Alloy		0.0499	X	X		X

NOTES

(1) HL = Hysteresis Loop
SSS = Simplified Steady State
SPP = Sine Pulse Propagation

(2) Reference GR/EP Laminate

(3) Standard Bonded Joint with Elastic Adhesive

(4) Includes Fiberglass Strips for Elastic Elements

AD-A174 914 PASSIVELY DAMPED JOINTS FOR ADVANCED SPACE STRUCTURES 2/2
(U) MCDONNELL DOUGLAS ASTRONAUTICS CO HUNTINGTON BEACH
CA J H PEEBLES ET AL. 28 MAR 86 MDC-H2334
UNCLASSIFIED AFOSR-TR-86-2075 F49620-83-C-0117 F/G 22/2 NL

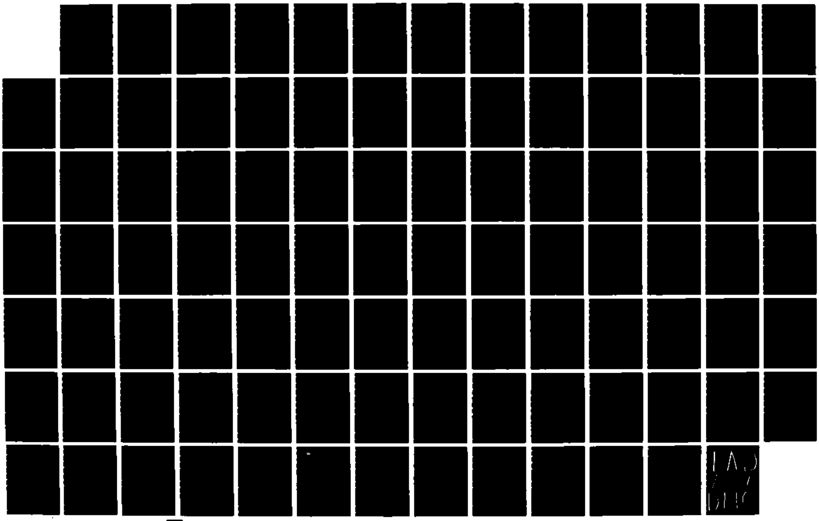

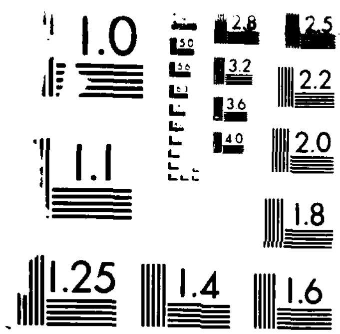

RESOLUTION TEST CHART

Table D-3. Relative* Performance Parameters of Passively Damped Joints

Specimen Number	VEM Name	Damping Benefit	Stiffness Penalty	Merit Factor
1	ISD 110	15.983	67.246	0.238
3	EC 2216	12.783	2.652	4.820
5	DYAD 606	7.910	27.468	0.288
7	EA 9326	0.924	2.460	0.376
9	SMRD 100F90	2.783	6.858	0.406
11	RTV 630	0.828	11.178	0.074
15**	EC 2216	4.583	1.084	4.228
18**	DYAD 606	4.394	1.624	2.706
21	Rubber/Plastic Alloy	8.338	10.487	0.795

*With respect to the reference specimen data given in Table F-1 of Appendix F.

**Includes elastic element.

Because the specimens are all the same size, it can be interpreted as the damping benefit that is achievable with a given design configuration per unit value of stiffness penalty. Note that the stiffness of the joints could be improved by reducing the VEM layer thickness when feasible.

Of the joints tested, only specimens 3, 15 and 18 had a merit factor higher than 1.0. Specimens 3 and 15 used the EC 2216 viscoelastic material as adhesive layers, whereas specimen 18 used DYAD 606. The elastic glass fiber elements included in specimen 15 and a reduction in VEM layer thickness reduce the stiffness penalty to less than half the stiffness penalty of specimen 3, but at the cost of an even higher reduction in the damping benefit. A similar addition of elastic glass fiber elements to specimen 18, along with a 50% reduction in VEM layer thickness, reduce the stiffness penalty to less than 6% of that achieved by specimen 5 while only reducing the damping benefit by 42%. Clearly, the addition of stiffening elastic elements to the joints is beneficial. The results of specimen 18 demonstrate that an initially poor performing joint (specimen 5) can be transformed into a high performer by the inclusion of return-to-zero features.

The ISD 110 viscoelastic material used in specimen 1 provides the highest damping enhancement but its merit factor is low because of the serious reduction in stiffness. A thinner bond line is probably not practical in this case. The other materials do not display good damping-stiffness tradeoffs at these low frequencies either because of poor damping performance, like that of EA 9326 and RTV 630, or high stiffness penalty, like that associated with DYAD 606. However, the DYAD 606 and the rubber/plastic alloy could possibly be cast in thinner layers to minimize the stiffness reduction.

The frequency effect on the damping and stiffness characteristics of selected specimens is shown in Figs. D-5 and D-6, respectively. These figures are based on test data generated by the simplified steady state approach since it is more closely related to conventional measurement and interpretation concepts. A least-square fitting routine is used for drawing the "best fit" line between the data points of the same specimen. Four representative specimens of passively damped joints have been selected for these figures along with the standard elastic joint (specimen 14). Specimens 1 and 3 represent, respectively, the behavioral pattern associated with soft and stiff viscoelastic

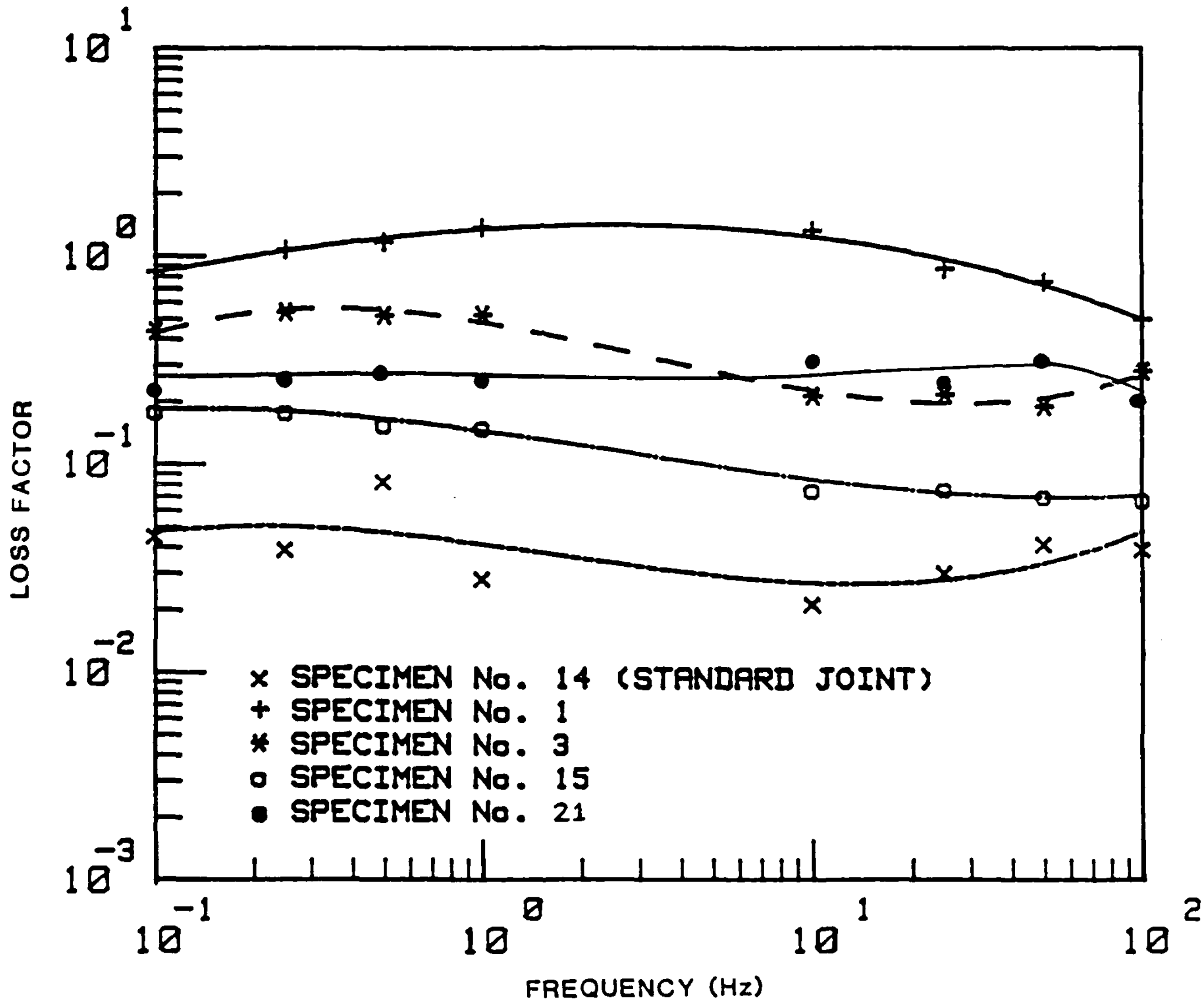

Figure D-5. Frequency Effect on Loss Factor of Joint Specimens

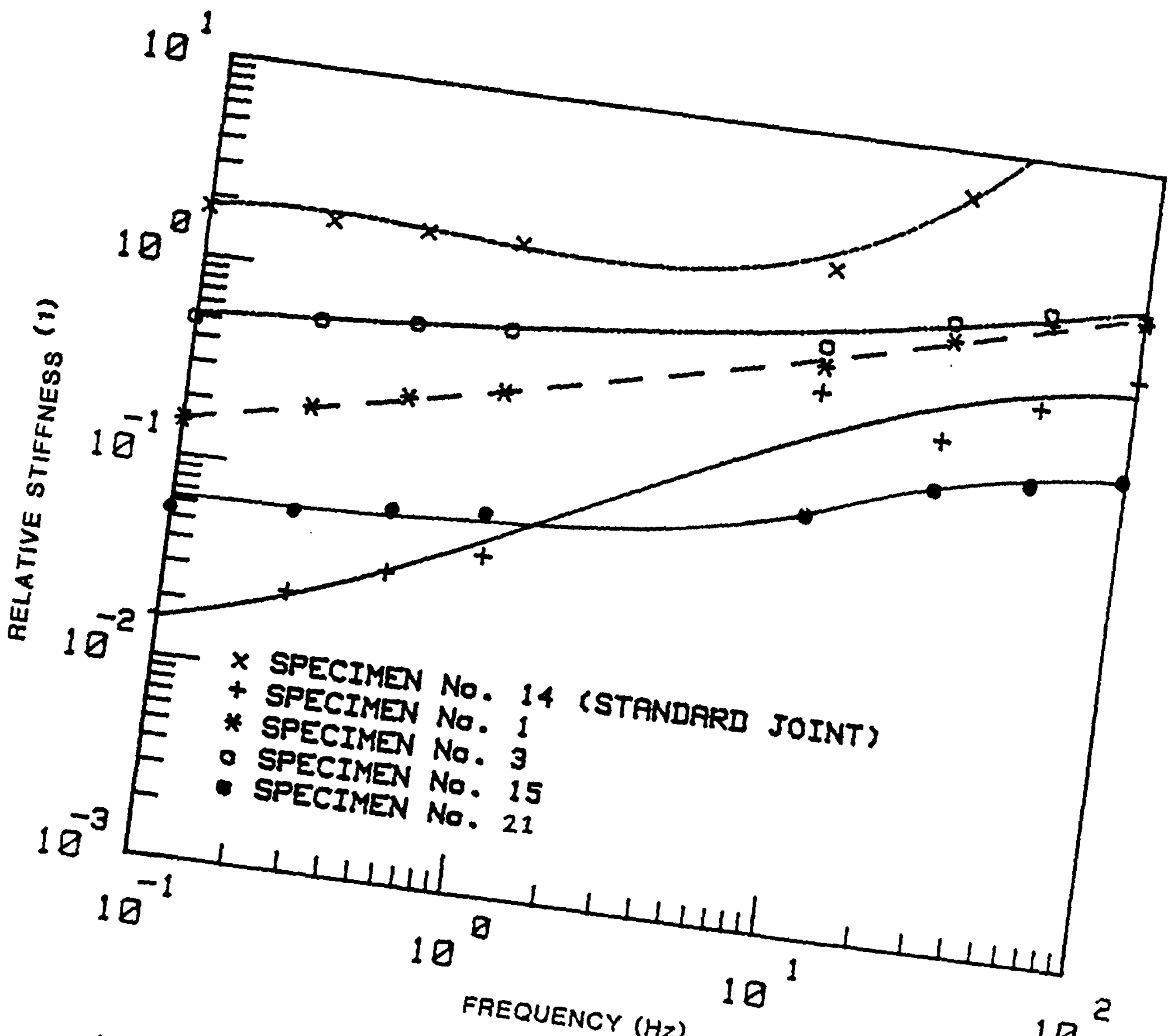

(1) - THE REFERENCE STIFFNESS IS 1,024,902 N/cm (585,000 lb/in)

Figure D-6. <u>Frequency Effect on Axial Stiffness of Joint Specimens</u>

materials. The comparison between specimens 3 and 15 illustrates the effect of the elastic glass fiber strips on the performance of a passively damped joint with stiff viscoelastic layers. The data for specimen 21 indicates the performance of the new rubber plastic alloy material developed by MOAC.

It should be emphasized that the damping data in Fig. D-5 are expressed in terms of the measured loss factor of the joint rather than the material loss factor of the viscoelastic layers. The damping characteristics of soft joints, like specimen 1, are dominated by those of the viscoelastic materials, but as these materials become stiffer the joint loss factor is reduced from the damping material loss factor since the viscoelastic layers share less of the total strain energy stored in the joint (Ref. D-3). Therefore, the trend displayed in Fig. D-6 showing the stiffness increasing with frequency consequently may yield a reduction in the damping performance of the joint at higher frequencies even for a viscoelastic material with a relatively flat loss factor-frequency behavior. The smaller stiffness penalties at frequencies above 10 Hz will improve significantly the merit factors given in Table D-3, especially for the softer materials like the ISD 110 used in specimen 1. The stiffness of specimen 3 approaches that of specimen 15 at the higher frequencies, so the glass fiber link is ineffective in this frequency range. Moreover, it seems to provide undesirable consequences, as the loss factor of specimen 15 is significantly lower than that of specimen 3 over the whole test frequency range. These results strengthen the conclusion derived in Appendix C and Ref. D-1 regarding the importance of appropriate matching between the stiffness levels of the elastic link and the VEM layers. The use of a lower stiffness elastic link in specimen 15 probably would have improved its stiffness-damping performance.

The validity of the three testing approaches adopted for this research program can be assessed by comparing the performance data versus frequency that each method produces. Figs. D-7 and D-8 illustrate the data correlation between the test methods for specimens 3 and 15, respectively.

In Figs. D-7a and D-8a the damping efficiency for the sine pulse method and the loss factor for the hysteresis and steady state methods are plotted versus frequency. The "damping efficiency" parameter provides a general measure of damping, which is not restricted to oscillatory loading like the commonly used

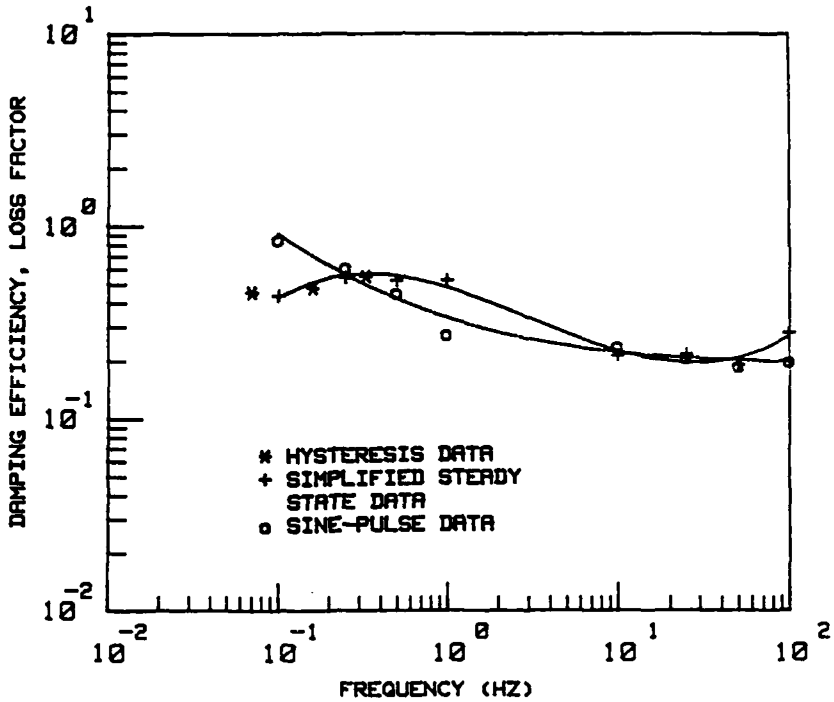

Figure D-7a. Damping Data Correlation for Specimen No. 3

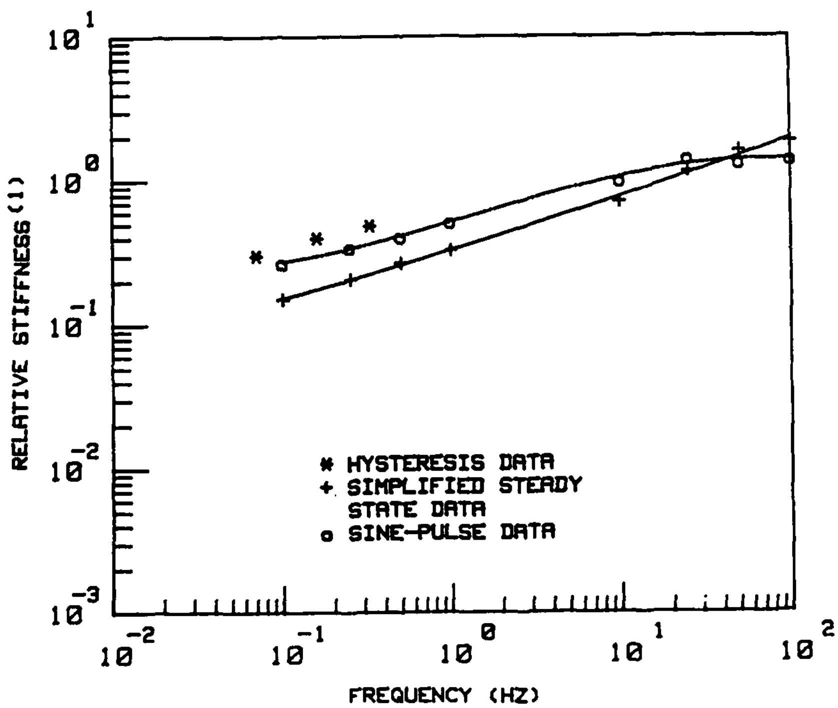

(1) - REFERENCE STIFFNESS EQUAL TO 1,024,902 N/cm (585,000 lb/in)

Figure D-7b. Stiffness Data Correlation for Specimen No. 3

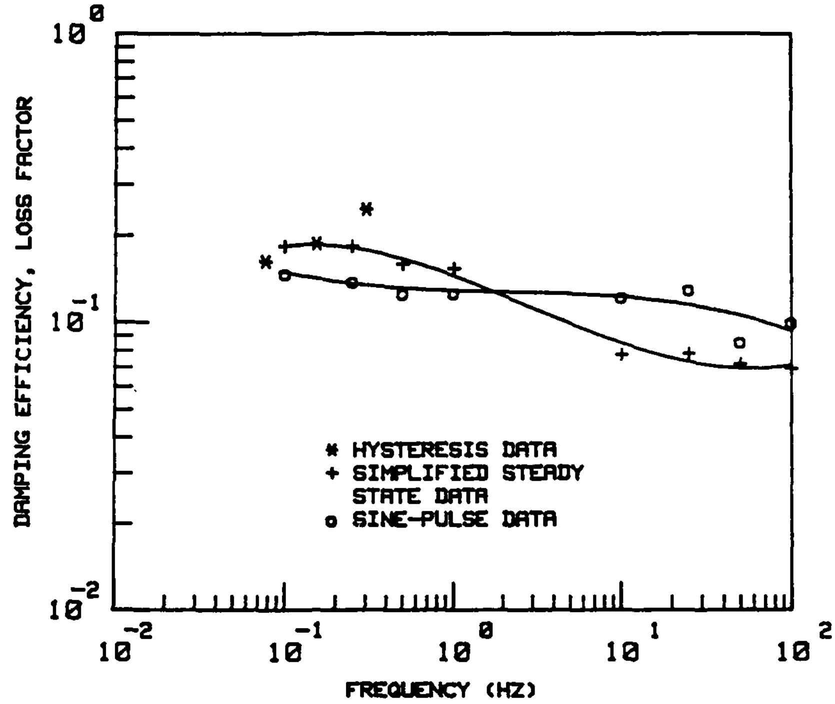

Figure D-8a. Damping Data Correlation for Specimen No. 15

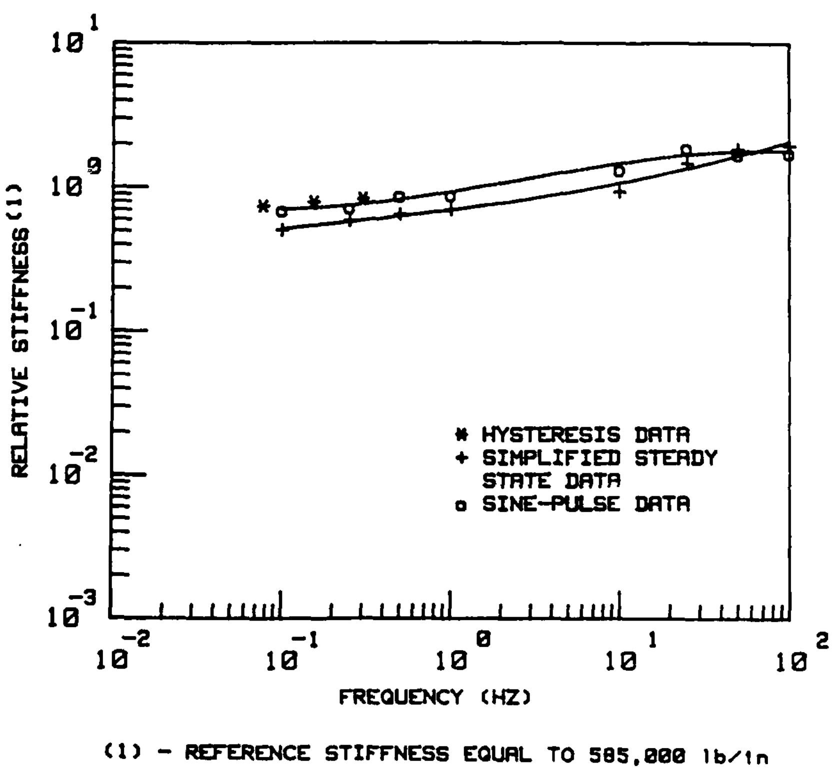

Figure D-8b. Stiffness Data Correlation for Specimen No. 15

"loss factor" parameter. These parameters have been defined in Appendix E. These figures show that the numerical values and the general trends described by the damping efficiency and loss parameters are relatively close, although they are generated by different testing and analysis techniques. While the sine-pulse and simplified steady state techniques predict a decrease in damping performance with frequency, the hysteresis loop method yields higher loss factors at higher frequencies. This is probably due to the effect of energy losses through the test fixture since the elasticity of the testing machine is not accounted for in the hysteresis loop analysis.

Figs. D-7b and D-8b show good stiffness correlation between the various methods. The lower stiffness values yielded by the simplified steady state technique in the 0.1-1 Hz frequency range indicate that the unloaded sensitivity of the piezoelectric displacement transducer may be slightly lower than the average value extrapolated to this range from test data measured at 10 Hz (refer to Appendix G for transducer characteristics).

Figs. D-7 and D-8 have demonstrated good agreement between the various test methods and low scatter within each method. The low scatter is particularly remarkable compared with existing damping property data.

High and Low Temperature Results

Nine specimens (identified in Table D-2) were tested at low and elevated temperatures. Data were obtained at four temperatures, -50, 25, 75 and 200°F, and also at four frequencies, .25, 1.0, 25.0, and 100.0 Hz using the simplified steady state method. The steady state method was selected for these tests because of its simplicity, the output was more directly related to conventional measures of damping, and the test setup fit within the Blue M environmental chamber at GIT.

As indicated in the equations presented in Appendix E, the simplified steady state method requires the accurate determination of the test fixture's stiffness if it is not infinite relative to the specimen's stiffness. The test fixture's equivalent compliance, C, is a calibration term that corrects for the stiffness contributions of the test fixture, motion transducer, and load cell. This factor is both frequency and temperature dependent. In order to obtain accurate results, precise determination of C at each temperature and

frequency is essential. An aluminum bar equal in length to specimen 1, with a known axial stiffness of 225,000 lb/in, was mounted in the test fixture and used to evaluate the temperature/frequency dependency of C. Two assumptions were made: (1) the stiffness of the bar is constant over the temperature range of interest, and (2) no losses occur in the solid aluiminum bar (zero phase shift). Using these assumptions and the equation for the storage modulus (real part of K_s) presented in Appendix E, the values for C were experimentally determined and are given in Table D-4.

With the proper fixture calibration values determined, the joint specimens were tested at the prescribed temperature and frequency conditions. Figs. D-9 and D-10 show some existing damping properties for the viscoelastic materials used in specimens 3 and 9, respectively. Comparing these loss factor curves with the experimental results for specimens 3 and 9 in Figs. D-12 and D-14 shows a good correlation between the expected results and the experimental data.

For most of the specimens tested (see Figs. D-11 to D-19) the loss factor peaked at approximately room temperature and dropped sharply at the low and high temperatures. This behavior was expected since most of the viscoelastic materials were designed to perform best at room temperature. However, the rubber/plastic alloy employed in specimen 21 demonstrated the smallest temperature and frequency dependence (see Fig. D-19). This material was specially blended using several damping materials having different glass transition points, thus creating a material with moderate damping over a broad temperature range.

Examination of the loss factor dependence on frequency also agrees generally with the expected trends. At low temperatures, the loss factor decreased as frequency increased. At high temperatures, the loss factor increased as frequency increased.

Because of some inconsistencies encountered when trying to gather data at low temperature using the simplified steady state method, an error analysis was performed to assess the sensitivity of the governing equations to variations in the measured inputs and outputs. Differentiation of the basic loss factor equation $\eta = [\cos \phi - (A/B)\ C]/\sin \phi$ with respect to the measured output

Table D-4. Test Fixture Equivalent Compliance Values
C (in/lb x 10^6)

Temp. (°F)	Frequency (Hz) 0.25	1.0	25.0	100.0
-50	1.83926	1.76644	0.98428	0.68993
25	1.96639	1.97014	1.21924	0.91579
75	2.53239	2.56789	1.79701	1.45514
200	4.49586	4.86958	3.93724	3.78987

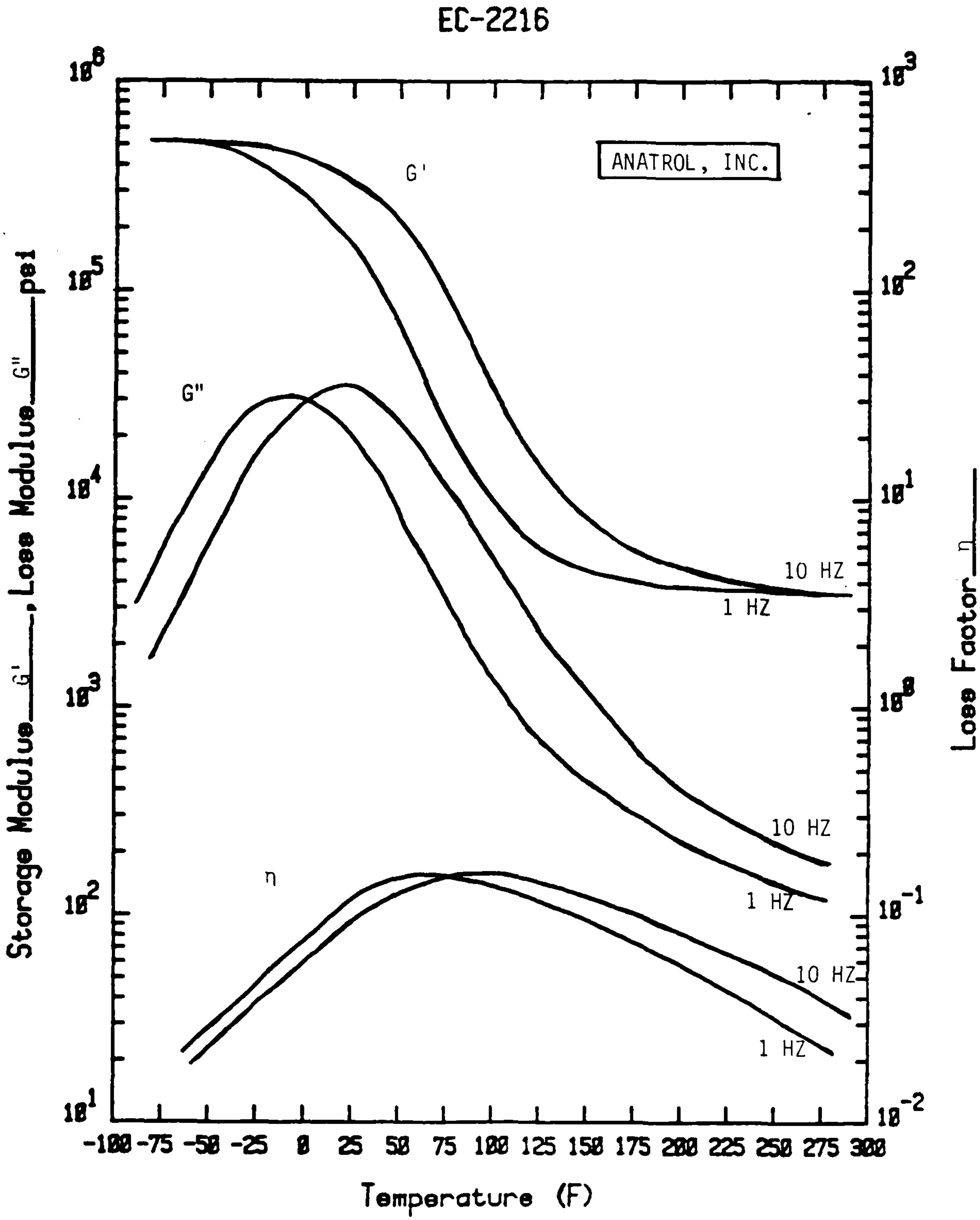

Figure D-9. Damping Properties of EC 2216 - Specimen No. 3

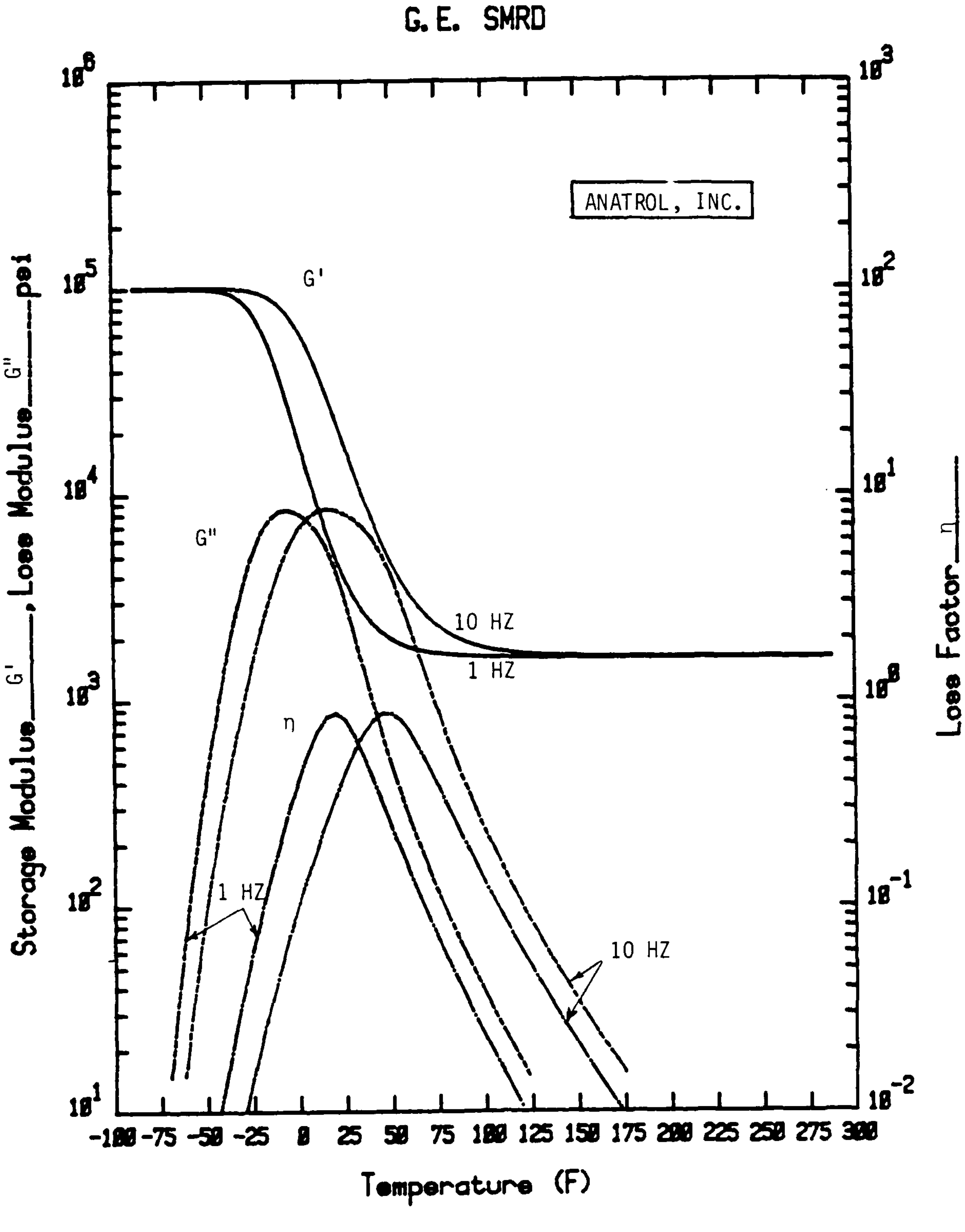

Figure D-10. Damping Properties of SMRD 100F90 - Specimen No. 9

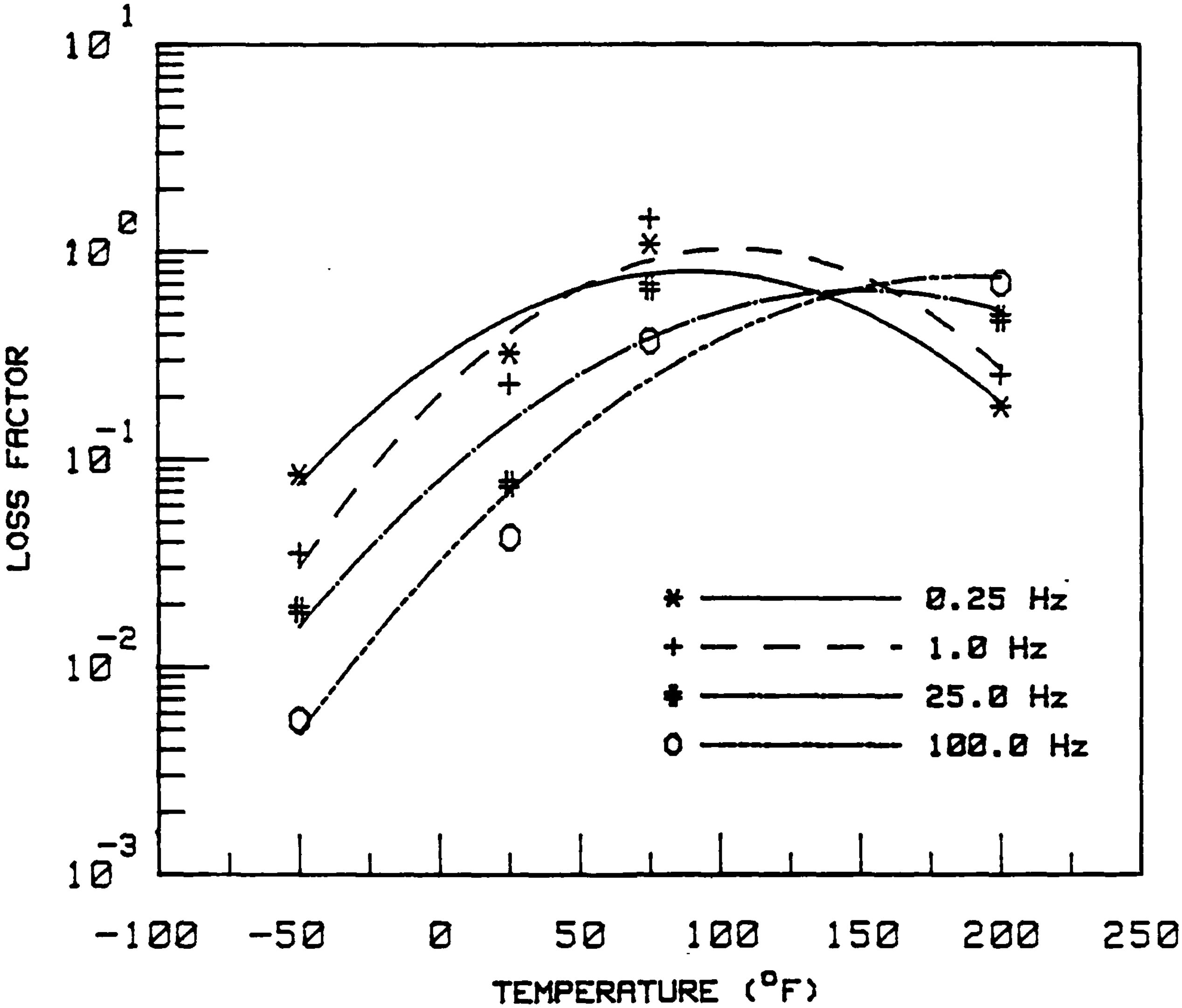

Figure D-11. Temperature/Frequency Effect on Loss Factor of Specimen No. 1

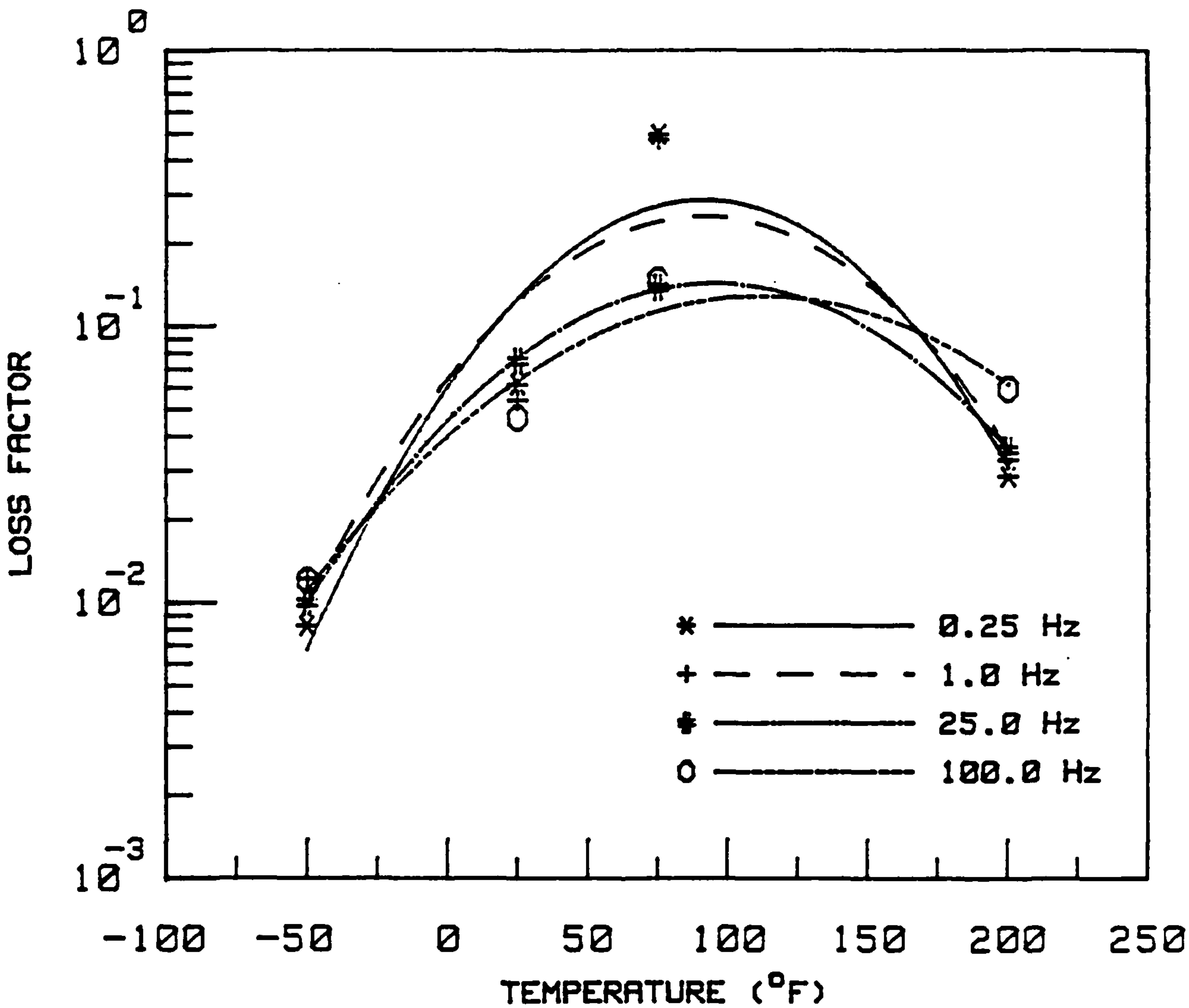

Figure D-12. Temperature/Frequency Effect on Loss Factor of Specimen No. 3

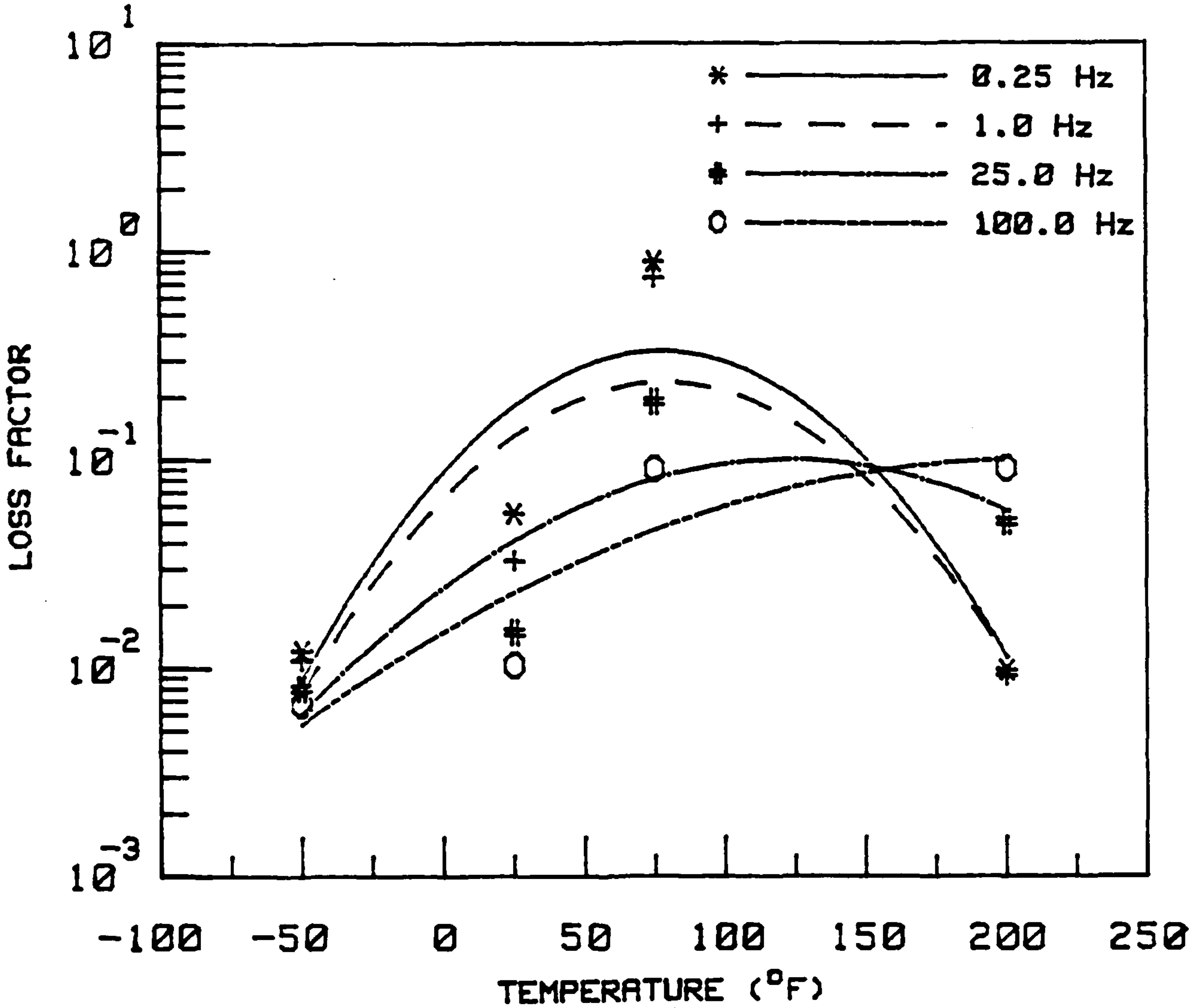

Figure D-13. Temperature/Frequency Effect on Loss Factor of Specimen No. 5

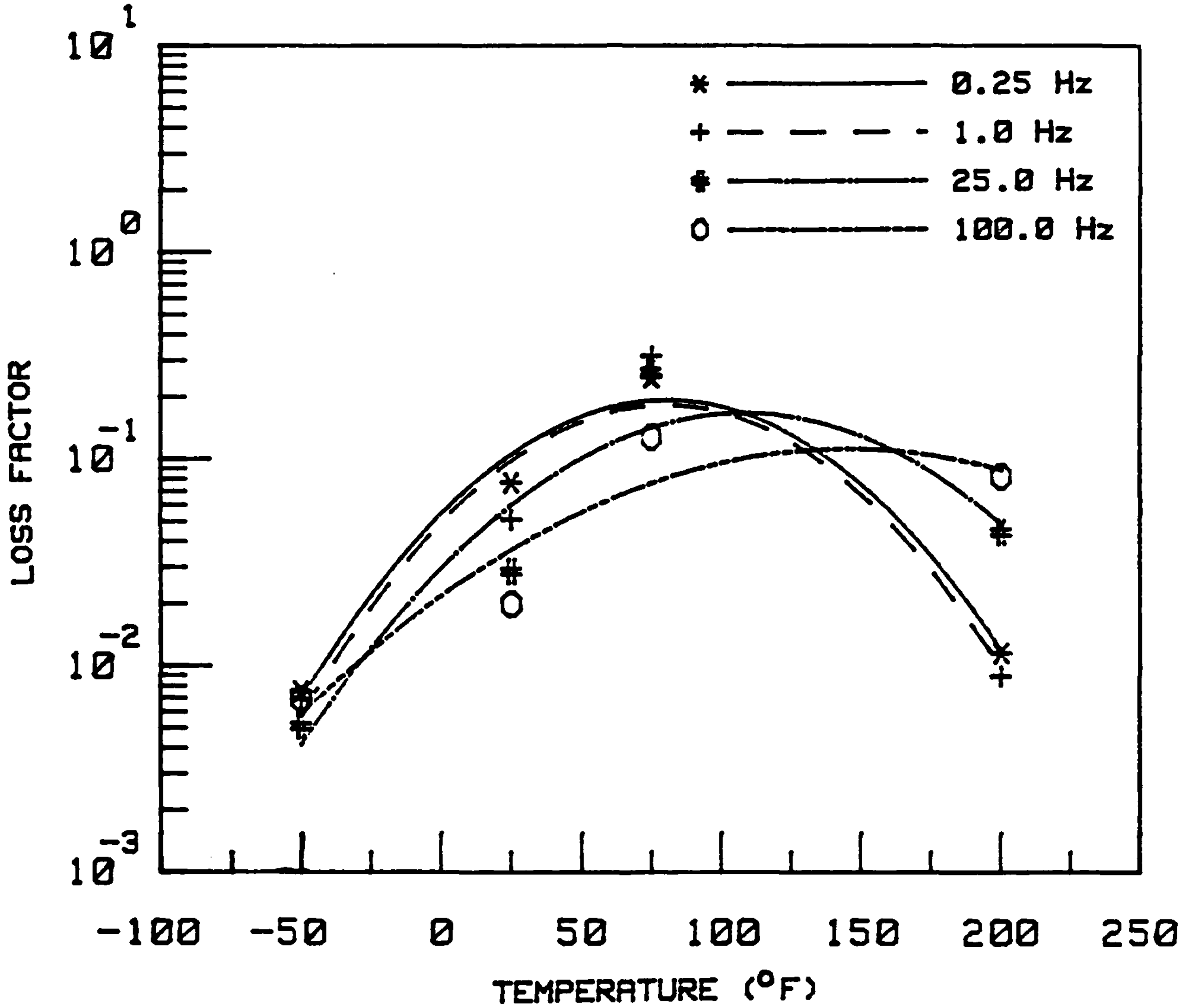

Figure D-14. Temperature/Frequency Effect on Loss Factor of Specimen No. 9

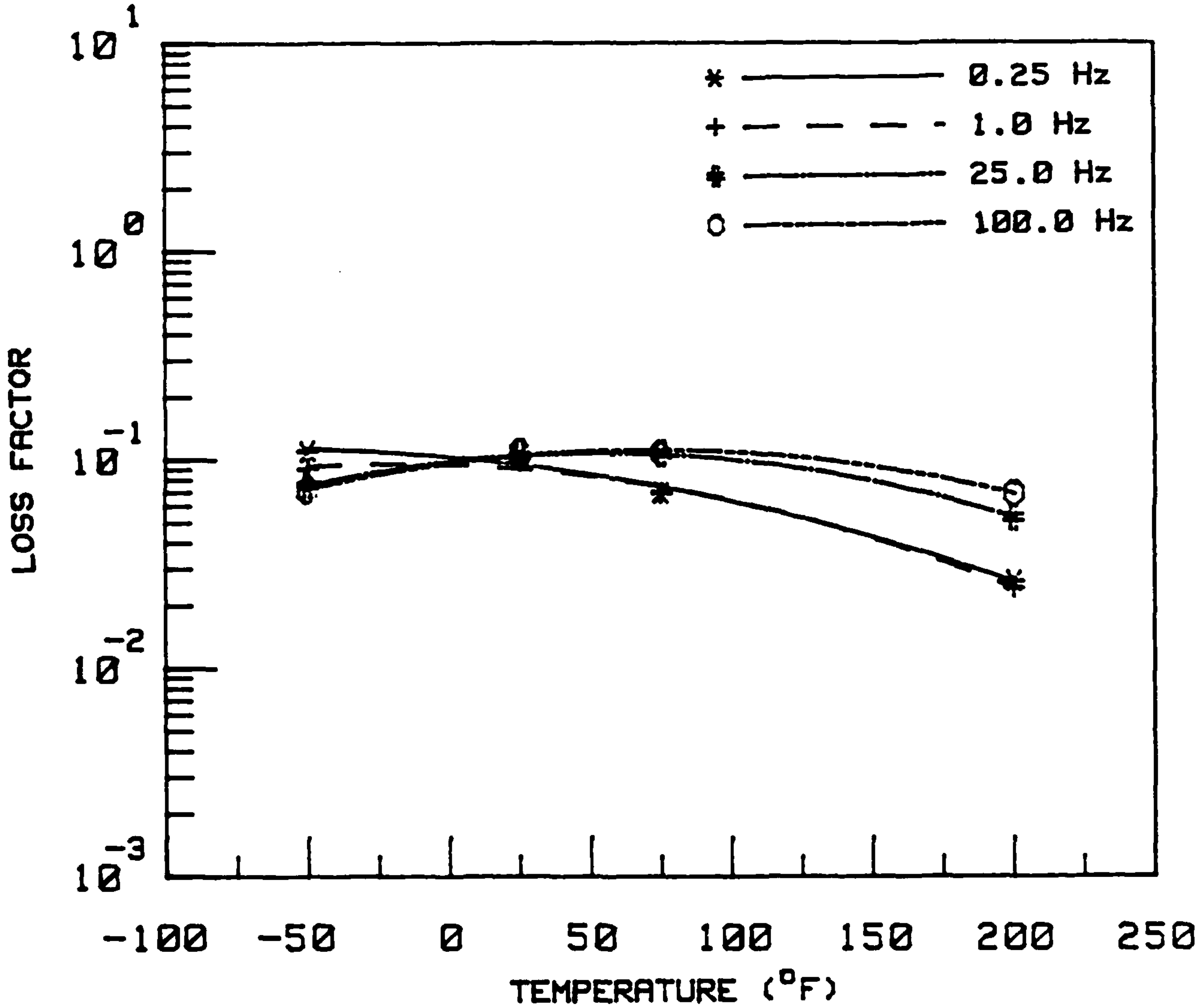

Figure D-15. Temperature/Frequency Effect on Loss Factor of Specimen No. 11

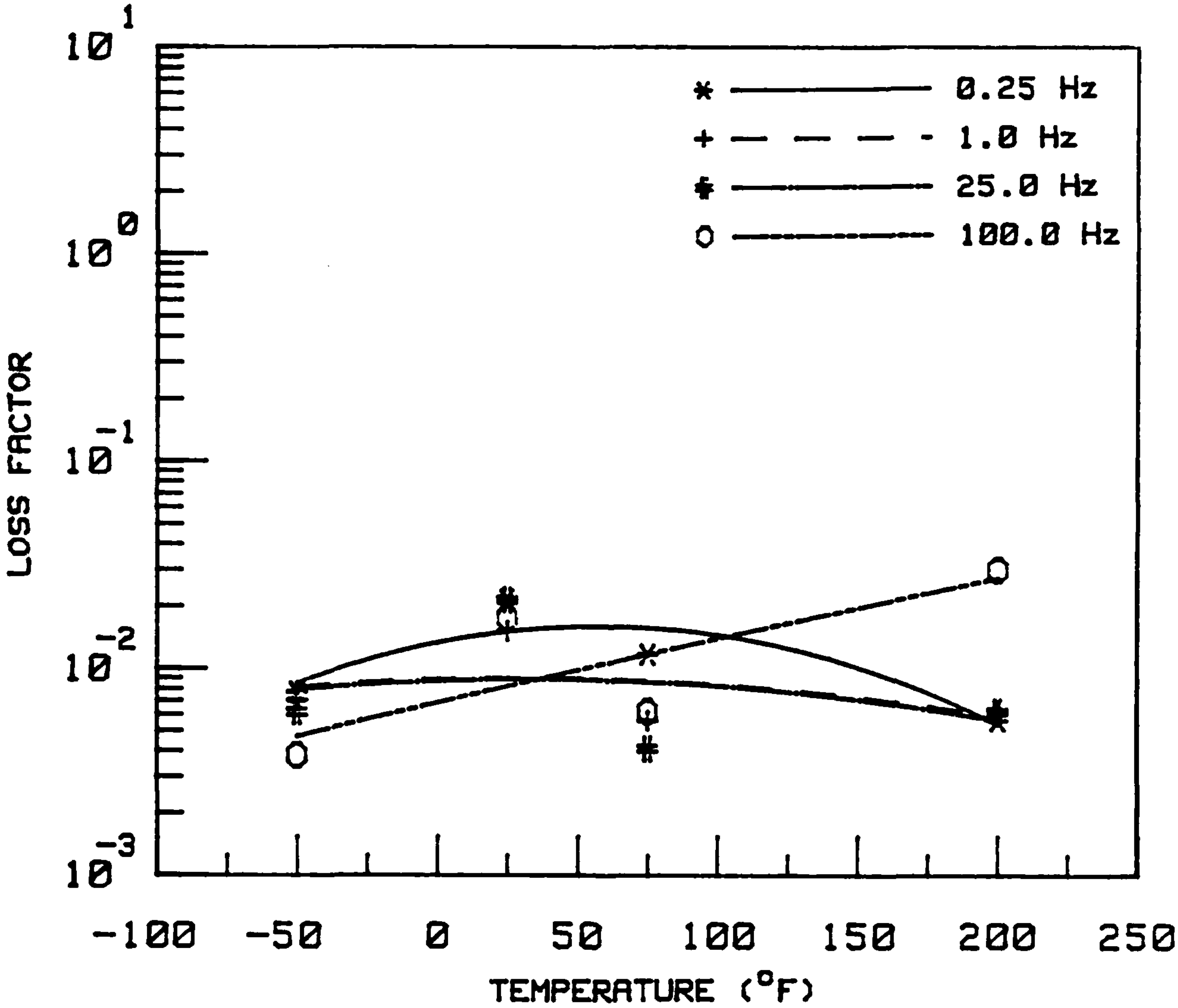

Figure D-16. Temperature/Frequency Effect on Loss Factor of Specimen No. 13

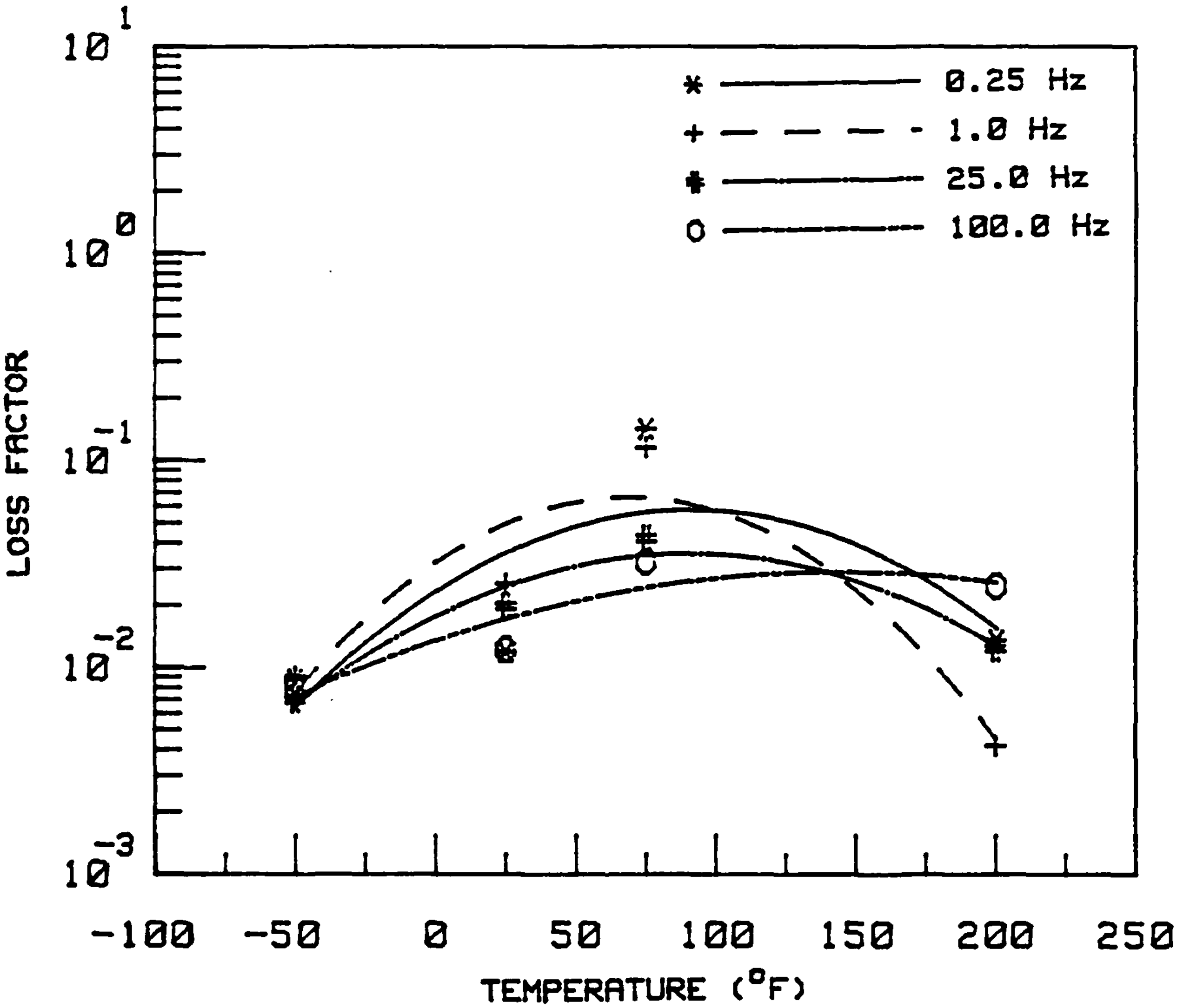

Figure D-17. Temperature/Frequency Effect on Loss Factor of Specimen No. 15

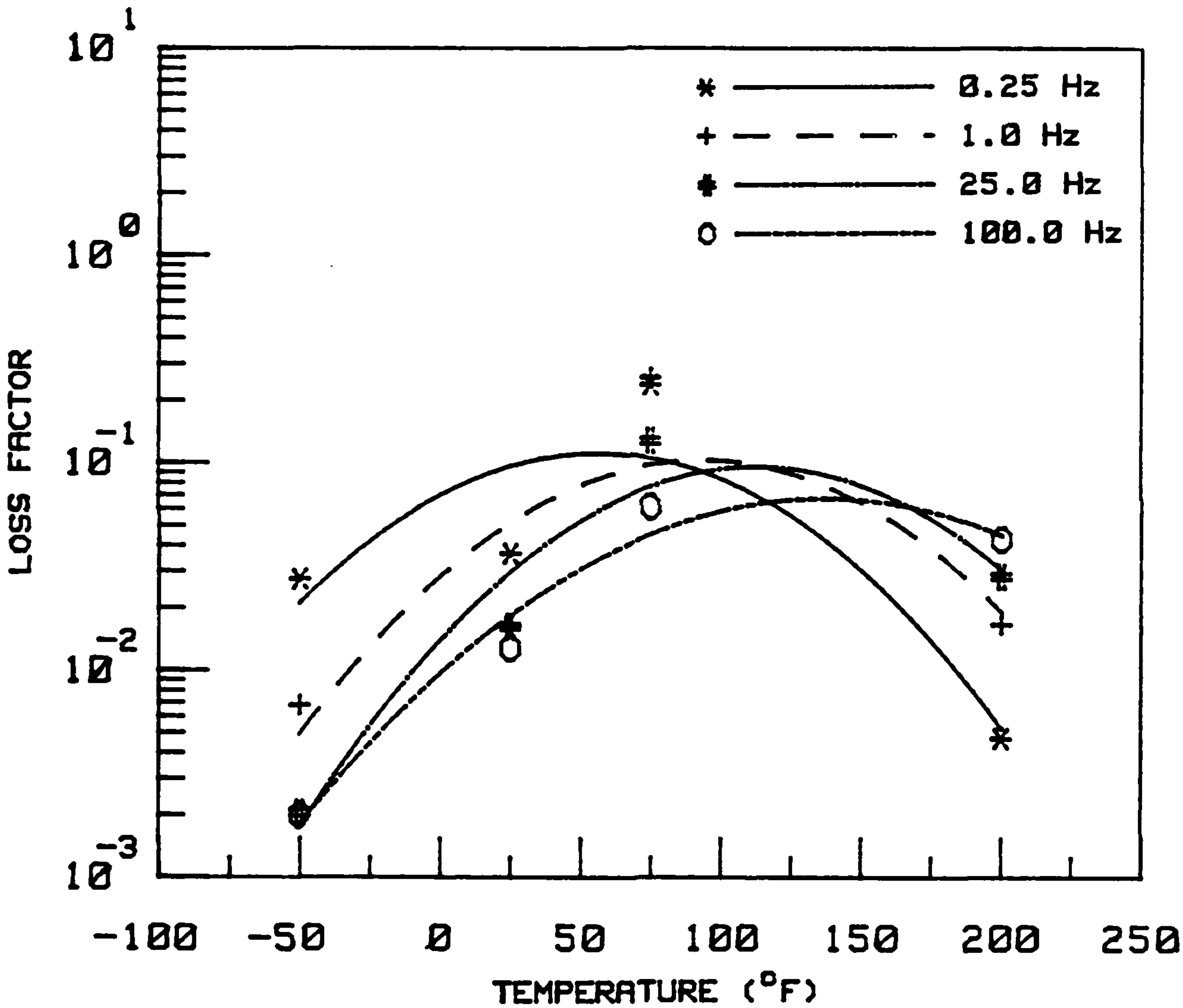

Figure D-18. Temperature/Frequency Effect on Loss Factor of Specimen No. 18

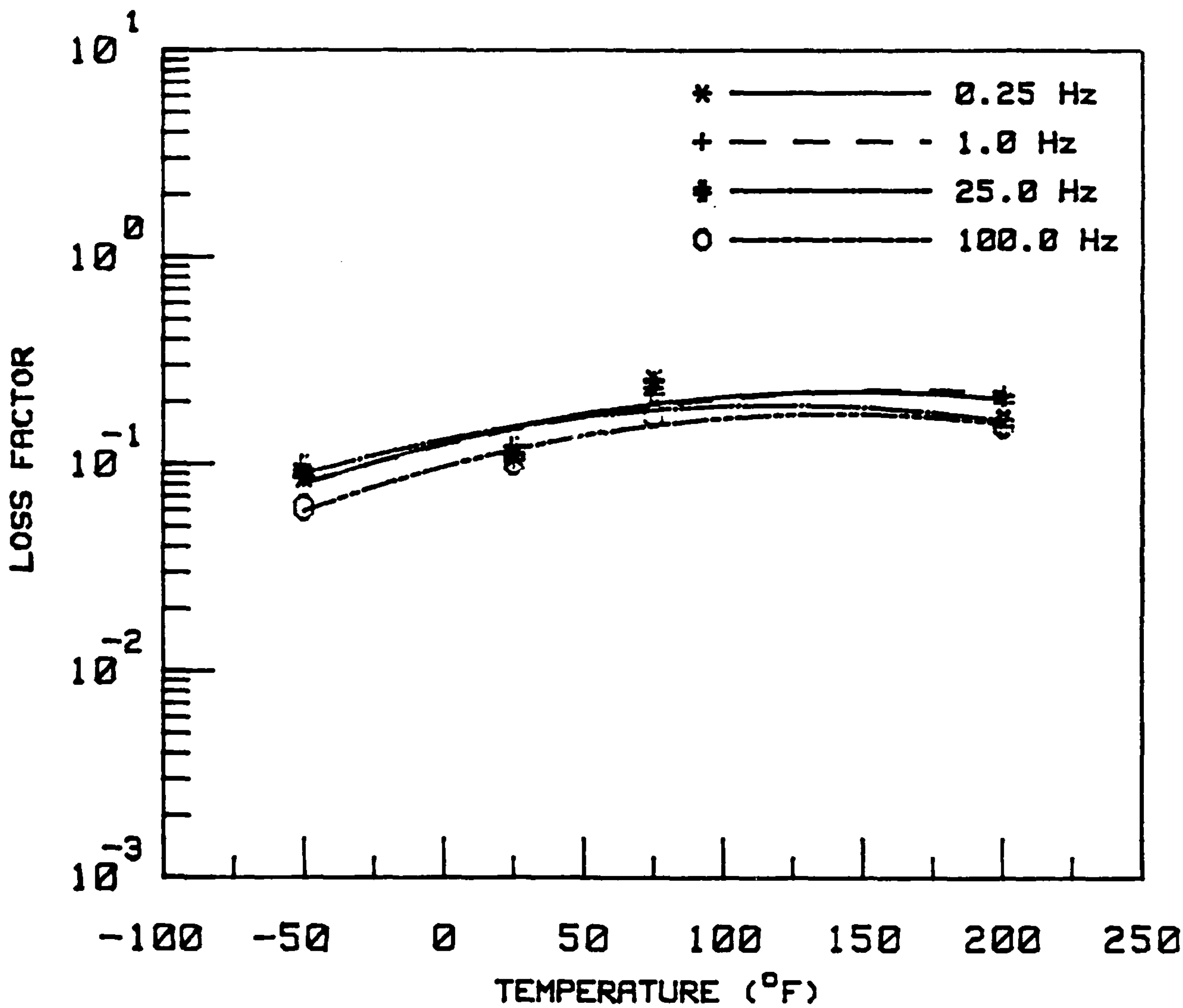

Figure D-19. Temperature/Frequency Effect on Loss Factor of Specimen No. 21

amplitude B, the phase angle ϕ, and the test fixture compliance C revealed that the computed loss factor is very sensitive to measurement error of the phase angle. Using data from specimen 1 at room temperature, a 1% error in ϕ will produce a 21% change in the loss factor. The loss factor is much less sensitive to changes in B or C. An improved method of determining the phase shift should be used. The "zero-crossing" method used is not very accurate, especially when the output signal is non-sinusoidal, as is often the case. The shape of the output signal is more sinusoidal at low temperatures, consequently the low temperature results are more accurate. The quality of the output signal and, therefore, the accuracy of the phase shift measurement, can be improved by isolating the test fixture from any external vibration sources, precisely aligning the specimen and test fixture to ensure pure axial motion, and meticulously cleaning all electrical connections between the load cell and charge amplifier. Alternatively, a more accurate phase shift measurement might be obtained by employing averaging and ensembling techniques or Fourier fitting the output data. Harmonic or other curve fitting methods like these can be used to estimate the phase shift with a great deal of statistical accuracy.

Additional tabulated results for each of the specimens are provided in Appendix F. Examination of the storage modulus and dissipative modulus shown in these tables also correlates with the expected trends. The moduli could not be plotted since there are not enough data points to generate the cubic curves.

References

D-1. R. W. Trudell. Passively Damped Joints for Advanced Space Structures - Annual Technical Report. McDonnell Douglas Astronautics Co. report MDC H1178, June 1984.

D-2. R. W. Trudell, et al. Passively Damped Joints for Advanced Space Structures. Presented at the Vibration Damping Workshop, sponsored by AFFDL, February 1984, and published in the proceedings.

D-3. J. C. Prucz. Analytical and Experimental Methodology for Evaluating Passively Damped Structural Joints. Ph.D. Thesis submitted to Georgia Institute of Technology, May 1985.

Appendix E

EXPERIMENTAL PROCEDURE AND DATA REDUCTION

Introduction

The development of new test methods naturally spawns the development of new experimental procedures and data reduction techniques to support those methods. Such has been the case in this research program where innovative data reduction techniques have been developed and implemented to evaluate data produced by the simplified steady state and sine pulse propagation approaches. The test methods employed in this program have been previously described, compared, and their results evaluated in Appendix D. A detailed discussion of the experimental procedures, equipment, and data reduction techniques that support those test methods will be discussed in this appendix for:

a) Hysteresis-Loop Approach

b) Simplified Steady State Approach

c) Sine-Pulse Propagation Approach

Hysteresis-Loop Approach

The experimental setup used for the hysteresis-loop technique is shown in Fig. E-1a. The specimen is mounted vertically in an Instron Universal Testing Machine and a cyclic axial load is applied to it by the moving crosshead of the machine. A strain gage load cell built in the fixed crosshead measures the resultant load on the specimen. The relative axial displacement between the edges of the joint section of the specimen is measured by a linear variable differential transformer (LVDT) extensometer. The testing machine is controlled by presetting the vertical speed of the moving crosshead to prescribed values. However, the resultant loading frequencies cannot be directly controlled and they are higher for stiffer specimens, even at the same speed of the crosshead. Although the resultant time histories of load and deformation are triangular rather than sinusoidal, the data may be related to the associated frequency due to the cyclic nature of the applied loading.

Preliminary testing at a single temperature and frequency condition were run at MDAC-HB on all the specimens. GIT testing was also only at room temperature, but at three different crosshead speeds (frequencies). The load and displacement time histories acquired at GIT were stored as voltage signals on separate channels of a Nicolet 4094A digital oscilloscope, after preliminary electronic filtering and amplification. Two DC Neff amplifiers, one of which has a built-in filter, and a KROHN-HITE 3342R filter were used for signal

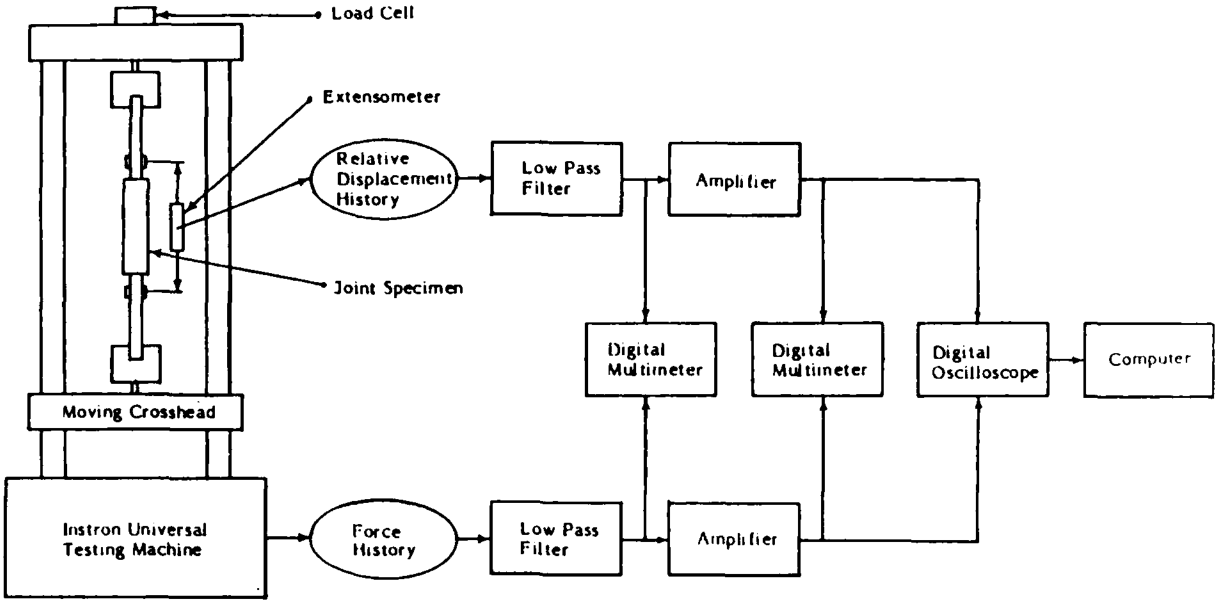

Figure E-1a. Experimental Setup for the Hysteresis Loop Approach

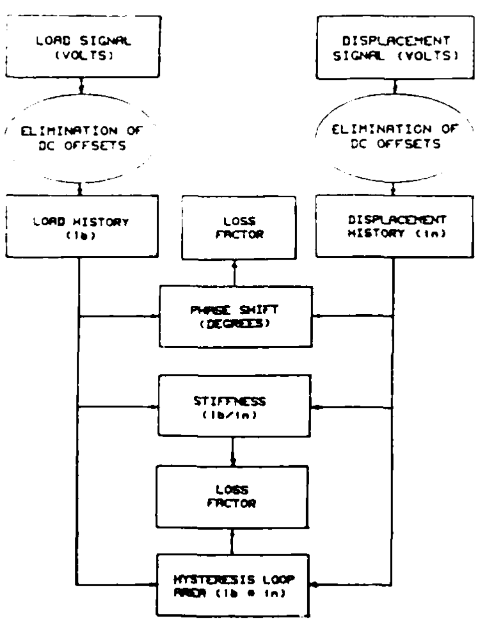

Figure E-1b. Data Analysis Flow for Hysteresis Loop

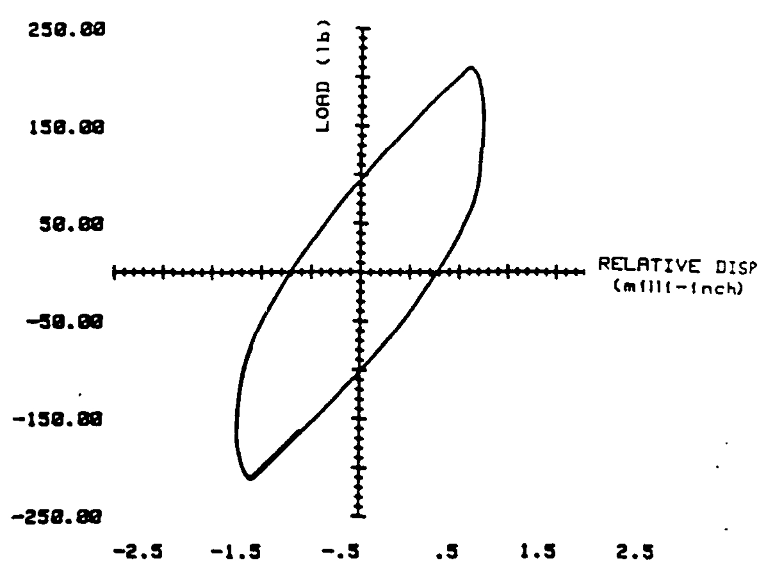

Figure E-1c. Hysteresis Loop of Specimen No. 3

conditioning. High frequency noise above 1 kHz was filtered out of the signals. The load gain factor was 200 and the displacement gain varied from one specimen to the other, its maximum value being 5. Digital multimeters were used for calibration and monitoring of the signal conditioning equipment. The sweep length of the digital oscilloscope was selected such that the acquired data covered at least one full loading cycle. The response signals from about ten successive cycles were automatically averaged by the oscilloscope for enhanced statistical reliability of the results. The data was subsequently recorded on a magnetic disk for future reference.

The digital data reduction was performed on an HP 9845B desk computer after the automatic transfer of the measured voltage signals from the memory unit of the Nicolet oscilloscope through a GPIB (General Purpose Interface Bus) interface system.

A schematic flow chart of the data analysis software is shown in Fig. E-1b. An ordering routine is first applied separately to the two voltage vectors corresponding to the load and displacement signals, respectively. The minimum and maximum values of each signal are thus determined and used to eliminate any DC component that may be included in the raw data because of the measurement or the signal conditioning equipment. The corresponding calibration and gain factors are subsequently used for calculating the real time histories of load and relative displacement.

The ratio between the maximum axial load and the maximum axial deformation yields the corresponding stiffness of the specimen. The damping characteristic is expressed in terms of the loss factor, which can be determined either from the phase shift between the zero crossings of the load and displacement variations with time, or from the area enclosed inside the resultant hysteresis loop. The second alternative has been chosen here since it does not require a high time resolution of the processed signals. A typical hysteresis loop is shown in Fig. E-1c. The corresponding expression of the loss factor is:

$$\eta = \frac{H_a}{2\pi U_{max}}$$

where the hysteresis loop area, H_a, is evaluated by numerical integration of the measured data in the load-displacement plane. The maximum strain energy stored in one cycle, U_{max}, is given by

$$U_{max} = \frac{P^2}{2K_j}$$

where P is the maximum applied external load and K_j is the joint stiffness.

Simplified Steady State Approach

The experimental setup and data analysis flow for the steady state approach are shown in Fig. E-2. The specimen is mounted horizontally in the specially designed fixture that was described in Appendix D. A more detailed discussion of the fixture design can be found in Ref. E-1. The basic measurements required by this technique consist of the applied input voltage to a custom designed piezoelectric motion transducer at one end of the specimen and a force measurement from a load cell at the opposite end of the specimen. The simplifying feature of this technique is that no displacement measurement is required - a definite advantage for the stiff joints anticipated for use in large space structures.

A harmonic voltage applied to the piezoelectric exciter generates a small axial harmonic motion which is transmitted through the test specimen, resulting in an axial harmonic force measured by the piezoelectric load cell. Mathematically, this input motion and output force can be described by the following equations:

$$X = A \cos \omega t \qquad \text{where } A = (\mu in/V)(V_{in})$$

$$F = B \cos (\omega t + \phi) \qquad \text{where } B = (lb/V)(V_{out})$$

The viscoelastic behavior of the test specimen induces a phase lag ϕ between the force history and the voltage applied to the exciter.

A Tektronix 5440 four channel analog oscilloscope is used for real time monitoring and adjustments of the various signals. Since peak voltages close to 300 volts are applied to the exciter, the corresponding signal is passed through a 60:1 attenuation box before it can be acquired on the oscilloscopes. In order to avoid possible signal distortions at very low frequencies because of the capacitor time constant of the piezoelectric load cell, an AVL charge amplifier with a long time constant setting is used for the charge to voltage conversion of the load data.

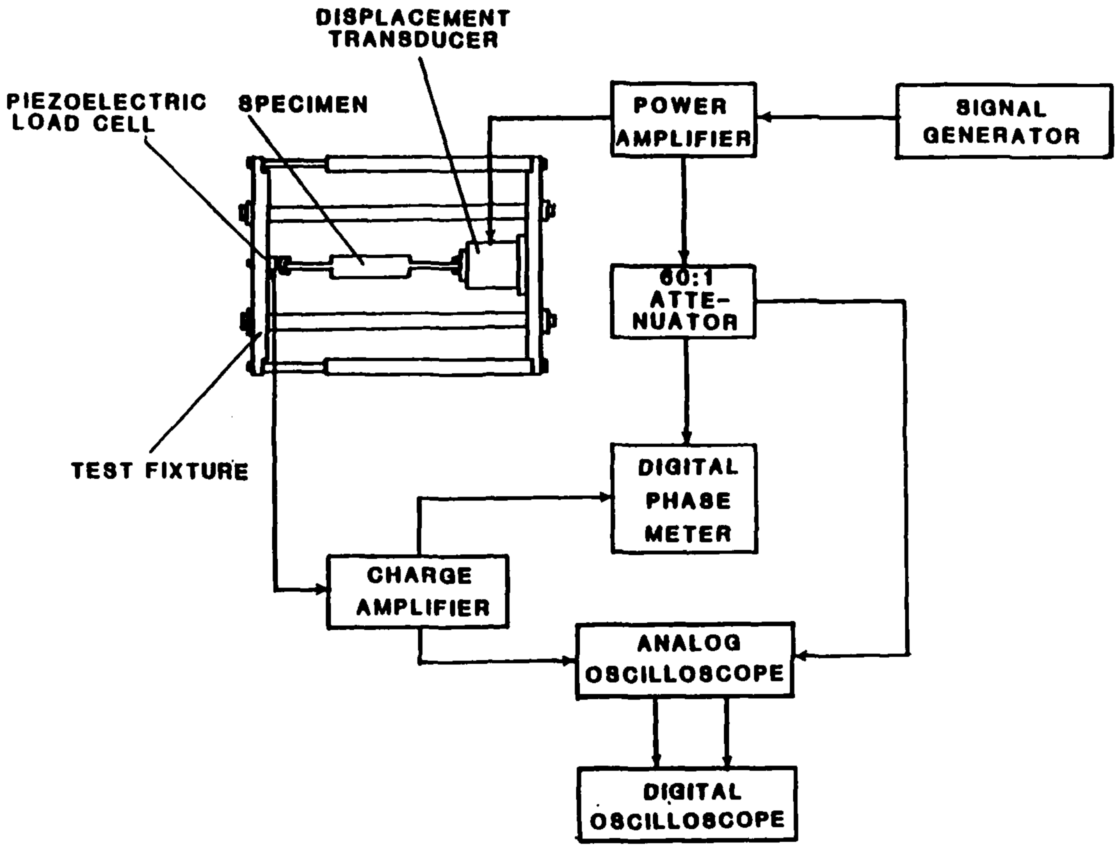

Figure E-2a. Experimental Setup for the Simplified Steady State Approach

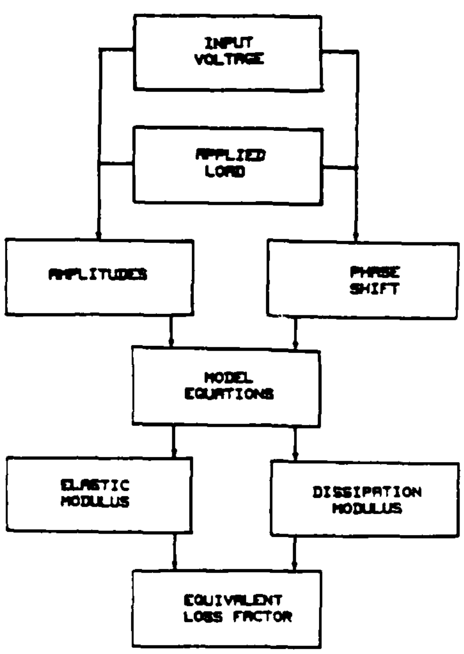

Figure E-2b. Data Analysis Flow for Simplified Steady State Approach

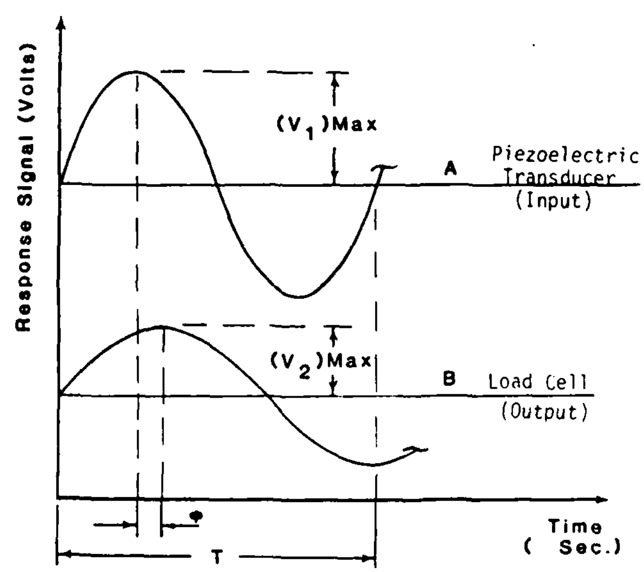

Figure E-2c. Sample Measurements for Simplified Steady State Approach

The time histories of the voltage applied to the exciter and the load cell response are acquired, averaged and analyzed on separate channels of a Nicolet 4094A digital oscilloscope. The complex stiffness of the test specimen is determined from the amplitudes of the applied voltage V_{in} and the resultant force V_{out} along with the phase shift ϕ between these two signals, which can be measured directly on the display screen of the digital oscilloscope as shown in the following figure.

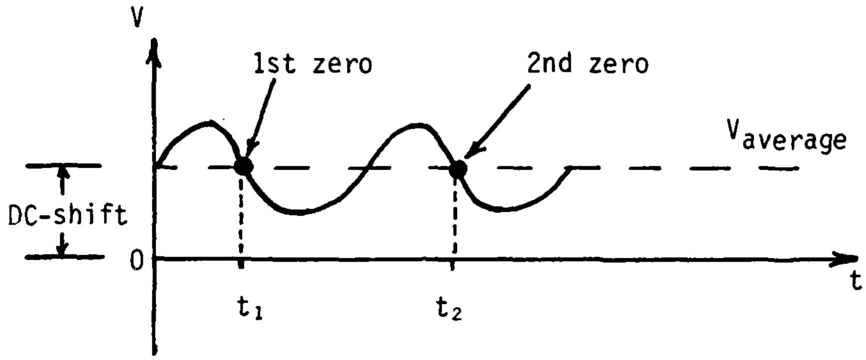

The load phase lag, with respect to the applied displacement, is determined by the difference between the zero-crossings of the corresponding load and displacement time waves. Therefore, the phase shift is given by

$$\phi = (2\pi)(\Delta T)(f)$$

where f = forcing frequency

and $$\Delta T = \frac{(t1_{in} - t1_{out}) + (t2_{in} - t2_{out})}{2}$$

Once the input/output amplitudes and corresponding phase shift are known, the complex stiffness and loss factor of the specimen can be determined from the following equations.

$$K_s = \left(\frac{X}{F} - C\right)^{-1} \quad \text{where } C = \sum_{i=1}^{n} \frac{1}{K_i}$$

$$\mathrm{re}(K_s) = \frac{\frac{B}{A}\cos\phi - \frac{B^2}{A^2}C}{1 - 2C\frac{B}{A}\cos\phi + \frac{B^2}{A^2}C^2} \qquad \text{(elastic stiffness, K')}$$

$$\mathrm{imag}(K_s) = \frac{\frac{B}{A}\sin\phi}{1 - 2C\frac{B}{A}\cos\phi + \frac{B^2}{A^2}C^2} \qquad \text{(dissipative stiffness, K")}$$

$$\eta_s = \frac{\mathrm{imag}(K_s)}{\mathrm{re}(K_s)}$$

where A = amplitude of applied motion
B = amplitude of resultant force
C = equivalent compliance of test fixture
K_s = specimen stiffness
η_s = specimen loss factor

The equivalent compliance C in the above equations is a correction term that accounts for the stiffness contributions of the test fixture, load cell, and displacement transducer. It can be neglected when the stiffness of the specimen is much lower than that of any of these elements. Accurate determination of C is essential if reliable data is to be obtained. For the room temperature tests, C was assumed to be constant with frequency. Using a reference specimen of known stiffness and the stiffness equations above, the value of C was computed to be 3.25×10^{-6} in/lb. However, this correction term can vary with frequency and temperature due to the inherent characteristics of the measurement devices and exciter.

In order to determine the joint stiffness, K_j, shown below,

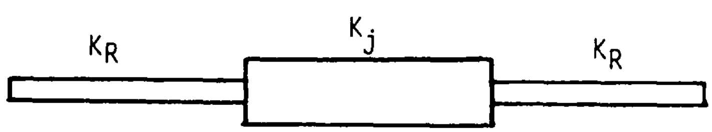

we use the following equation:

$$\frac{1}{K_S} = \frac{2}{K_R} + \frac{1}{K_J}$$

where K_S = overall specimen stiffness
K_R = stiffness of the two end members

or K_R = 1,755,000 lb/in.
$K_S = \sqrt{(K_S')^2 + (K_S'')^2}$

However, it has been suggested that the above formula for K_S may be incorrect and that the specimen stiffness is simply the real part, or the elastic stiffness, of the complex stiffness previously defined.

Sine-Pulse Propagation Approach

No custom-built test fixture or exciter are needed for application of the sine-pulse propagation method. Nevertheless, the facilities developed for the simplified steady state technique have been used also for the transient tests in order to facilitate data correlation between the two methods. The corresponding experimental setup is shown in Fig. E-3a. The voltage signal applied to the piezoelectric exciter is supplied and amplified by the same equipment as in the simplified steady state tests, but the continuous sine wave generated by the function generator is now gated to the desired pulse length. All the excitation pulses used in the tests contain just one full cycle. The stiffness and damping properties of the test specimen are determined by comparing the response signals from two identical PCB piezoelectric load cells mounted at its ends.

Force measurements from load cells are taken, rather than accelerations (see Fig. E-3c), due to the very low displacement amplitudes and frequencies generated by the piezoelectric motion transducer. The use of load cells requires the non-excited end of the specimen to be fixed. Whether the specimen end is fixed or free is unimportant - both suspension techniques produce results that agree very closely.

After passing through two identical AVL charge amplifiers, the two response signals are acquired on separate channels of a Nicolet 4094A digital oscilloscope. The specimen responses to consecutive identical pulses are

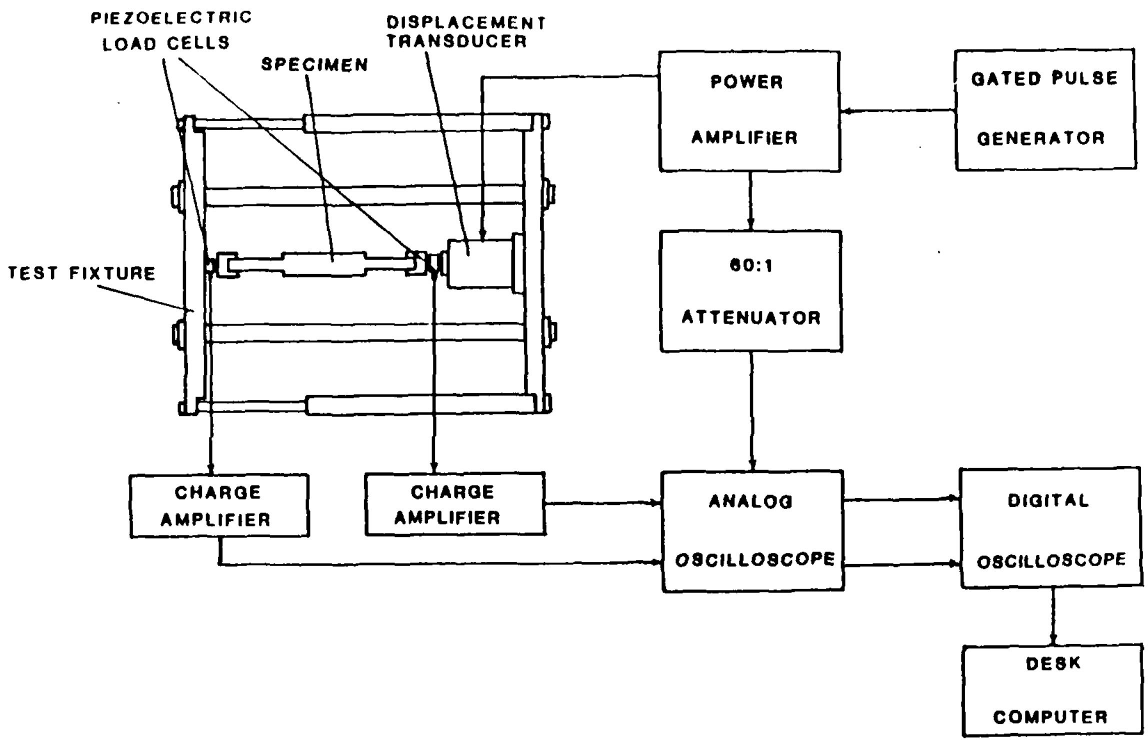

Figure E-3a. Experimental Setup for the Sine-Pulse Propagation Approach

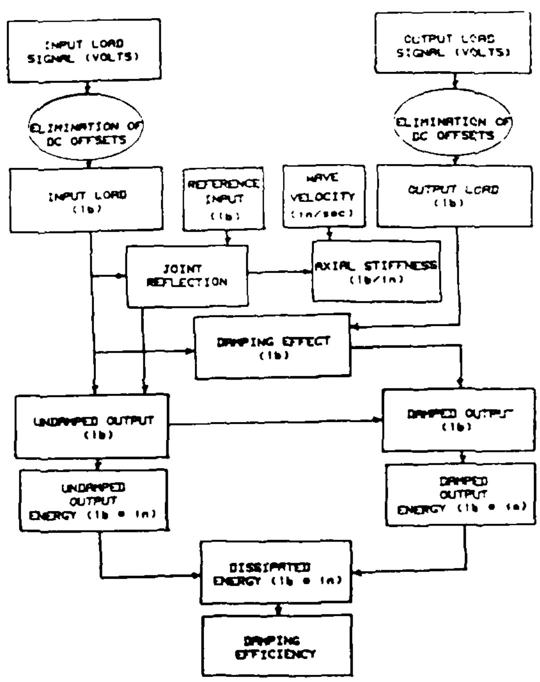

Figure E-3b. Data Analysis Flow for Sine-Pulse Approach

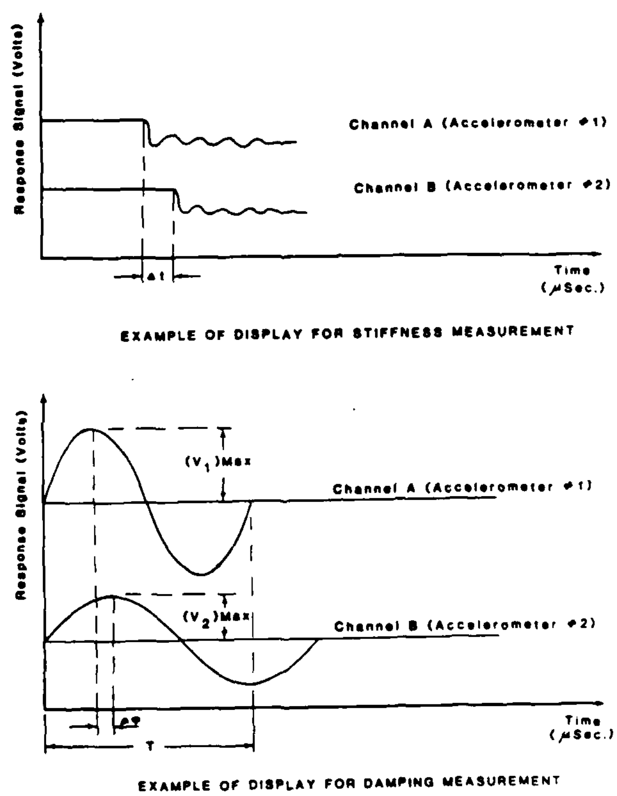

Figure E-3c. Sample Measurements for Sine Pulse Approach

automatically averaged by the oscilloscope and subsequently recorded on a magnetic disk for future reference and analysis. The pulse repetition rate is kept low enough to allow sufficient time for the disturbances caused by a previous pulse to die down before the next pulse is applied to the specimen.

The data reduction is performed, like in the hysteresis loop technique, on an HP 9845B desk computer. The input and output load signals acquired for each test are transferred separately through the GPIB interface system from the memory unit of the Nicolet oscilloscope to the computer memory. Fig. E-3b displays a schematic diagram of the data analysis procedure.

Since each data point represents an axial load at a particular instant of time, the strain energy level associated with it may be expressed as:

$$U_{1i}(t) = \frac{P_{1i}(t)^2}{2K_i}, \quad U_{2i}(t) = \frac{[P_{1i}(t) + D_i(t)]^2}{2K_i}$$

where the indices 1 and 2 refer to the input and output signals, respectively. In the case of an homogeneous specimen, the total energy dissipated by damping per cycle is

$$\Delta U = U_1 - U_2$$

where the total input and output energies per cycle, U_1 and U_2 are obtained by numerical time integration of the corresponding digital signals.

$$U_{1,2} = \sum_{t_k=1}^{T} U_{1i,2i}(t_k)$$

where T is the length of the excitation pulse. The damping efficiency of the specimen is defined by the ratio between the dissipated and the input energies per cycle.

$$\eta_e = \frac{\Delta U}{U_1}$$

In the case of a joint specimen, the measured load signals include the effects of wave reflections and refractions at the joint-member discontinuity interfaces. Force equilibrium and displacement continuity conditions at these interfaces dictate the signs and amplitudes of the resulting waves as a function of a reflection parameter which may be defined here as

$$\alpha_1 = \frac{c_i}{c_j}\,\frac{L_j}{L_i}\,\frac{K_j}{K_i}$$

where the index i refers to the member and the index j refers to the joint portion of the test specimen.

Since the joint damping affects only that part of the applied load that is transmitted through the joint, the reflection parameter α_1 must be evaluated before the damping effect can be separated from the measured signals. For this purpose, the input load signal of the joint specimen is compared with a reference input load signal for the same applied excitation. The reference specimen is a homogeneous bar with the same geometrical and material characteristics as the members of the joint specimen, so that the difference between the two signals is mainly due to the reflection at the member-joint interface, i.e.,

$$-R_{1j}(t) = |P_{1i}(t) - P_{1j}(t)|$$

The parameter α_1 is subsequently calculated and used in the evaluation of the damping effect according to the following formula:

$$D_j(t) = \text{FIT}\ P_{2j}(t) - P_{1j}(t) - \left[1 - \frac{4\alpha_1}{(\alpha_1 + 1)^2}\right] P_{1j}(t)$$

where the symbol FIT denotes the least-square fitting routine for elimination of the multiple reflections effect.

The above equation for $D_j(t)$ is derived by considering the major components included in the measured load signals $P_{1j}(t)$ and $P_{2j}(t)$ and extracting the damping signal $D_j(t)$ from their difference.

The separation between the effects on the difference signal $[P_{2j}(t) - P_{1j}(t)]$ of multiple reflections and damping and direct joint reflections relies upon the different character of their time variations. Unlike the damping and the joint reflection effects which display a smooth, monotonic trend all over the pulse length, the multiple reflections effect is characterized by high frequency oscillations above and below the main difference signal, much like "white noise" in electronic systems. This observation is supported both by test data and the results of wave system simulations like those shown in Fig. E-4.

Computation of the "damping efficiency" of the joint is similar to that of a homogeneous bar except that the refracted portion of the applied signal for the calculation of U_1 and its combination with the damping signal $D_j(t)$ for the calculation of U_2 are used as defined below.

$$U_{1j}(t) = \frac{1}{2K_j}\left[\frac{2\alpha_1}{\alpha_1 + 1} P_{1j}(t)\right]^2$$

$$U_{2j}(t) = \frac{1}{2K_j}\left[\frac{2\alpha_1}{\alpha_1 + 1} P_{1j}(t) + D_j(t)\right]^2$$

The axial stiffness of the reference homogeneous specimen, K_1, is evaluated from the propagation velocity of the applied stress pulse through the specimen, c_1. The time delay, Δt, between the moments in which the pulse front reaches the two load cells is measured with an accuracy of about 1 μs when the data is acquired by the Nicolet 4094A oscilloscope at its maximum sampling rate. Since no significant dispersion is expected to occur for low frequency sine-pulses, the extensional modulus of the homogeneous specimen can be calculated from $E_1 = \rho_1 c_1^2$. It is subsequently utilized for the evaluation of K_1 in the reflection parameter equation since the member of the joint has the same cross section and material properties as the reference specimen, but a different length.

In the case of a joint specimen, the pulse propagation from one end to the other is a more complex process because of the discontinuous interfaces between

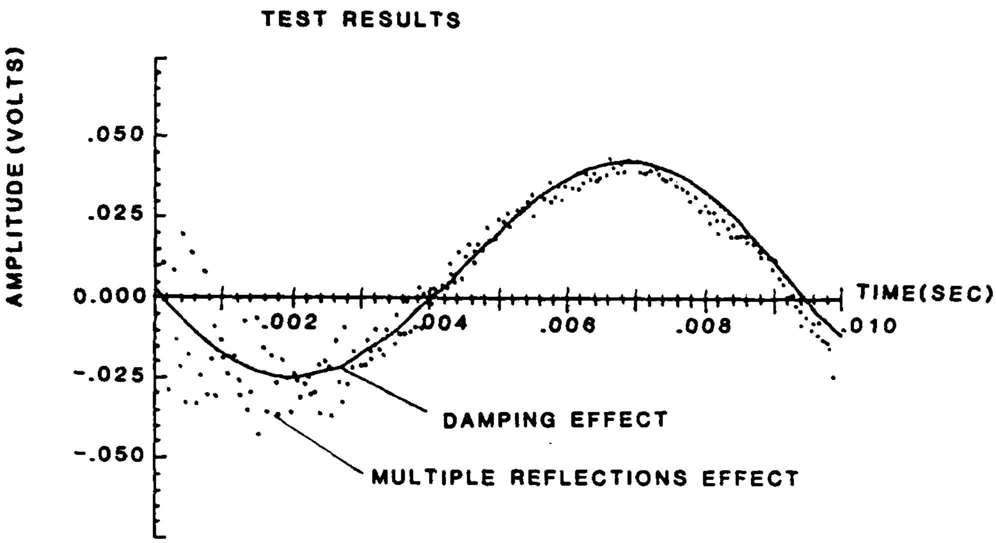

Figure E-4a. Difference Signal Between Output and Input Test Data for a Composite Continuous Bar

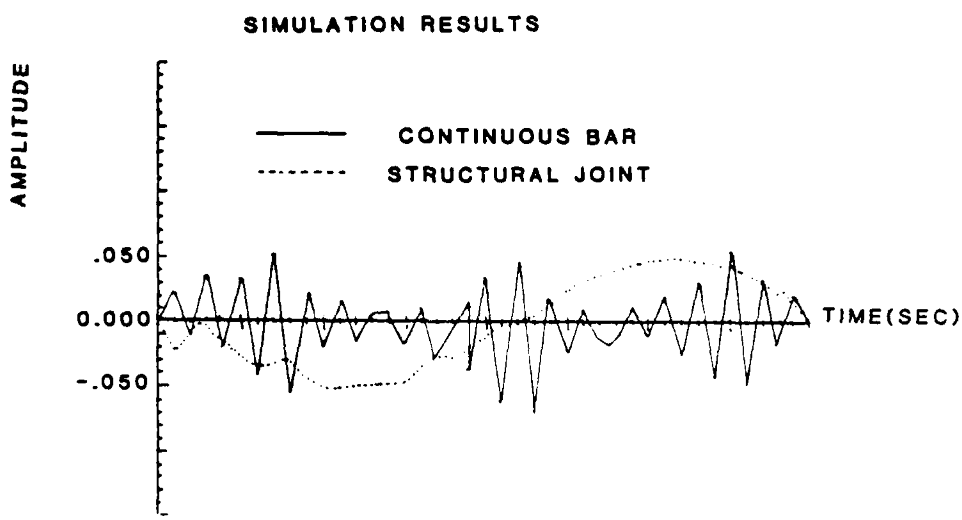

Figure E-4b. Difference Signals Between Output and Input Simulation Results

the different components of the joint. The axial stiffness K_j is approximately evaluated in this case by using the reflection parameter equation for α_j where the wave velocity c_j is determined separately like c_i by measuring the propagation time of the pulse front between the two load cells. A square pulse, rather than a sine pulse, is used for these measurements in order to make the pulse front more visible and facilitate its accurate location on the screen of the digital oscilloscope. Although some signal dispersion occurs in this case because of the high frequency components of the pulse, it does not significantly affect the accuracy of the results, if the measurements are taken over a short propagation distance of the pulse signal.

References

E-1. J. C. Prucz. Analytical and Experimental Methodology for Evaluating Passively Damped Structural Joints. Ph.D. Thesis submitted to Georgia Institute of Technology, May 1985.

Appendix F

JOINT DAMPING DATA

Introduction

This appendix contains the tabular form of the test data obtained from the hysteresis, steady-state, and sine pulse propagation test methods. All of the data presented here was acquired from testing performed at GIT. Summary plots and the narrative evaluation of this data was presented in Appendix D.

The following experimental results are presented in this appendix:

a) Hysteresis Loop Results (Room Temperature)

b) Simplified Steady State Results (Room Temperature)

c) Sine Pulse Results (Room Temperature)

d) Simplified Steady State Results (High and Low Temperature)

Hysteresis Loop Results (Room Temperature)

Tables F-1 to F-3 present the room temperature hysteresis loop test results for three crosshead speeds, 0.05, 0.1 and 0.2 in/sec, respectively. Included in each table is the frequency, loss factor, and axial stiffness for each specimen tested by this method. The procedure for calculating the loss factor and stiffness from the hysteresis loop is described in detail in Appendix E.

Simplified Steady State Results (Room Temperature)

Tables F-4 to F-15 present the room temperature simplified steady state test results. Each table, which corresponds to a particular specimen, provides the applied displacement and load as well as the resulting phase difference, elastic stiffness, dissipative stiffness, joint stiffness, and loss factor for prescribed frequencies between 0.1 and 100 Hz. The procedure for computing these parameters from the measured output is described in Appendix E.

Sine Pulse Results (Room Temperature)

Tables F-16 and F-17 show the damping performance of specimens 3 and 15 in terms of the damping efficiency parameter ($\eta_e = \Delta U/U_1$) and the commonly used loss factor ($\eta = \Delta U/2\pi U_{max}$) for frequencies from 0.1 to 100 Hz. A quarter of the total strain energy associated with the input pulse signal has been chosen to estimate the maximum strain energy stored per cycle, which is required for the loss factor evaluation. The "phase difference" parameter included in

Tables F-16 and F-17 represents the phase shift between the force and displacement time histories as determined from the equation

$$\phi = \tan^{-1}(\eta)$$

Table F-18 shows the propagation velocity, c_j, of a square longitudinal pulse through various test specimens. The equivalent extensional modulus ($E_j = \rho_j c_j^2$) is calculated as if the specimen were a homogeneous bar with an equivalent density of

$$\rho_j = \rho v \frac{V_v}{V_t} + \rho e \frac{V_e}{V_t}$$

where

ρ_v = density of viscoelastic material
ρ_e = density of elastic elements
V_v = volume of viscoelastic material
V_e = volume of elastic elements
V_t = total volume of the joint

The equivalent cross-sectional area is subsequently evaluated from the equation $A_j = K_j L_j / E_j$, where the estimation for K_j is based on the hysteresis stiffness data for the corresponding specimen and L_j is the length of the joint. The axial stiffness characteristics shown in Tables F-19 and F-20 are subsequently computed by substituting the wave velocities given in Table F-18 and the measured reflection parameters, α_1, into the equation below.

$$\alpha_1 = \frac{c_i}{c_j} \frac{L_j}{L_i} \frac{K_j}{K_i}$$

Simplified Steady State Results (High and Low Temperature)

Tables F-21 to F-56 present the low and elevated temperature results. Data were obtained using the simplified steady state approach at four temperatures (-50°, 25°, 75°, and 200°F) and four frequencies (0.25, 1.0, 25.0, 100.0 Hz). The data reduction procedure is identical to that used to obtain the steady state room temperature results.

Table F-1. Hysteresis Loop Results for Crosshead Speed of 0.05 in/sec

Specimen Number	Frequency (Hz)	Loss Factor	Axial Stiffness (Lb/In)
13*	0.078	0.0355	471,196
1	0.033	0.5674	7,007
3	0.070	0.4538	177,675
5	0.016	0.2808	17,154
7	0.072	0.0328	191,536
9	0.044	0.0988	68,708
11	0.033	0.0294	42,152
15	0.077	0.1627	434,760

* Reference homogeneous specimen with the same graphite/epoxy laminate as the adherends of the joint specimens and the same cross section.

Table F-2. Hysteresis Loop Results for Crosshead Speed of 0.1 in/sec.

Specimen Number	Frequency (Hz)	Loss Factor	Axial Stiffness (Lb/In)
13[1]	0.158	0.1107	509,947
1	0.092	0.6221	11,197
3	0.159	0.4777	234,902
5	0.039	0.3605	21,300
7	0.143	0.1077	191,102
9	0.091	0.1562	72,278
11	0.066	0.0766	42,461
15	0.154	0.1870	462,801

(1) Reference homogeneous specimen.

Table F-3. Hysteresis Loop Results for Crosshead Speed of 0.2 in/sec

Specimen Number	Frequency (Hz)	Loss Factor	Axial Stiffness (Lb/In)
13(1)	0.308	0.2281	523,123
1	0.286	0.7589	20,139
3	0.328	0.5470	285,096
5	0.099	0.4694	28,688
7	0.280	0.2714	196,263
9	0.189	0.3110	77,908
11	0.130	0.1491	43,062
15	0.301	0.2470	486,673

(1) Reference homogeneous specimen.

Table F-4. Steady State Test Data at Room Temperature for Specimen No. 1

Frequency (Hz)	Amplitude Data: Displacement (In x 10^6)	Amplitude Data: Load (Lb)	Phase Difference (Degrees)	Elastic Stiffness (Lb/In)	Dissipative Stiffness (Lb/In)	Joint Stiffness (Lb/In)	Loss Factor
0.1	79.00	0.713	39.114	7,050	5,957	9,328	0.8450
0.25	79.62	1.095	45.270	9,650	10,402	14,422	1.0779
0.5	79.77	1.562	46.833	13,248	15,574	20,934	1.1756
1.0	79.63	2.127	50.042	16,561	22,855	29,162	1.3800
10	71.17	10.40	30.705	137,531	182,464	308,933	1.3267
25	63.04	7.35	26.573	129,071	112,044	212,263	0.8681
50	60.33	8.77	20.449	199,810	150,224	349,567	0.7518
100	59.45	9.80	12.616	300,672	149,295	543,693	0.4965

Table F-5. Steady State Test Data at Room Temperature for Specimen No. 3

Frequency (Hz)	Amplitude Data: Displacement (In x 10^6)	Amplitude Data: Load (Lb)	Phase Difference (Degrees)	Elastic Stiffness (Lb/In)	Dissipative Stiffness (Lb/In)	Joint Stiffness (Lb/In)	Loss Factor
0.1	78.46	5.08	18.753	73,773	32,202	88,624	0.4365
0.25	78.58	6.38	21.194	94,003	50,847	121,695	0.5409
0.5	78.54	7.48	19.323	118,091	61,629	157,045	0.5219
1.0	78.39	8.40	18.375	139,983	73,497	192,852	0.5250
10	69.12	10.23	6.282	276,228	58,950	416,515	0.2134
25	61.68	10.54	5.466	370,933	80,313	668,784	0.2165
50	58.52	10.75	4.354	443,463	84,222	929,559	0.1899
100	58.15	11.03	6.066	466,052	130,418	1,079,095	0.2798

Table F-6. Steady State Test Data at Room Temperature for Specimen No. 5

Frequency (Hz)	Amplitude Data Displacement (In x 10^6)	Load (Lb)	Phase Difference (Degrees)	Elastic Stiffness (Lb/In)	Dissipative Stiffness (Lb/In)	Joint Stiffness (Lb/In)	Loss Factor
0.1	80.4	2.76	36.198	28,673	24,350	39,302	0.8492
0.25	80.51	4.06	36,944	41,926	39,674	61,785	0.9463
0.5	80.49	5.31	34.317	58,329	53,778	87,223	0.9220
1.0	80.42	6.81	30.635	82,251	71,603	124,527	0.8705
10	72.19	10.52	11.862	247,438	100,687	384,060	0.4069
25	63.84	11.15	8.325	370,570	127,230	707,866	0.3433
50	60.99	11.58	5.985	467,963	129,380	1,086,897	0.2765
100	60.10	11.96	4.158	544,111	112,495	1,514,711	0.2068

Table F-7. Steady State Test Data at Room Temperature for Specimen No. 7

Frequency (Hz)	Amplitude Data Displacement (In x 10^6)	Load (Lb)	Phase Difference (Degrees)	Elastic Stiffness (Lb/In)	Dissipative Stiffness (Lb/In)	Joint Stiffness (Lb/In)	Loss Factor
0.1	80.24	7.84	1.062	142,988	3,883	170,898	0.0272
0.25	80.28	7.95	1.440	145,972	5,412	175,245	0.0371
0.5	80.24	8.04	1.422	148,498	5,467	178,894	0.0368
1.0	80.03	8.07	1.278	149,913	4,975	180,922	0.0332
10	71.57	7.73	1.926	166,088	8,608	205,203	0.0518
25	63.28	7.68	2.205	199,937	12,720	259,614	0.0636
50	60.45	7.77	2.421	219,964	15,983	294,582	0.0726
100	59.55	7.90	2.699	232,085	19,257	317,016	0.0830

Table F-8. Steady State Test Data at Room Temperature for Specimen No. 9

Frequency (Hz)	Amplitude Data: Displacement ($In \times 10^6$)	Load (Lb)	Phase Difference (Degrees)	Elastic Stiffness (Lb/In)	Dissipative Stiffness (Lb/In)	Joint Stiffness (Lb/In)	Loss Factor
0.1	80.13	4.49	8.298	67,324	12,036	74,173	0.1787
0.25	80.16	4.97	12.150	74,426	20,184	84,544	0.2712
0.5	80.12	5.48	28.746	67,899	49,903	93,217	0.7350
1.0	79.94	6.05	14.706	93,427	32,888	111,649	0.3520
10	71.57	8.75	14.022	180,924	76,501	253,088	0.4228
25	63.28	9.76	11.812	272,751	116,896	448,374	0.4286
50	60.42	10.45	9.027	357,571	131,789	673,633	0.3686
100	59.52	11.02	5.940	440,950	116,192	949,333	0.2635

Table F-9. Steady State Test Data at Room Temperature for Specimen No. 11

Frequency (Hz)	Amplitude Data: Displacement ($In \times 10^6$)	Load (Lb)	Phase Difference (Degrees)	Elastic Stiffness (Lb/In)	Dissipative Stiffness (Lb/In)	Joint Stiffness (Lb/In)	Loss Factor
0.1	80.78	3.39	2.754	48,482	2,700	51,402	0.0557
0.25	80.85	3.50	3.622	50,222	3,701	53,424	0.0737
0.5	80.78	3.59	3.892	51,830	4,124	55,268	0.0796
1.0	80.73	3.69	3.582	53,486	3,933	57,122	0.0735
10	72.40	3.82	4.806	63,256	6,423	68,549	0.1015
25	64.02	3.92	5.625	75,706	9,318	83,540	0.1231
50	61.17	4.05	5.841	83,432	10,888	93,063	0.1305
100	60.35	4.13	5.724	87,100	11,243	97,590	0.1291

Table F-10. Steady State Test Data at Room Temperature for Specimen No. 13

Frequency (Hz)	Amplitude Data		Phase Difference (Degrees)	Elastic Stiffness (Lb/In)	Dissipative Stiffness (Lb/In)	Joint Stiffness (Lb/In)	Loss Factor
	Displacement (In x 10^6)	Load (Lb)					
0.1	78.74	12.35	0.432	320,067	4,924	503,937	0.0154
0.25	78.51	12.38	0.450	322,374	5,185	509,688	0.0161
0.5	78.73	12.38	0.225	321,668	2,584	507,848	0.0080
1.0	78.57	12.38	0.216	322,739	2,493	510,520	0.0077
10	77.00	11.42	0.216	340,394	2,703	556,149	0.0079
25	62.48	11.13	0.180	422,935	3,155	816,485	0.0075
50	59.83	11.08	0.270	465,235	5,508	990,393	0.0118
100	59.11	11.06	0.288	477,840	6,133	1,049,343	0.0128

Table F-11. Steady State Test Data at Room Temperature for Specimen No. 14

Frequency (Hz)	Amplitude Data		Phase Difference (Degrees)	Elastic Stiffness (Lb/In)	Dissipative Stiffness (Lb/In)	Joint Stiffness (Lb/In)	Loss Factor
	Displacement (In x 10^6)	Load (Lb)					
0.1	78.42	14.73	1.044	481,795	22,558	1,071,009	0.0468
0.25	78.51	14.79	0.899	484,348	19,605	1,083,024	0.0405
0.5	78.58	14.86	1.890	487,604	41,776	1,106,491	0.0857
1.0	78.22	14.78	0.648	488,925	14,324	1,105,186	0.0293
10	70.19	13.63	0.468	526,700	11,670	1,318,310	0.0221
25	61.92	13.28	0.540	706,513	21,964	3,634,810	0.0311
50	59.17	13.19	0.675	808,649	34,611	10,427,726	0.0428
100	58.35	13.20	0.612	854,565	34,522	33,748,214	0.0404

Table F-12. Steady State Test Data at Room Temperature for Specimen No. 15

Frequency (Hz)	Amplitude Data: Displacement (In x 10^6)	Amplitude Data: Load (Lb)	Phase Difference (Degrees)	Elastic Stiffness (Lb/In)	Dissipative Stiffness (Lb/In)	Joint Stiffness (Lb/In)	Loss Factor
0.1	78.67	10.19	6.047	218,442	40,129	297,360	0.1837
0.25	78.72	10.83	5.760	243,185	44,569	344,219	0.1833
0.5	78.61	11.24	4.851	262,295	41,717	380,869	0.159
1.0	78.37	11.50	4.572	275,988	42,331	409,523	0.1534
10	70.15	11.26	2.106	334,372	25,737	542,811	0.0770
25	61.98	11.16	1.845	432,477	33,630	857,853	0.0777
50	59.25	11.15	1.593	482,239	34,538	1,076,703	0.0716
100	58.37	11.08	1.512	493,777	34,049	1,135,323	0.0689

Table F-13. Steady State Test Data at Room Temperature for Specimen No. 16

Frequency (Hz)	Amplitude Data: Displacement (In x 10^6)	Amplitude Data: Load (Lb)	Phase Difference (Degrees)	Elastic Stiffness (Lb/In)	Dissipative Stiffness (Lb/In)	Joint Stiffness (Lb/In)	Loss Factor
0.1	80.12	14.31	3.240	419,466	56,708	667,723	0.1352
0.25	80.28	14.79	2.700	453,985	53,435	756,002	0.1177
0.5	80.27	15.04	2.232	475,500	47,458	814,475	0.0998
1.0	80.12	15.18	1.494	491,544	33,394	858,472	0.0679
10	71.68	14.32	0.702	568,834	19,870	1,121,020	0.0349
25	63.42	14.09	0.742	797,624	37,191	2,580,660	0.0466
50	60.37	14.09	0.603	964,267	42,013	5,840,827	0.0436
100	59.81	14.15	0.450	1,021,568	34,693	8,813,848	0.0340

Table F-14. Steady State Test Data at Room Temperature for Specimen No. 18

Frequency (Hz)	Amplitude Data Displacement (In x 10^6)	Load (Lb)	Phase Difference (Degrees)	Elastic Stiffness (Lb/In)	Dissipative Stiffness (Lb/In)	Joint Stiffness (Lb/In)	Loss Factor
0.1	80.03	7.83	7.704	139,826	27,851	165,324	0.1992
0.25	80.07	8.61	10.395	156,922	44,656	193,650	0.2846
0.5	80.03	9.38	11.457	176,164	58,390	226,091	0.3315
1.0	79.80	10.12	10.674	201,193	65,332	265,809	0.3247
10	71.32	12.15	6.678	361,992	95,734	586,366	0.2645
25	63.08	12.55	5.422	530,824	143,685	1,172,099	0.2707
50	60.26	12.86	4.221	663,584	160,799	2,002,686	0.2418
100	59.37	13.15	2.754	770,381	132,589	3,184,719	0.1721

Table F-15. Steady State Test Data at Room Temperature for Specimen No. 21

Frequency (Hz)	Amplitude Data Displacement (In x 10^6)	Load (Lb)	Phase Difference (Degrees)	Elastic Stiffness (Lb/In)	Dissipative Stiffness (Lb/In)	Joint Stiffness (Lb/In)	Loss Factor
0.1	74.62	2.09	11.124	30,024	6,506	31,836	0.2167
0.25	74.63	2.36	13.410	33,989	9,062	36,646	0.2666
0.5	74.58	2.61	14.310	37,787	10,921	41,179	0.2890
1.0	74.33	2.85	12.978	42,235	11,163	45,974	0.2643
10	65.91	3.84	14.832	67,604	22,262	77,458	0.3293
25	58.17	4.31	11.565	93,373	25,332	108,737	0.2713
50	55.83	4.74	13.230	109,876	36,049	133,191	0.3281
100	55.09	5.20	8.928	131,715	30,009	159,672	0.2278

Table F-16. Pulse Method Damping Data for Specimen No. 3

Frequency (Hz)	Stress Level (Psi)	Damping Efficiency	Loss Factor	Phase Difference (Degrees)
0.1	4.568	0.8656	0.5511	28.86
0.25	5.493	0.6191	0.3941	21.51
0.5	6.167	0.4566	0.2906	16.20
1.0	6.678	0.2776	0.1767	10.02
10	7.514	0.2409	0.1382	7.87
25	7.542	0.2093	0.1332	7.59
50	7.608	0.1901	0.1210	6.90
100	7.606	0.2011	0.1280	7.29

Table F-17. Pulse Method Damping Data for Specimen No. 15

Frequency (Hz)	Stress Level (Psi)	Damping Efficiency	Loss Factor	Phase Difference (Degrees)
0.1	8.097	0.1490	0.0949	5.42
0.25	8.414	0.1397	0.0889	5.08
0.5	8.633	0.1271	0.0809	4.62
1.0	8.778	0.1277	0.0813	4.65
10	8.484	0.1231	0.0809	4.62
25	8.337	0.1307	0.0832	4.76
50	8.281	0.0861	0.0548	3.14
100	8.360	0.1004	0.0639	3.66

Table F-18. Stiffness Estimation fromWave Velocity Data

Specimen Number	Propagation Time (μsec)	Wave Velocity (In/Sec)	Equivalent Modulus (Psi x 10^{-6})	Equivalent Cross-Section (In^2)
13	30	333,333	15.65	0.225
14	25	400,000	22.30	0.324
1	45	222,222	6.88	0.0098
3	37	270,270	9.84	0.143
5	35	285,714	10.95	0.0105
7	40	250,000	8.45	0.136
9	38	263,158	9.02	0.048
11	45	222,222	6.95	0.037
15	37	270,270	10.24	0.271

Table F-19. Pulse Method Stiffness and Reflection Data for Specimen No. 3

Frequency (Hz)	Maximum Load (Lb)	Reflection Parameter (α_1)	Reflection Coefficient (A_{1R})	Transmission Coefficient (A_{1T})	Axial Stiffness (Lb/In)
0.1	4.568	0.3355	-0.497	0.5024	159,726
0.25	5.493	0.4278	-0.401	0.5992	203,668
0.5	6.167	0.5056	-0.328	0.6716	240,707
1.0	6.678	0.6387	-0.220	0.7795	304,074
10	7.514	1.2289	0.103	1.1027	585,058
25	7.542	1.7393	0.270	1.2699	828,051
50	7.608	1.6246	0.238	1.2380	773,444
100	7.606	1.7047	0.260	1.2605	811,578

Table F-20. Pulse Method Stiffness and Reflection Data for Specimen No. 15

Frequency (Hz)	Maximum Load (Lb)	Reflection Parameter (α_1)	Reflection Coefficient (A_{1R})	Transmission Coefficient (A_{1T})	Axial Stiffness (Lb/In)
0.1	8.097	0.8668	-0.0714	0.9286	412,668
0.25	8.414	0.9068	-0.0489	0.9511	431,712
0.5	8.633	1.0906	0.0433	1.0433	519,216
1.0	8.778	1.1011	0.0481	1.0481	524,215
10	8.484	1.6505	0.2454	1.2454	785,775
25	8.337	2.3380	0.4008	1.4008	1,113,082
50	8.281	2.1014	0.3551	1.3551	1,000,440
100	8.360	2.1647	0.3680	1.3680	1,030,576

Table F-21. Steady State Test Data at -50°F for Specimen No. 1

Frequency (Hz)	Amplitude Data Displacement (in x 10^6)	Amplitude Data Load (lb)	Phase Difference (degrees)	Elastic Stiffness (lb/in)	Dissipative Stiffness (lb/in)	Joint Stiffness (lb/in)	Loss Factor
0.25	81.83	16.27	3.074	311,786	26,410	483,625	0.08471
1.0	81.49	19.02	1.188	396,753	14,001	724,189	0.03529
25.0	64.37	17.88	0.788	382,139	7,229	676,936	0.01892
100.0	60.54	17.98	0.252	373,396	2,065	649,977	0.005531

Table F-22. Steady State Test Data at +25°F for Specimen No. 1

Frequency (Hz)	Amplitude Data Displacement (in x 10^6)	Amplitude Data Load (lb)	Phase Difference (degrees)	Elastic Stiffness (lb/in)	Dissipative Stiffness (lb/in)	Joint Stiffness (lb/in)	Loss Factor
0.25	81.41	12.63	12.600	209,184	68,025	274,660	0.3252
1.0	81.12	14.19	8.532	257,793	59,358	365,034	0.2303
25.0	64.59	15.05	3.118	324,344	24,698	514,499	0.07615
100.0	60.26	15.53	1.836	336,945	14,139	546,974	0.04196

Table F-23. Steady State Test Data at 75°F for Specimen No. 1

Frequency (Hz)	Amplitude Data Displacement (in x 10^6)	Amplitude Data Load (lb)	Phase Difference (degrees)	Elastic Stiffness (lb/in)	Dissipative Stiffness (lb/in)	Joint Stiffness (lb/in)	Loss Factor
0.25	82.34	0.94	46.260	7,859	8,551	11,795	1.0832
1.0	81.83	1.80	53.064	12,901	18,593	23,230	1.4411
25.0	64.71	7.50	29.160	110,188	74,259	156,587	0.6739
00.0	61.07	10.29	17.028	187,385	69,410	258,751	0.3704

Table F-24. Steady State Test Data at 200°F for Specimen No. 1

Frequency (Hz)	Amplitude Data		Phase Difference (degrees)	Elastic Stiffness (lb/in)	Dissipative Stiffness (lb/in)	Joint Stiffness (lb/in)	Loss Factor
	Displacement (in x 10^6)	Load (lb)					
0.25	81.45	0.14	10.035	1,652	294	1,681	0.1783
1.0	81.08	0.15	14.112	1,770	449	1,830	0.2537
25.0	64.12	0.22	25.110	3,127	1,487	3,477	0.4757
100.0	60.26	0.34	34.344	4,758	3,339	5,852	0.7017

Table F-25. Steady State Test Data at -50°F for Specimen No. 3

Frequency (Hz)	Amplitude Data		Phase Difference (degrees)	Elastic Stiffness (lb/in)	Dissipative Stiffness (lb/in)	Joint Stiffness (lb/in)	Loss Factor
	Displacement (in x 10^6)	Load (lb)					
0.25	81.76	11.97	0.0675	488,501	1,919	1,101,955	0.00393
1.0	81.53	12.04	0.540	486,702	15,128	1,092,934	0.0310
25.0	65.02	10.89	0.360	426,082	6,809	828,253	0.0160
100.0	61.18	10.72	0.6480	402,895	10,486	744,916	0.0260

Table F-26. Steady State Test Data at 25°F for Specimen No. 3

Frequency (Hz)	Amplitude Data		Phase Difference (degrees)	Elastic Stiffness (lb/in)	Dissipative Stiffness (lb/in)	Joint Stiffness (lb/in)	Loss Factor
	Displacement (in x 10^6)	Load (lb)					
0.25	81.64	9.98	0.630	207,316	3,866	271,448	0.0186
1.0	81.38	10.08	0.468	209,664	2,898	275,487	0.0138
25.0	64.66	9.05	0.540	215,559	3,130	285,755	0.0145
100.0	60.91	8.78	0.576	206,599	2,976	270,221	0.0144

Table F-27. Steady State Test Data at 75°F for Specimen No. 3

Frequency (Hz)	Amplitude Data: Displacement (in x 10^6)	Amplitude Data: Load (lb)	Phase Difference (degrees)	Elastic Stiffness (lb/in)	Dissipative Stiffness (lb/in)	Joint Stiffness (lb/in)	Loss Factor
0.25	78.58	6.38	21.195	89,586	44,571	112,940	0.4975
1.0	78.39	8.78	18.378	137,919	65,735	184,993	0.4766
25.0	61.68	10.54	5.467	243,584	33,716	341,649	0.1384
100.0	58.15	11.04	6.066	258,622	38,050	372,320	0.1471

Table F-28. Steady State Test Data at 200°F for Specimen No. 3

Frequency (Hz)	Amplitude Data: Displacement (in x 10^6)	Amplitude Data: Load (lb)	Phase Difference (degrees)	Elastic Stiffness (lb/in)	Dissipative Stiffness (lb/in)	Joint Stiffness (lb/in)	Loss Factor
0.25	81.06	1.74	1.485	23,800	683	24,473	0.0287
1.0	80.81	1.76	1.692	24,321	803	25,028	0.0330
25.0	63.87	1.66	1.845	28,991	1,040	30,001	0.0359
100.0	60.08	1.70	3.042	31,707	1,888	32,954	0.0595

Table F-29. Steady State Test Data at -50°F for Specimen No. 5

Frequency (Hz)	Amplitude Data: Displacement (in x 10^6)	Amplitude Data: Load (lb)	Phase Difference (degrees)	Elastic Stiffness (lb/in)	Dissipative Stiffness (lb/in)	Joint Stiffness (lb/in)	Loss Factor
0.25	81.25	15.64	0.450	297,915	3,622	451,047	0.01216
1.0	80.93	15.65	0.414	293,562	3,221	441,144	0.01097
25.0	63.95	13.98	0.360	278,688	2,231	408,391	0.008007
100.0	60.12	13.86	0.324	274,006	1,842	398,415	0.006724

Table F-30. Steady State Test Data at 25°F for Specimen No. 5

Frequency (Hz)	Amplitude Data Displacement (in x 10^6)	Amplitude Data Load (lb)	Phase Difference (degrees)	Elastic Stiffness (lb/in)	Dissipative Stiffness (lb/in)	Joint Stiffness (lb/in)	Loss Factor
0.25	82.50	15.18	2.025	287,603	15,937	427,823	0.05542
1.0	82.28	15.34	1.188	294,598	9,658	443,489	0.03279
25.0	65.06	13.98	0.630	291,228	4,339	435,894	0.01490
100.0	61.15	14.03	0.468	290,389	3,002	434,017	0.01034

Table F-31. Steady State Test Data at 75°F for Specimen No. 5

Frequency (Hz)	Amplitude Data Displacement (in x 10^6)	Amplitude Data Load (lb)	Phase Difference (degrees)	Elastic Stiffness (lb/in)	Dissipative Stiffness (lb/in)	Joint Stiffness (lb/in)	Loss Factor
0.25	80.51	4.06	36.945	41,733	37,361	59,833	0.8952
1.0	80.41	6.81	30.636	79,566	59,267	111,861	0.7449
25.0	63.84	11.15	8.325	220,710	41,823	301,932	0.1895
100.0	60.10	11.96	4.158	245,866	22,207	343,505	0.0903

Table F-32. Steady State Test Data at 200°F for Specimen No. 5

Frequency (Hz)	Amplitude Data Displacement (in x 10^6)	Amplitude Data Load (lb)	Phase Difference (degrees)	Elastic Stiffness (lb/in)	Dissipative Stiffness (lb/in)	Joint Stiffness (lb/in)	Loss Factor
0.25	81.40	0.78	0.540	10,093	99	10,211	0.0098
1.0	80.97	0.79	0.504	10,230	94	10,352	0.0092
25.0	63.95	0.75	2.745	12,213	613	12,401	0.0503
100.0	60.10	0.78	4.932	13,584	1,233	13,854	0.0908

Table F-33. Steady State Test Data at -50°F for Specimen No. 9

Frequency (Hz)	Amplitude Data: Displacement (in x 10^6)	Amplitude Data: Load (lb)	Phase Difference (degrees)	Elastic Stiffness (lb/in)	Dissipative Stiffness (lb/in)	Joint Stiffness (lb/in)	Loss Factor
0.25	81.44	16.56	0.270	324,940	2,446	516,026	0.007529
1.0	81.11	16.62	0.252	321,023	2,212	506,217	0.006892
25.0	64.08	14.86	0.225	300,527	1,529	457,063	0.005089
100.0	60.29	14.69	0.328	292,875	2,012	439,596	0.006873

Table F-34. Steady State Test Data at 25°F for Specimen No. 9

Frequency (Hz)	Amplitude Data: Displacement (in x 10^6)	Amplitude Data: Load (lb)	Phase Difference (degrees)	Elastic Stiffness (lb/in)	Dissipative Stiffness (lb/in)	Joint Stiffness (lb/in)	Loss Factor
0.25	81.73	14.42	2.880	269,064	20,740	388,051	0.07708
1.0	81.41	14.73	1.872	280,759	14,265	412,853	0.05081
25.0	64.26	13.62	1.215	285,647	8,169	423,510	0.02860
100.0	60.49	13.73	0.900	286,433	5,680	425,239	0.01983

Table F-35. Steady State Test Data at 75°F for Specimen No. 9

Frequency (Hz)	Amplitude Data: Displacement (in x 10^6)	Amplitude Data: Load (lb)	Phase Difference (degrees)	Elastic Stiffness (lb/in)	Dissipative Stiffness (lb/in)	Joint Stiffness (lb/in)	Loss Factor
0.25	80.16	4.97	12.150	68,900	17,106	77,241	0.2483
1.0	79.94	6.05	14.706	85,167	26,708	99,364	0.3136
25.0	62.28	9.76	11.812	184,991	48,559	244,563	0.2625
100.0	59.52	11.02	5.940	224,039	28,501	304,117	0.1272

Table F-36. Steady State Test Data at 200°F for Specimen No. 9

Frequency (Hz)	Amplitude Data		Phase Difference (degrees)	Elastic Stiffness (lb/in)	Dissipative Stiffness (lb/in)	Joint Stiffness (lb/in)	Loss Factor
	Displacement (in x 10^6)	Load (lb)					
0.25	81.00	1.99	0.585	27,598	316	28,496	0.0115
1.0	80.75	1.98	0.450	27,876	248	28,791	0.0089
25.0	63.80	1.84	2.250	32,426	1,437	33,703	0.0443
100.0	60.02	1.90	4.140	35,932	2,957	37,593	0.0823

Table F-37. Steady State Test Data at -50°F for Specimen No. 11

Frequency (Hz)	Amplitude Data		Phase Difference (degrees)	Elastic Stiffness (lb/in)	Dissipative Stiffness (lb/in)	Joint Stiffness (lb/in)	Loss Factor
	Displacement (in x 10^6)	Load (lb)					
0.25	81.12	6.30	5.400	89,971	9,929	100,250	0.1104
1.0	80.88	6.78	4.428	97,901	8,903	110,195	0.09094
25.0	63.84	7.11	3.870	124,718	9,478	145,381	0.07599
100.0	60.06	7.48	3.744	135,902	9,731	160,808	0.07161

Table F-38. Steady State Test Data at 25°F for Specimen No. 11

Frequency (Hz)	Amplitude Data		Phase Difference (degrees)	Elastic Stiffness (lb/in)	Dissipative Stiffness (lb/in)	Joint Stiffness (lb/in)	Loss Factor
	Displacement (in x 10^6)	Load (lb)					
0.25	81.42	3.97	5.310	53,729	5,526	57,233	0.1029
1.0	81.09	4.26	5.040	58,336	5,741	62,490	0.09843
25.0	64.07	4.70	5.400	80,052	8,313	88,088	0.1039
100.0	60.26	5.11	5.760	91,284	9,986	101,883	0.1094

Table F-39. Steady State Test Data at 75°F for Specimen No. 11

Frequency (Hz)	Amplitude Data: Displacement (in x 10^6)	Amplitude Data: Load (lb)	Phase Difference (degrees)	Elastic Stiffness (lb/in)	Dissipative Stiffness (lb/in)	Joint Stiffness (lb/in)	Loss Factor
0.25	80.85	3.50	3.622	47,481	3,306	50,326	0.0696
1.0	80.73	3.69	3.582	50,359	3,484	53,561	0.0692
25.0	64.02	3.92	5.625	66,037	7,064	71,852	0.1069
100.0	60.35	4.13	5.724	72,879	7,831	79,980	0.1075

Table F-40. Steady State Test Data at 200°F for Specimen No. 11

Frequency (Hz)	Amplitude Data: Displacement (in x 10^6)	Amplitude Data: Load (lb)	Phase Difference (degrees)	Elastic Stiffness (lb/in)	Dissipative Stiffness (lb/in)	Joint Stiffness (lb/in)	Loss Factor
0.25	81.90	3.38	1.215	50,716	1,321	53,845	0.0261
1.0	81.09	3.31	1.116	50,950	1,238	54,107	0.0243
25.0	64.92	3.19	2.430	60,772	3,197	65,384	0.0526
100.0	60.98	3.30	3.132	67,852	4,672	73,712	0.0688

Table F-41. Steady State Test Data at -50°F for Specimen No. 13

Frequency (Hz)	Amplitude Data: Displacement (in x 10^6)	Amplitude Data: Load (lb)	Phase Difference (degrees)	Elastic Stiffness (lb/in)	Dissipative Stiffness (lb/in)	Joint Stiffness (lb/in)	Loss Factor
0.25	82.09	17.36	0.270	346,017	2,668	571,289	0.007712
1.0	81.77	17.35	0.252	339,278	2,386	553,149	0.007034
25.0	64.62	15.54	0.270	314,955	1,944	491,292	0.006173
100.0	60.80	15.40	0.180	306,925	1,168	472,027	0.003807

Table F-42. Steady State Test Data at 25°F for Specimen No. 13

Frequency (Hz)	Amplitude Data		Phase Difference (degrees)	Elastic Stiffness (lb/in)	Dissipative Stiffness (lb/in)	Joint Stiffness (lb/in)	Loss Factor
	Displacement (in x 10^6)	Load (lb)					
0.25	81.84	15.70	0.765	307,882	6,601	474,294	0.02144
1.0	81.63	15.68	0.540	309,074	4,687	477,129	0.01517
25.0	64.43	14.04	0.900	296,643	6,346	448,138	0.02140
100.0	60.76	13.98	0.792	291,401	5,103	436,282	0.01751

Table F-43. Steady State Test Data at 75°F for Specimen No. 13

Frequency (Hz)	Amplitude Data		Phase Difference (degrees)	Elastic Stiffness (lb/in)	Dissipative Stiffness (lb/in)	Joint Stiffness (lb/in)	Loss Factor
	Displacement (in x 10^6)	Load (lb)					
0.25	78.65	12.38	0.450	234,906	2,752	320,809	0.0117
1.0	78.57	12.38	0.216	234,449	1,315	319,934	0.0056
25.0	62.48	11.13	0.180	231,258	943	314,019	0.0041
100.0	59.11	11.06	0.288	229,126	1,409	310,105	0.0062

Table F-44. Steady State Test Data at 200°F for Specimen No. 13

Frequency (Hz)	Amplitude Data		Phase Difference (degrees)	Elastic Stiffness (lb/in)	Dissipative Stiffness (lb/in)	Joint Stiffness (lb/in)	Loss Factor
	Displacement (in x 10^6)	Load (lb)					
0.25	81.41	7.91	0.180	172,354	961	214,485	0.0056
1.0	81.08	7.83	0.360	182,264	2,161	230,063	0.0119
25.0	64.56	7.07	0.203	192,488	1,195	246,582	0.0062
100.0	60.70	6.92	0.972	200,952	6,008	260,757	0.0299

Table F-45. Steady State Test Data at -50°F for Specimen No. 15

Frequency (Hz)	Amplitude Data		Phase Difference (degrees)	Elastic Stiffness (lb/in)	Dissipative Stiffness (lb/in)	Joint Stiffness (lb/in)	Loss Factor
	Displacement (in x 10^{6})	Load (lb)					
0.25	81.87	20.62	0.270	469,171	4,118	520,342	0.008779
1.0	81.61	20.63	0.288	456,681	4,147	505,023	0.009082
25.0	64.53	18.52	0.288	399,869	2,801	436,450	0.007005
100.0	60.72	18.48	0.360	385,168	3,063	418,995	0.007953

Table F-46. Steady State Test Data at 25°F for Specimen No. 15

Frequency (Hz)	Amplitude Data		Phase Difference (degrees)	Elastic Stiffness (lb/in)	Dissipative Stiffness (lb/in)	Joint Stiffness (lb/in)	Loss Factor
	Displacement (in x 10^{6})	Load (lb)					
0.25	81.02	16.76	0.405	348,541	4,152	578,202	0.01191
1.0	80.76	16.73	0.864	349,946	8,918	582,079	0.02548
25.0	63.79	14.88	0.810	325,814	6,437	518,234	0.01976
100.0	60.00	15.07	0.539	326,243	3,993	519,319	0.01224

Table F-47. Steady State Test Data at 75°F for Specimen No. 15

Frequency (Hz)	Amplitude Data		Phase Difference (degrees)	Elastic Stiffness (lb/in)	Dissipative Stiffness (lb/in)	Joint Stiffness (lb/in)	Loss Factor
	Displacement (in x 10^{6})	Load (lb)					
0.25	78.72	10.84	5.760	190,939	27,119	247,180	0.1420
1.0	78.38	11.51	4.572	209,662	24,185	277,889	0.1154
25.0	61.74	11.16	1.845	235,617	9,901	322,494	0.0420
100.0	58.38	11.08	1.512	232,994	7,553	317,450	0.0324

Table F-48. Steady State Test Data at 200°F for Specimen No. 15

Frequency (Hz)	Amplitude Data: Displacement (in x 10^6)	Amplitude Data: Load (lb)	Phase Difference (degrees)	Elastic Stiffness (lb/in)	Dissipative Stiffness (lb/in)	Joint Stiffness (lb/in)	Loss Factor
0.25	81.30	6.57	0.495	126,942	1,722	148,426	0.0136
1.0	81.03	6.56	0.144	133,788	555	157,857	0.0042
25.0	64.13	5.97	0.450	147,056	1,823	176,676	0.0124
100.0	60.30	6.03	0.882	160,828	3,986	196,980	0.0248

Table F-49. Steady State Test Data at -50°F for Specimen No. 18

Frequency (Hz)	Amplitude Data: Displacement (in x 10^6)	Amplitude Data: Load (lb)	Phase Difference (degrees)	Elastic Stiffness (lb/in)	Dissipative Stiffness (lb/in)	Joint Stiffness (lb/in)	Loss Factor
0.25	81.68	20.34	0.855	459,141	12,642	963,043	0.02754
1.0	81.38	20.47	0.216	452,724	3,071	935,235	0.006785
25.0	77.68	18.60	0.090	313,336	643	487,636	0.002055
100.0	60.52	18.59	0.090	389,645	776	700,852	0.001993

Table F-50. Steady State Test Data at 25°F for Specimen No. 18

Frequency (Hz)	Amplitude Data: Displacement (in x 10^6)	Amplitude Data: Load (lb)	Phase Difference (degrees)	Elastic Stiffness (lb/in)	Dissipative Stiffness (lb/in)	Joint Stiffness (lb/in)	Loss Factor
0.25	81.28	15.61	1.305	308,393	11,291	475,509	0.03661
1.0	80.99	15.69	0.576	313,446	5,097	487,630	0.01626
25.0	63.95	14.11	0.675	301,856	4,865	460,145	0.01612
100.0	60.15	14.07	0.576	297,577	3,807	450,274	0.01279

Table F-51. Steady State Test Data at 75°F for Specimen No. 18

Frequency (Hz)	Amplitude Data: Displacement (in x 10^6)	Amplitude Data: Load (lb)	Phase Difference (degrees)	Elastic Stiffness (lb/in)	Dissipative Stiffness (lb/in)	Joint Stiffness (lb/in)	Loss Factor
0.25	80.07	8.61	10.395	134,235	31,941	163,729	0.2379
1.0	79.80	10.12	10.674	165,575	42,687	212,373	0.2578
25.0	63.08	12.55	5.422	264,844	33,871	383,773	0.1279
100.0	59.37	13.15	2.754	282,018	17,322	416,737	0.0614

Table F-52. Steady State Test Data at 200°F for Specimen No. 18

Frequency (Hz)	Amplitude Data: Displacement (in x 10^6)	Amplitude Data: Load (lb)	Phase Difference (degrees)	Elastic Stiffness (lb/in)	Dissipative Stiffness (lb/in)	Joint Stiffness (lb/in)	Loss Factor
0.25	81.04	4.42	0.203	72,323	338	78,820	0.0047
1.0	80.76	4.44	0.702	75,034	1,255	82,062	0.0167
25.0	63.90	4.12	1.215	86,348	2,454	95,811	0.0284
100.0	60.07	4.20	1.800	95,005	4,062	106,638	0.0428

Table F-53. Steady State Test Data at -50°F for Specimen No. 21

Frequency (Hz)	Amplitude Data: Displacement (in x 10^6)	Amplitude Data: Load (lb)	Phase Difference (degrees)	Elastic Stiffness (lb/in)	Dissipative Stiffness (lb/in)	Joint Stiffness (lb/in)	Loss Factor
0.25	81.54	13.22	3.474	229,918	19,904	311,550	0.08657
1.0	81.29	13.99	3.528	245,921	21,799	341,677	0.08865
25.0	64.34	15.01	4.230	301,103	28,931	458,397	0.09608
100.0	60.50	15.92	2.880	320,677	19,715	505,358	0.06148

Table F-54. Steady State Test Data at 25°F for Specimen No. 21

Frequency (Hz)	Amplitude Data Displacement (in x 10^6)	Load (lb)	Phase Difference (degrees)	Elastic Stiffness (lb/in)	Dissipative Stiffness (lb/in)	Joint Stiffness (lb/in)	Loss Factor
0.25	81.38	9.43	4.860	148,974	16,422	179,437	0.1102
1.0	81.03	9.95	4.572	160,793	16,976	196,867	0.1056
25.0	63.95	10.15	5.399	195,306	22,918	251,221	0.1173
100.0	60.15	10.77	4.896	213,021	21,844	281,312	0.1025

Table F-55. Steady State Test Data at 75°F for Specimen No. 21

Frequency (Hz)	Amplitude Data Displacement (in x 10^6)	Load (lb)	Phase Difference (degrees)	Elastic Stiffness (lb/in)	Dissipative Stiffness (lb/in)	Joint Stiffness (lb/in)	Loss Factor
0.25	74.63	2.36	13.410	32,790	8,389	35,204	0.2559
1.0	74.33	2.85	12.978	40,377	10,137	43,704	0.2511
25.0	58.17	4.31	11.565	79,688	18,069	90,101	0.2267
100.0	55.09	5.20	8.928	102,309	17,729	117,770	0.1733

Table F-56. Steady State Test Data at 200°F for Specimen No. 21

Frequency (Hz)	Amplitude Data Displacement (in x 10^6)	Load (lb)	Phase Difference (degrees)	Elastic Stiffness (lb/in)	Dissipative Stiffness (lb/in)	Joint Stiffness (lb/in)	Loss Factor
0.25	81.30	0.85	10.755	10,725	2,139	11,075	0.1995
1.0	81.08	0.94	11.448	12,014	2,581	12,463	0.2149
25.0	64.29	1.16	8.370	19,084	3,024	19,757	0.1585
100.0	60.42	1.30	8.064	23,165	3,577	24,083	0.1544

Appendix G

PIEZOELECTRIC TRANSDUCER DEVELOPMENT

Introduction

To obtain good generic damping data from the simplified steady state test method, an absolute displacement input was required. The use of piezoelectric materials, which are very stiff and produce an absolute displacement directly proportional to an applied voltage, was a logical choice for construction of a displacement transducer. Wilcoxon Research of Bethesda, Maryland was selected to design and manufacture the device as per the specifications described in Appendix D. Subsequent testing with the transducer revealed that it had the proper piezoelectric characteristics but certain properties of its mechanical construction produced results that were questionable. These uncertainties were eventually resolved when the actual properties of the piezoelectric transducer (determined by test) were compared with the physical laws that govern its behavior. To present our understanding of those relationships, the following topics will be discussed in this appendix:

a) Unloaded Transducer Characteristics

b) Loaded Transducer Characteristics

c) Summary of Performance

Unloaded Transducer Characteristics

The development history of the test apparatus, and particularly the piezoelectric shaker (more properly called a positioner or actuator) is worthy of discussion because in the final analysis everything worked pretty much as expected and the difficulties encountered along the way were largely the result of failure to appreciate all of the consequences of that very basic relationship

$$\ddot{X}(t) = -\omega^2 x \sin \omega t \tag{G-1}$$

and $$|X| = \frac{|\ddot{X}|}{\omega^2}$$

The first difficulty encountered was reported in the first annual report (Ref. 4 of the main report) which was a nonlinearity due to an inappropriate crystal choice by the manufacturer. The manufacturer rectified this problem (at no cost) and shipped the transducer to GIT in June. The results provided by the

manufacturer showed extremely good linearity and flat frequency response over the range tested (100 to 1000 Hz). The only surprise was that the transducer sensitivity rating of 0-3 μin/volt was in terms of peak μin per rms volt. This result meant that a 40% higher power supply voltage was required to obtain the full ±100 μin range (or nearly 500 volts 0 to peak). Since this posed a basic feasibility problem it was decided to live with a ±70 μin capability instead, because the response is still in the appropriate order of magnitude. The calibration data provided by the manufacturer is given in Annex A of this appendix.

GIT attempted to duplicate the measurements and encountered two problems: (1) what appeared to be a noisy and distorted output, and (2) rising sensitivity at frequencies below 100 Hz. The transducer was returned to the manufacturer for evaluation. They found the cause of the second problem but were unable to duplicate the first problem. The cause of the second problem was radial strain of the exciter crystal being transmitted to the accelerometer that GIT had cemented to the transducer face. Piezoelectric accelerometers are somewhat sensitive to case strain and thus can act as a load cell. The displacement transducer output really is independent of frequency from 0 Hz to about 1/3 of the internal resonance frequency (over 5 kHz). However, when a constant displacement is measured with an accelerometer, the output of the accelerometer increases with the square of the frequency (Eq. G-1). The case strain effect, which is a load transfer due to the radial component of the strain in the crystal, is also independent of frequency. An error signal (not acceleration related) is generated by the accelerometer that is correspondingly independent of frequency. At some point in the low frequency range as one decreases frequency the case strain signal is no longer trivial compared to the decreasing acceleration related output. The data provided by the manufacturer is given in Fig. G-1 (from Annex B) along with a curve fit of the data. If the above hypothesis is indeed correct then the equation below can be used to define the sensitivity of the transducer as a function of frequency, f:

$$(S) = a + bf^{-2} \qquad \text{(G-2)}$$

where S = the apparent sensitivity based on accelerometer output divided by ω^2 and the excitation voltage

a = true displacement response

b = case strain constant

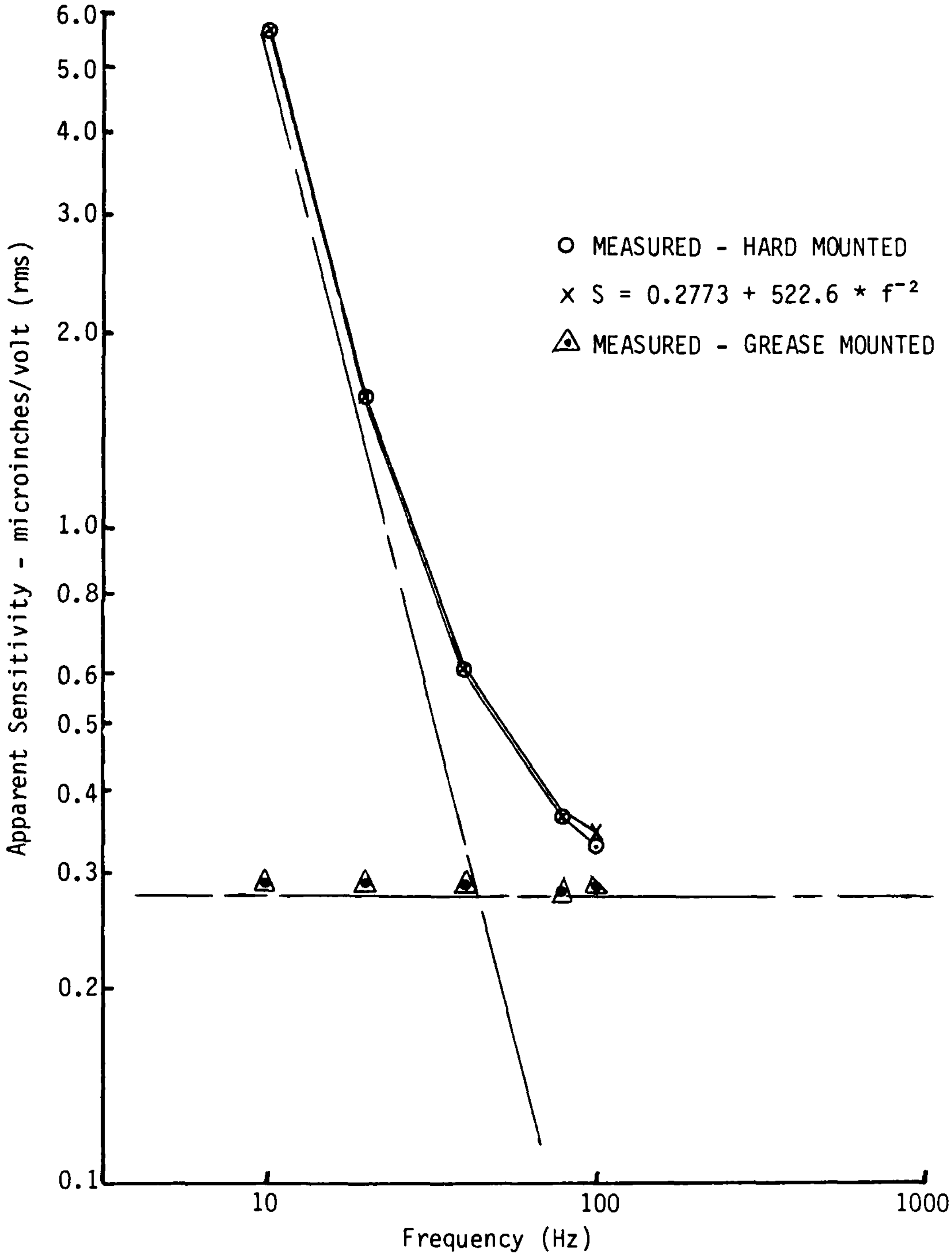

Figure G-1. Effect of Case Strain on Accelerometer-Based Sensitivity

As can be seen in the figure, the fit is virtually exact and the "a" term comes out within 2% of the values measured with the same accelerometer isolated by grease. These results satisfactorily support the case strain hypothesis.

The first problem, namely the distorted noisy signal, ultimately was also traced to Eq. G-1. Since the piezoelectric transducer is a pure displacement device for an applied voltage independent of frequency, an accelerometer will effectively pre-emphasize the higher frequency residuals at a slope of +12 dB per octave. It was discovered that the digital function generator used by GIT to generate sine waves did so using a numerically synthesized procedure with a digital-to-analog converter providing the transformation to voltage. The resulting output consisted of a series of tiny "stairsteps" approximating a sine wave. While nearly invisible on an oscilloscope, because of the small Δt, the displacement transducer followed the stairsteps faithfully. The effective double differentiation of these stairsteps accomplished by the accelerometer raised their significance from trivial in the displacement domain to overwhelming in the acceleration domain. After an old bridge-type analog signal generator was found, the problem was largely cleared up.

Some noise and harmonic distortion were still present, principally because of the low acceleration levels associated with these small motions and the inevitable pre-emphasis produced by the accelerometer. Output signal quality was checked by forcing a load cell with the transducer to get rid of the pre-emphasis. Harmonic distortion was well under 1% with this approach and agreed reasonably well with the accelerometer results de-emphasized by 12 dB per octave. This result cleared up all of the questions associated with the unloaded response of the transducer.

Loaded Transducer Characteristics

The simplified steady state method of complex stiffness measurement is based on providing stiff low loss restraints for the specimen compared to the specimen stiffness. This includes having a very stiff displacement exciter. If this condition is not met, it is of no theoretical consequence as long as the stiffness of the remainder of the structural loop is known. The practical

consequence, however, is loss of sensitivity. It is therefore highly desirable to meet the high fixture and stiffness conditions. The transducer was therefore designed to have a stiffness well in excess of 2×10^6 lb/in.

An aluminum calibration bar with a theoretical axial stiffness of about 231,000 lb/in. was provided to GIT so that a fixture stiffness check could be made. With this bar in place it was determined that the apparent sensitivity of the displacement transducer fell to about 0.14 μin/volt down from an unloaded value of 0.2 μin/volt. This result was much lower than expected because the calculated added flexibility of the fixture to the bar was only around 2-3%, and the transducer in a self resonance test had a demonstrated stiffness of at least 5×10^6 lb/in. An accelerometer survey did confirm that nothing else was vibrating consequentially in the fixture including the rear face of the transducer. It was therefore concluded that there must be some unaccounted flexibility in the transducer or its attachments internally. The loss of sensitivity, although more significant than desired, did not affect the testing because a value of flexibility was determined for the correction term required by the method. This value is determined as follows:

$$F' = K_S \hat{X}' \tag{G-3}$$

where F' = lb/volt output

K_S = specimen stiffness

$\hat{X}'$ = apparent displacement sensitivity

150 volts yielded about 5 lb load reading, giving

$F' = .0333$ lb/volt

$K = 231{,}000$

thus $X' = .144$ μin/volt

If the flexibility is inside the transducer, then it is in series with the specimen and the following equation can be written:

$$F' = \left[\frac{1}{K_S} + \frac{1}{K_T}\right]^{-1} X' \tag{G-4}$$

where K_T = transducer stiffness

X' = unloaded transducer sensitivity = 0.2 μin/volt

Substituting values gives

$$K_T \approx 598{,}000 \text{ lb/in.}$$

The experimentation was carried out with this value.

During a lull in the testing for a GIT facility change, the transducer was shipped to MDAC-HB for some load/deflection testing to check its internal stiffness.

Three series of compression tests were run on the transducer to determine the stiffness of the device. During test series 1 the transducer table was uniformly loaded up to 1000 lb using the test setup shown in Fig. G-2a. After running the initial test the transducer was rotated to the 120° and 240° positions to establish the consistency of the test setup (the extensometer had to be removed prior to each rotation). The transducer was then rotated the final 120° to its original position to establish the repeatability of the results. The experimental results for the uniformly loaded condition are presented in Fig. G-3a. These results indicate a high load range (200-1000 lb) stiffness of 4.4-5.0 million lb/in. and a low load range (0-200 lb) stiffness of 500,000-900,000 lb/in.

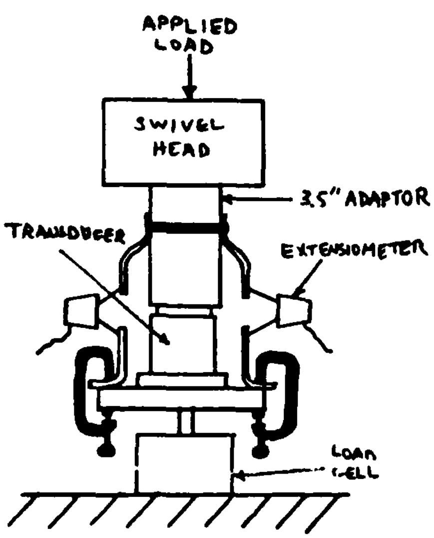

Figure 2a. Uniform Load

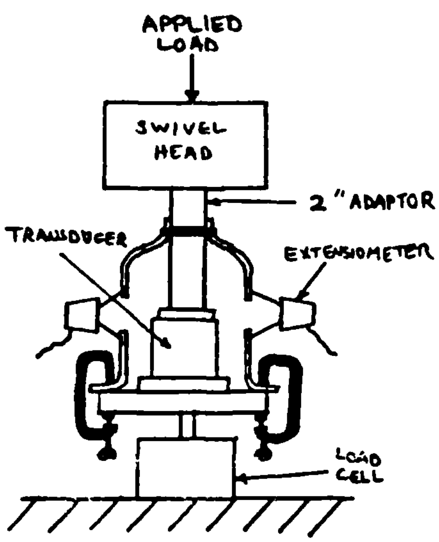

Figure 2b. Nonuniform Load

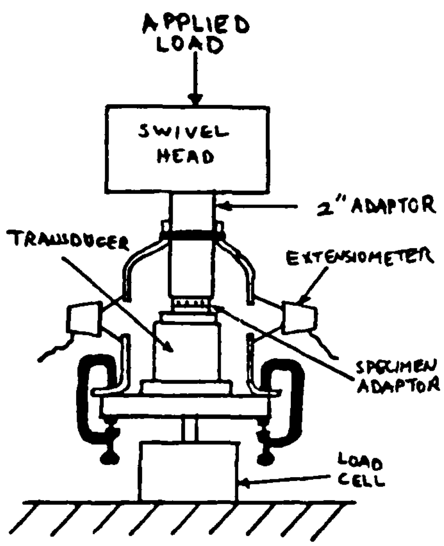

Figure 2c. Specimen Adaptor

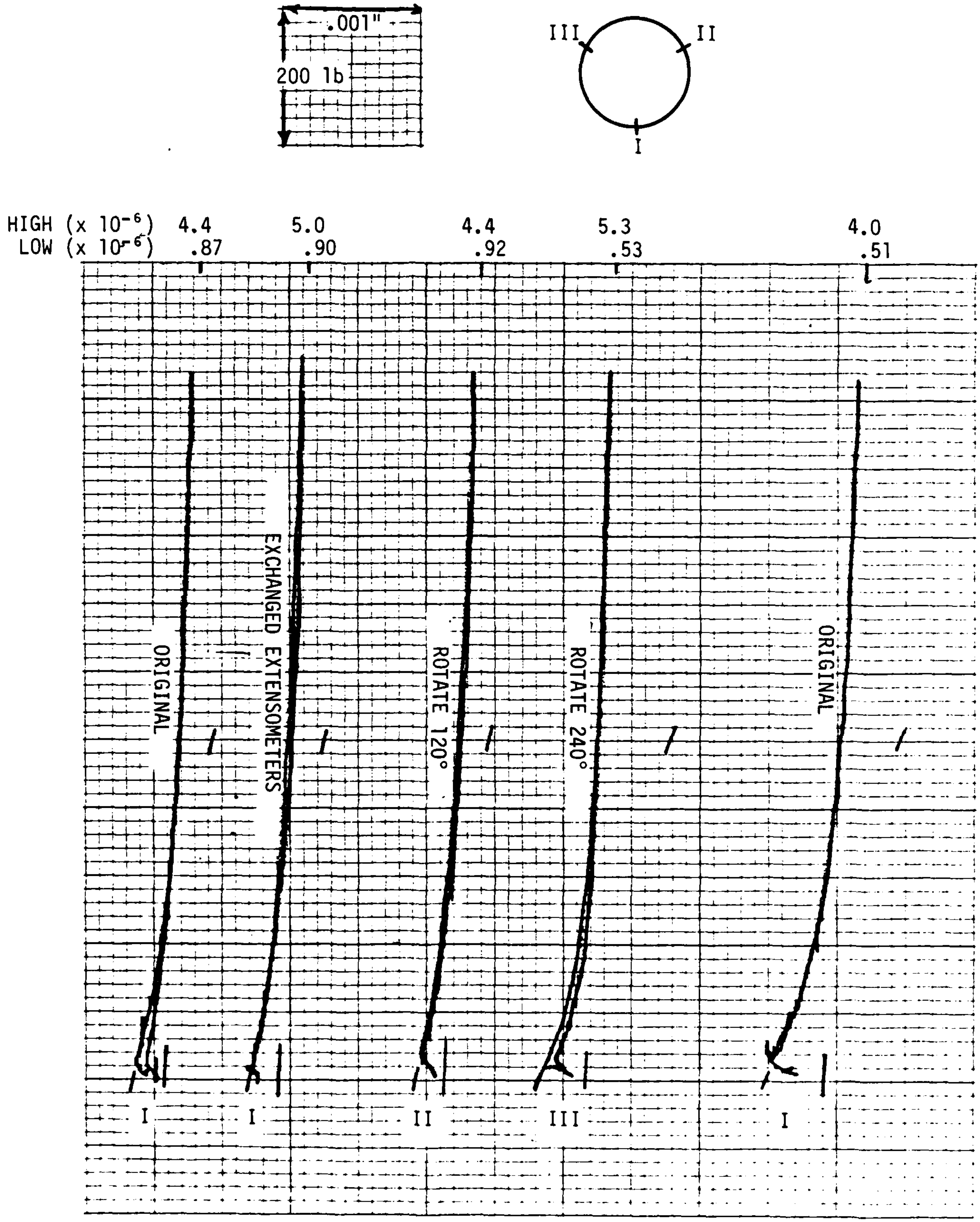

Figure G-3a. Uniform Load Across Table

For test series 2 the transducer table was loaded over a smaller area to establish any variation in stiffness due to nonuniform loading of the table. The test setup is shown in Fig. G-2b and the experimental results are presented in Fig. G-3b. The high load stiffness is 4.4-5.3 million lb/in. and the low load stiffness is 430,000-500,000 lb/in.

For test series 3 the specimen adaptor was bolted to the transducer table and then loaded up to 1000 lb to determine the influence of the adaptor on the transducer's stiffness. The test setup is shown in Fig. G-2c and the experimental results are presented in Fig. 3c. The high load stiffness is 1.5 to 2.5 million lb/in. and the low load stiffness is 500,000 to 600,000 lb/in.

During test series 1 and 2, with a 1000 lb load on the transducer table, a voltage of 150 was applied to the transducer with the correct polarity to cause relaxation. The measured load on the transducer dropped by approximately 9 lb due to the applied voltage. The Instron test machine was then loaded head to head with just the transducer removed in order to determine the machine foundation stiffness. The deflections were based on the loading jack screw travel and the load was read from the same cells used to test the transducer. Fig. G-4 shows the result, which is about 315,000 lb/in.

Using the 9 lb change in load, a test machine stiffness of 315,000 lb/in., and a high load transducer stiffness of 5 million lb/in. in Eq. G-4, the unloaded sensitivity of the transducer is computed to be 0.205 μin/volt. This 0 Hz result, when multiplied by $\sqrt{2}$ to rationalize units, is nearly the exact result obtained by the manufacturer nine months earlier using AC methods.

The suspected 500,000 lb/in. transducer stiffness computed from joint specimen test results has been verified. The stiffness of the transducer in the low load range (0-200 lb) is essentially unaffected by table load distribution or the presence of the specimen adaptor. In the high load range (200-1000 lb) the specimen adaptor does introduce some additional flexibility, reducing the overall stiffness by approximately 60%. These experimental results indicate that there are elements within the transducer that are not fully seated. The self resonance tests conducted seemed to indicate much higher stiffness and such a test is definitely a low load test. A review of the effect of end conditions on the self resonant frequency of a bar shows that frequency is

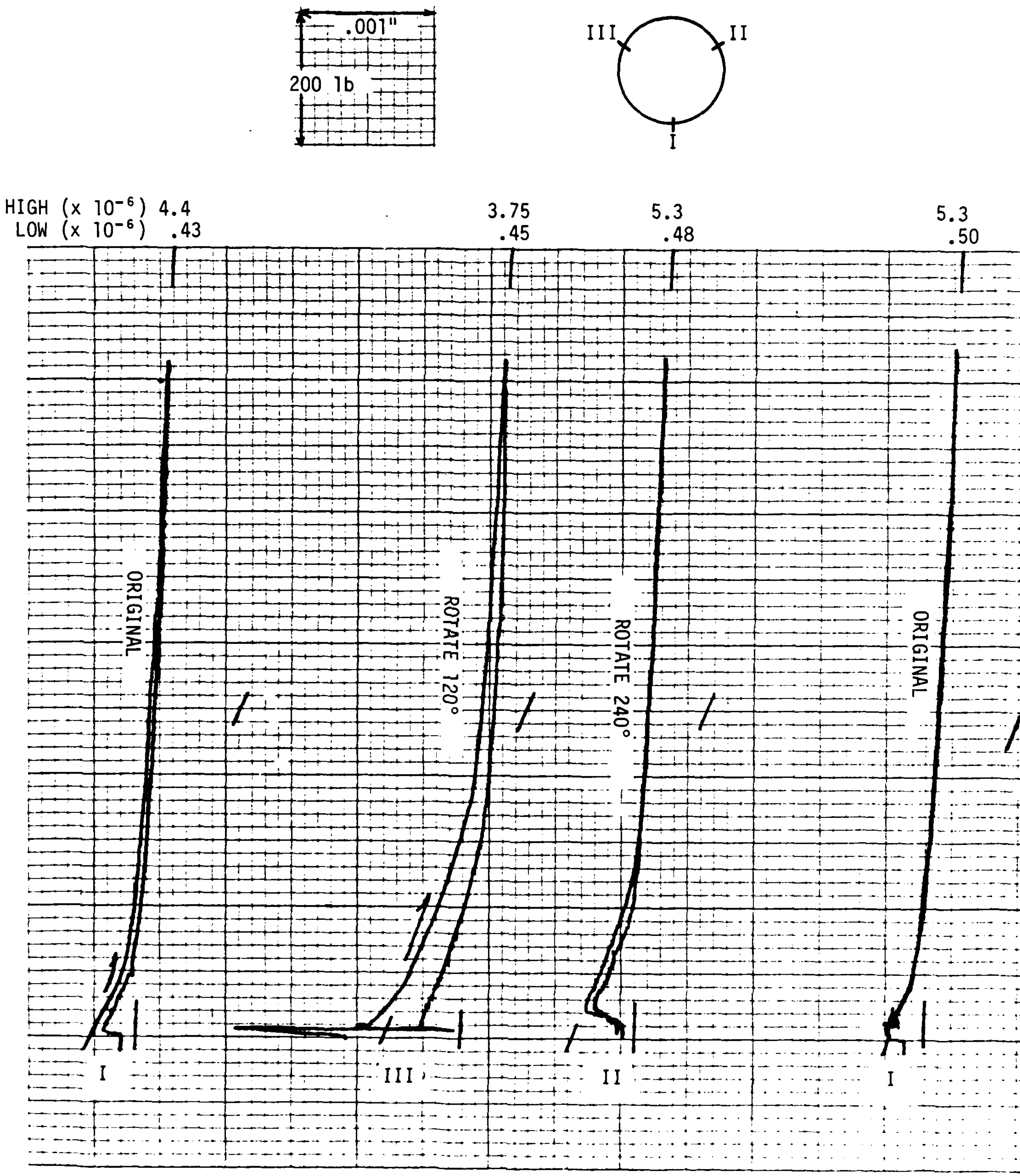

Figure G-3b. Smaller Loading Area - 2" Diameter

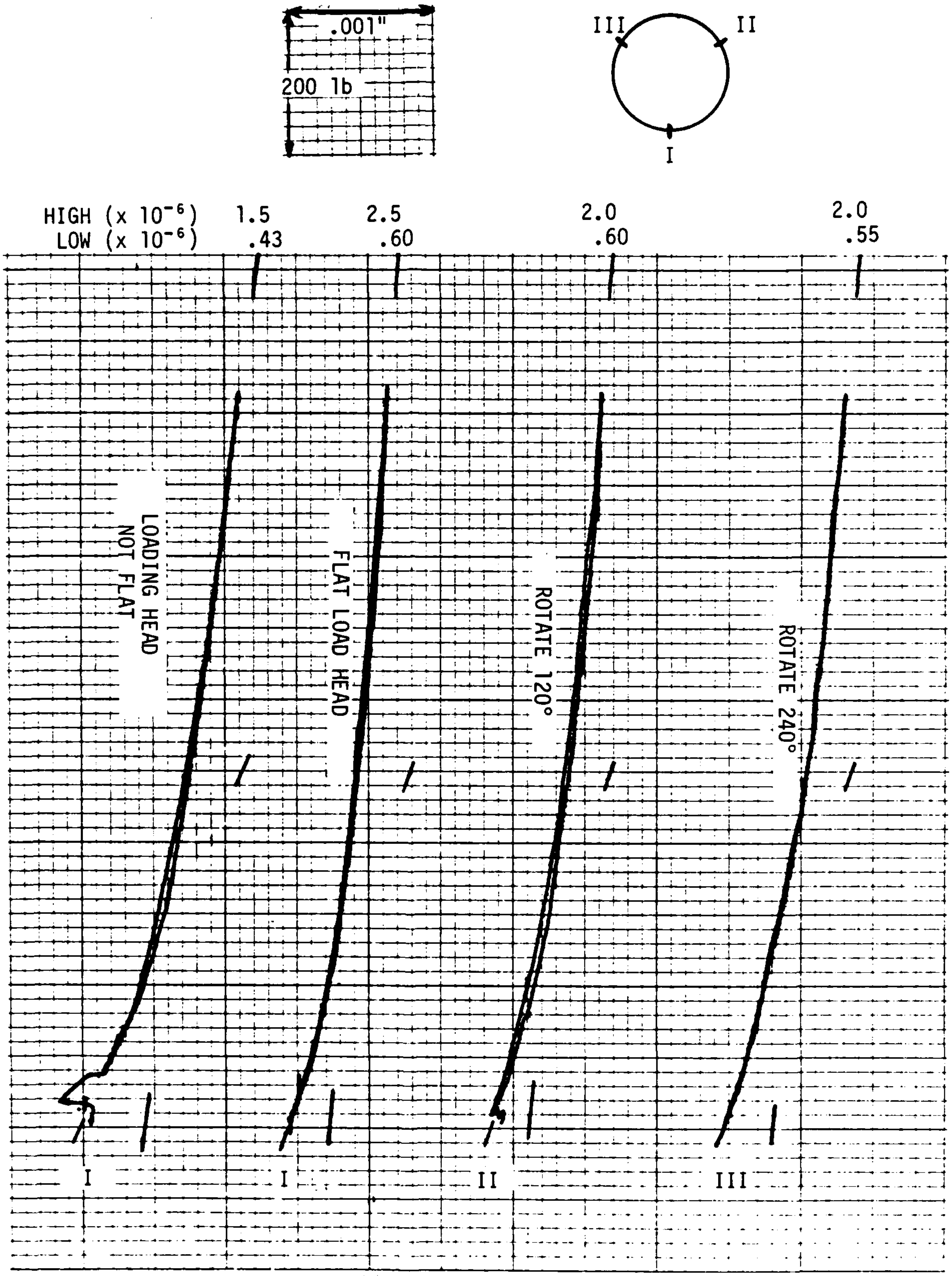

Figure G-3c. Loaded with Specimen Adapter on Table

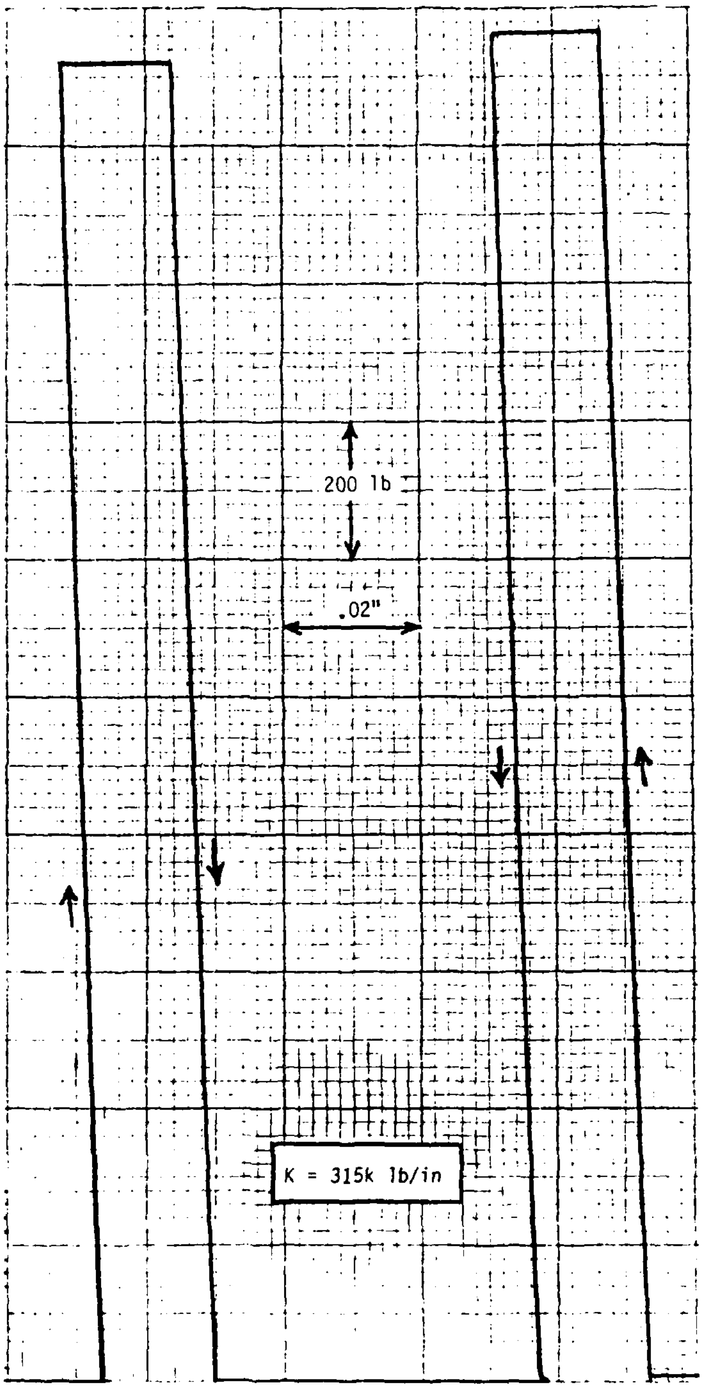

Figure G-4. Frame and Load Cell Stiffness

unaffected by changing from blocked to free end conditions. It is only affected by the properties of the bar itself. A simple calculation using the properties of ceramics shows that the ceramic disc stack should have a resonant frequency in the neighborhood of 5 kHz, which is about the observed value. It is therefore concluded that the disc stack (the bar) is well seated because 400,000 to 600,000 stiffness in the stack would lead to far lower self resonances.

The load head, on the other hand, is only 3/4 inch thick and is preloaded only at one point in the center. This arrangement leads to the possibility that a slight warpage (on the order of a few ten thousandths of an inch) might result from the preloading point (1000 lb at the center). Except for larger-than-desired flexibility at low loads, the nonlinear character of these high load range tests does not affect the GIT testing because the load range involved in the testing is only a few lbs. If higher stiffness in the low load range is desired, the stack would have to be preloaded to higher levels and a thicker load head used to avoid warpage and a reccurrence of the problem. A summary table of the test results is presented below.

		Stiffness	
Test Series	Description	Low Load 0-200 lb (x 10^{-3} lb/in)	High Load 200-1000 lb (x 10^{-6} lb/in)
1	Uniform Load	500-900	4.4-5.0
2	Nonuniform Load	430-500	4.4-5.3
3	Specimen Adaptor	550-600	1.5-2.5

These results were obtained at room temperature. Low temperature testing at GIT has also suggested that the transducer may be sensitive to temperature variations. To account for this factor, the compliance of the transducer and load cells mounted in the test fixture was experimentally determined as a function of both temperature and frequency using a reference specimen. These compliance values (listed in Appendix D) were used to compute the results from the simplified steady state methods for all the environmental testing.

Summary of Performance

The Wilcoxon displacement transducer performs within the intent of the design requirements placed on it. The transducer has successfully performed in the test program at all frequencies and loads and with all specimens. The historical discussion presented here serves to illustrate the cautions that must be observed with using a near-true position transducer. All of the design objectives, including the stiffness, could be met with minor redesigns of the transducer. Results of the GIT testing, discussed elsewhere, indicate that the simplified steady-state method using a piezoelectric exciter can greatly improve the accuracy and ease of complex modulus measurements.

Appendix G - Annex A

WILCOXON INITIAL CALIBRATION DATA

June 27, 1984

GEORGIA INSTITUTE OF TECHNOLOGY

PIEZOELECTRIC SHAKER

The Piezoelectric shaker was tested in the calibration laboratory at Wilcoxon Research. The shaker was driven by a 500 W audio amplifier. A 60 pound blocking mass was used to "back" the shaker and a reference accelerometer was used to measure the acceleration.

The transfer function, between accelerometer output and shaker input signal, was measured using a Hewlett Packard Spectrum Analyzer. The test results were tabulated and graphed for your convenience.

The shaker assembly was heated to 230°C and returned to room temperature in order to achieve the initial drop in sensitivity expected in a compressed crystal stack of this type. However, during our subsequent temperature test, the sensitivity dropped 6% after 16 hours at 200°C. Therefore, the data describing displacement as a function of temperature is given in percent change rather than measured displacement. Although the shaker has been temperature cycled, it is probable that an additional drop in sensitivity will occur as a result of high temperature duty.

Additional data indicating displacement (in micro inches peak per volt rms) as a function of drive voltage and frequency are provided. These data were taken after temperature cycling.

If we can be of any further help don't hesitate to contact our product engineering department.

I. Displacement as a function of drive voltage, d(V):

V in	xFunc	peak in/V rms $\times 10^{-7}$	
			f=504 Hz 25°C
20	5.12×10^{-2}	2.97×10^{-6}	
50	5.10×10^{-2}	2.96×10^{-6}	
100	5.11×10^{-2}	2.97×10^{-6}	
150	5.09×10^{-2}	2.96×10^{-6}	
200	5.10×10^{-2}	2.96×10^{-6}	
250	5.10×10^{-2}	2.96×10^{-6}	
300	5.14×10^{-2}	2.99×10^{-6}	

II. Displacement as a function of temperature, d(T): f=504 Hz; V in=100 V rms.

T°C	Calculated Displacement % Deviation
-40	8.4
0	6.0
25	0
100	0.8
150	8.0
200	16.3

* Allow 1% experimental error. (No loading block)

III. Displacement as a function of frequency, d(f):

Frequency	XFunc	peak in /V rms $\times 10^{-7}$	25°C/100 Vrms.
100	2.05×10^{-3}	3.06×10^{-6}	
200	7.99×10^{-3}	2.98×10^{-6}	
300	1.82×10^{-2}	3.02×10^{-6}	
400	3.20×10^{-2}	2.99×10^{-6}	
504	5.14×10^{-2}	3.02×10^{-6}	
600	7.42×10^{-2}	3.08×10^{-6}	
696	9.89×10^{-2}	3.05×10^{-6}	
800	1.30×10^{-1}	3.03×10^{-6}	
896	1.67×10^{-1}	3.11×10^{-6}	
1000	2.07×10^{-1}	3.09×10^{-6}	

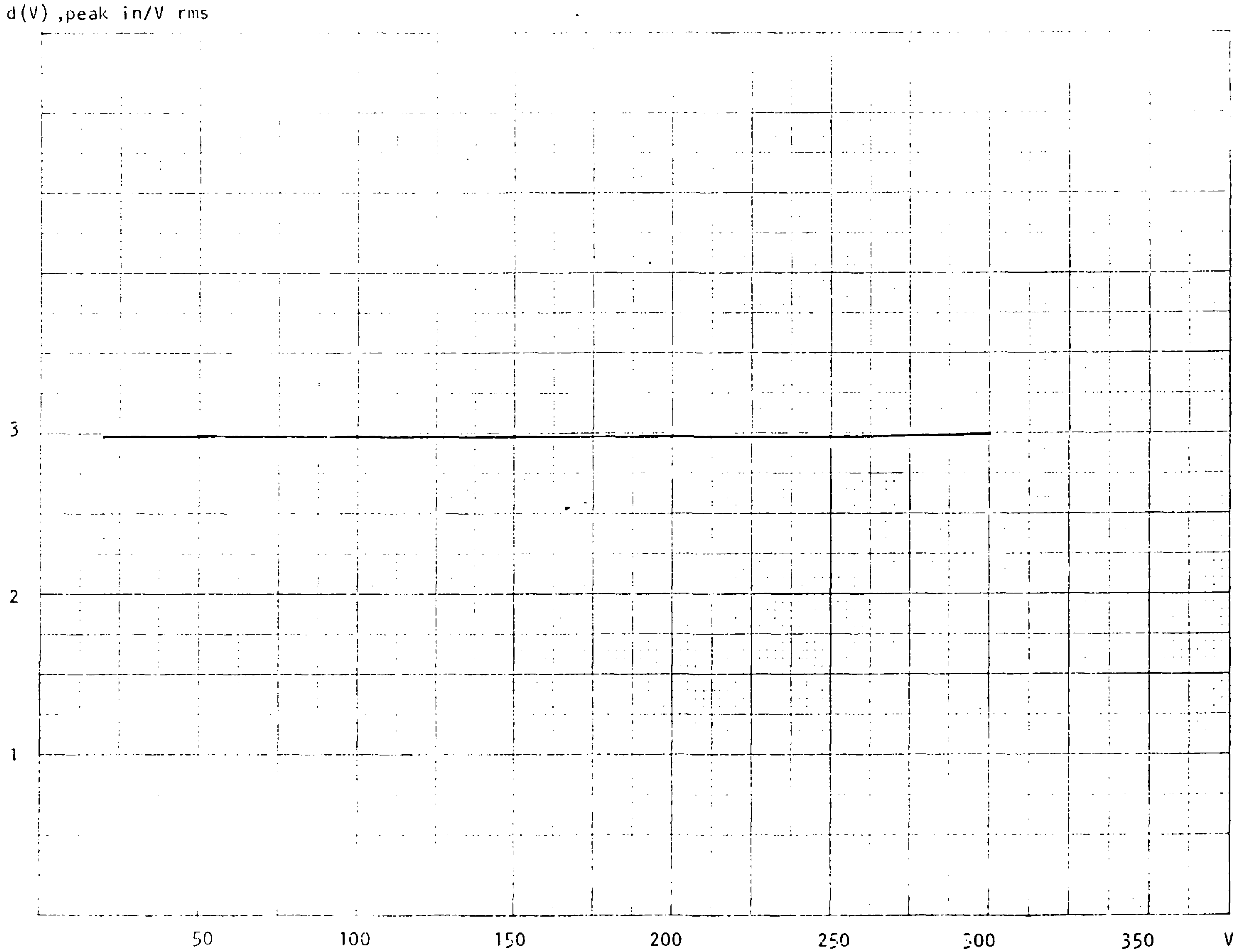

(Fig. 1)

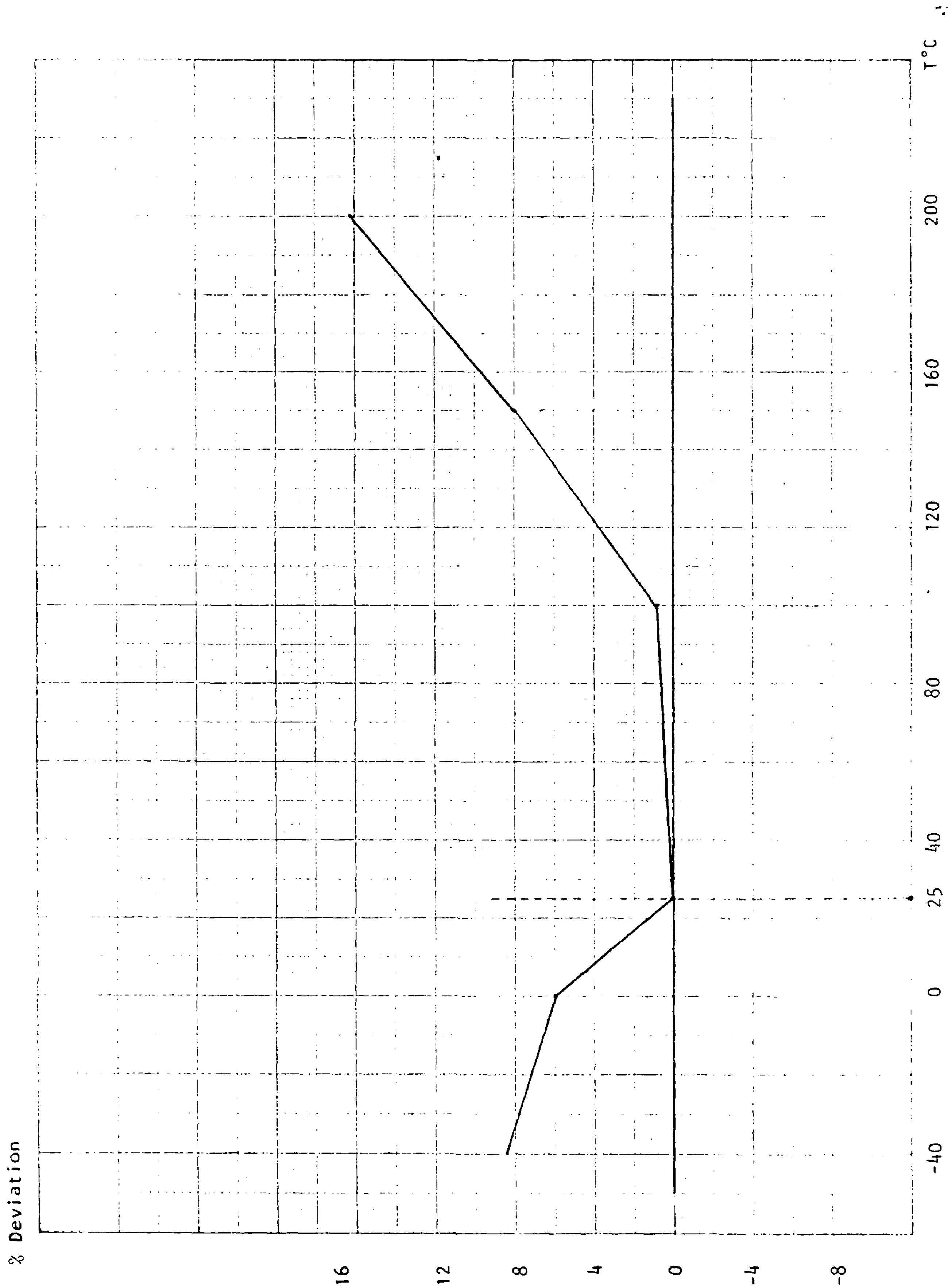

(Fig. 2)

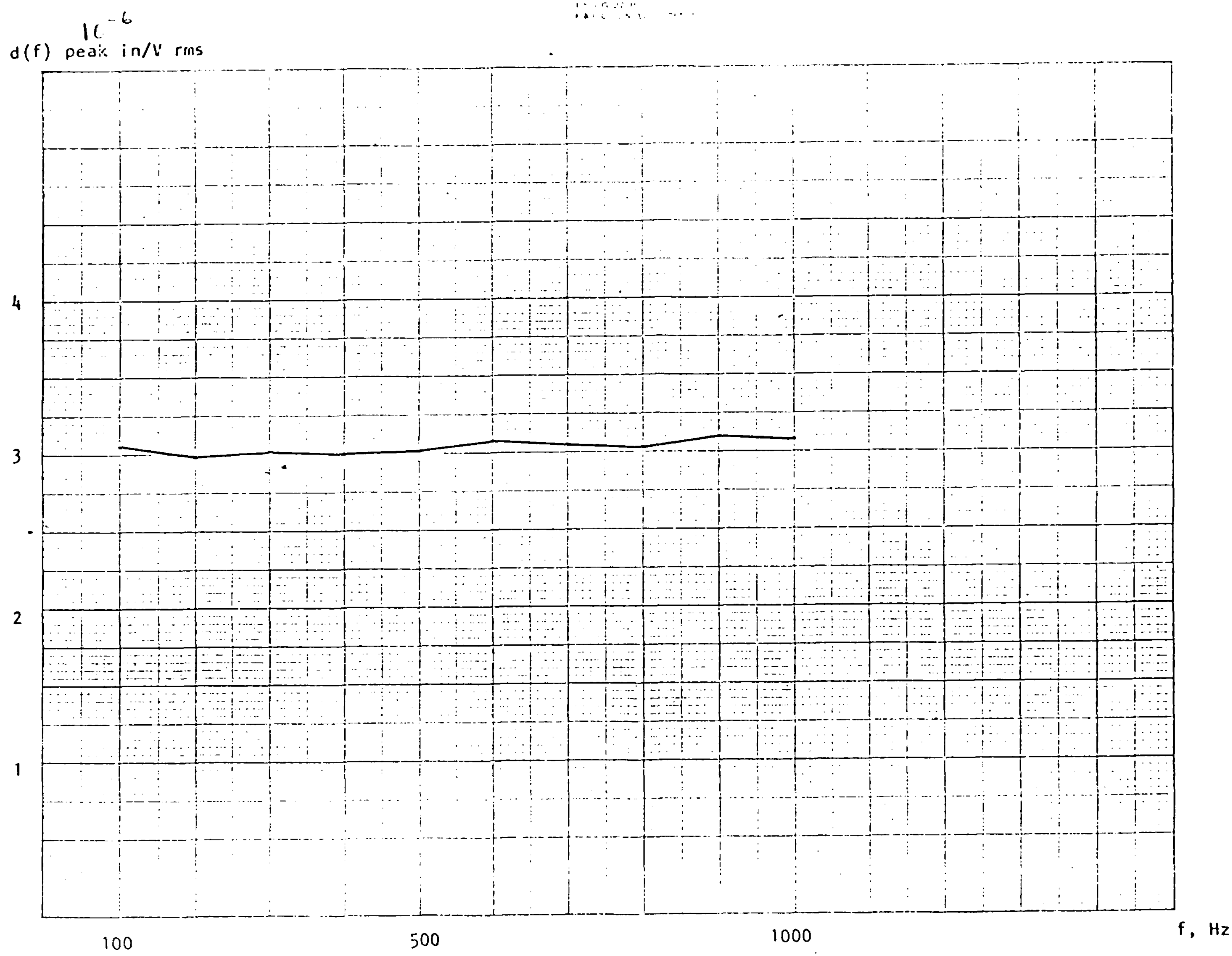

(Fig. 3)

Appendix G - Annex B

WILCOXON ADDITIONAL CALIBRATION DATA

WILCOXON RESEARCH

P.O. Box 5798 • Bethesda, Maryland 20014
(301) 770-3790 • Telex: 898-342 • Cable: WILSEARCH

MECHANICAL AND ELECTRONIC DEVELOPMENT • INSTRUMENTS AND SPECIAL DEVICES

27 August 1984

Dr. Ambul Reddy
Georgia Institute of Technology
888 Hemphill Avenue, N.W.
Aerospace Engineering
Atlanta, Georgia 30332

Dear Dr. Reddy:

We have concluded from our tests that the apparent non-linearity as a function of frequency of your shaker is due to straining of the mounting surface. In addition to the axial displacement of the mounting table, there is also a "stretching" or strain in the transaxial plane caused by radial expansion of the crystals. If we assume that this strain is independent of frequency, then the ratio of strain-to-acceleration increases by $1/f^2$.

Because all accelerometers have some amount of strain sensitivity, a significant error can result at low frequencies. The test results below were obtained with an accelerometer having reasonably low strain sensitivity, tightly screwed to the mounting table. Drive voltage was 100 Vrms.

DISPLACEMENT (apparent)
μ in/Vrms

10 Hz	20 Hz	40 Hz	80 Hz	100 Hz
5.5	1.6	.60	.36	.32

These data show an apparent increase in displacement with a decrease in frequency.

The same accelerometer was then unscrewed and attached with a thin layer of grease only. This greatly reduced transaxial coupling. The results are listed below.

DISPLACEMENT
μ in/Vrms

	10 Hz	20 Hz	40 Hz	80 Hz	100 Hz
50 V	.15 to .21	.24	.27	.28	.28
100 V	.18 to .33	.25	.27	.28	.28
200 V	.11 to .49	.27	.28	.28	.28

These data show a much more consistent output, except in the 10 Hz range. The non-repeatable character of the 10 Hz data was a result of room vibrations and low (less than 200 μV) acceleration signals.

The shaker was then isolated from room vibration and a very sensitive (10 V/g) accelerometer was used. This accelerometer also had very low strain sensitivity. The following data were obtained.

DISPLACEMENT
μ in/Vrms

	10 Hz	20 Hz	40 Hz	80 Hz	100 Hz
50 V	.28	.28	.28	.28	.28
100 V	.29	.28	.28	.28	.28
200 V	.29	.29	.29	.28	.29

In conclusion, it is necessary for one to eliminate strain sensitivity of the accelerometer in order to achieve correct results. Moreover, one should consider any effect of transaxial strain of the test specimen itself.

One practical way of eliminating the strain factor for the accelerometer would be to mount a standoff between the accelerometer and shake table. The length of the standoff should be one or more times the diameter of the accelerometer base. This would greatly reduce strain at the accelerometer.

Good luck with your testing.

Best Regards,

Clark Wilcoxon

Clark Wilcoxon

CW:ln

P.S. The transverse strain of the crystal steel interface = $d_{31} \frac{V}{t}$, where V is the voltage applied, t the thickness of the crystal in meters, and d_{31} is $200 \cdot 10^{-12}$ meters/volt. The strain is independent of frequency and the number of crystals, and is attenuated through the steel table depending on table thickness.

Fred Schloss
Chief Scientist

Appendix H

OUTGASSING AND CREEP TESTS

Introduction

Nonmetallics used on spacecraft must often meet JSC outgassing requirements to prevent contamination of optical surfaces. The standard outgassing test is ASTM E 595-77 as described in Ref. H-1. To meet the outgassing requirements of JSC specification SP-R-0022A (Ref. H-2) the total weight loss (TWL) of the material should be less than 1% and the volatile condensable material (VCM) level should be less than 0.1%.

The following topics will be discussed in this appendix:

1) Outgassing Tests
2) Creep Tests

Outgassing Tests

Outgassing results for VEM damping candidates and related materials are difficult to find. Some existing data were obtained from vendors and NASA-JSC (Ref. H-3) and are shown in Table H-1. This table indicates that, of the seven candidate damping materials selected for study by MDAC in this research program, only two had been tested and shown to meet JSC requirements - ISD 110 and SMRD 100 F90. Therefore, samples of the remaining five candidate materials were sent to NASA/White Sands Missile Base for outgassing evaluation. A description of the five specimens and the results of the tests are given in Table H-2. To improve the VEM outgassing characteristics, all specimens were vacuum-baked at elevated temperatures before being sent out for test.

The results of Table H-2 indicate that the outgassing of Soundcoat Dyad 606 and 3M EC 2216 are at acceptable levels. However, the VCM emissions of GE RTV 630 did not meet the criteria. The rubber/plastic alloy (MDAC L065-72A) and Hysol EA 9326 showed unacceptable performance for both the TWL and VCM requirements.

The fact that three of the selected VEM candidates failed the standard outgassing tests does not eliminate them from consideration as viable damping materials. The specimens tested at White Sands consisted of flat sheets of the raw material, whereas in an actual constrained layer or lap shear configuration the VEM sheet has only its edges exposed. The extremely low outgassing of the aluminum-foil-covered acrylic tapes in Table H-1 serves as an example

Table H-1. Outgassing Results for Damping Candidates and Related Materials

Material	TWL (Total Weight Loss, %)	VCM (Volatile Condensible Materials, %)	RML (Recovered Mass Loss, %)	Notes
GE SMRD 100 F90	1.00	0.10	--	
Scotchdamp ISD 110	1.51	0.03	0.84	Good
3M 467	4.24	0.02	0.43	High
"	0.83	0.04	--	Good (postcured 4 hrs at 38°C)
"	1.32	0.08	--	"
"	1.20	0.06	--	"
"	1.46	0.06	--	"
"	0.98	0.15	--	"
LD 400	12.82	6.35	--	High
Macbond IB 1200	1.56	0.05	--	Fair
3M Y966 Transfer Tape (Acrylic)	1.60	0.00	1.46	Fair-Good
" " " "	1.00	0.00	--	"
" " " "	1.02	0.01	--	"
Mystik 6468 Acrylic Transfer Tape	1.52	0.01	--	Fair
Mystic 7452 Al Foil/Acrylic	0.25	0.03	--	Good (shows shielding effect of foil)
Mystic 7453 Al Foil/Acrylic	0.64	0.04	--	" " " "
Permacel P11 Al Foil/Acrylic	0.36	0.01	--	" " " "
3M 425 Al Foil/Acrylic	0.14	0.07	--	" " " "
3M Y427 Al Foil/Acrylic	0.12	0.02	0.03	" " " "
3M 428 Al Foil/Acrylic	0.29	0.05	--	" " " "
3M Scotchdamp Y370	5.66	0.30	5.10	High
" " "	6.39	0.31	6.21	High (postcured 24 hrs at 50°C)
" " "	1.03	0.11	0.85	Good (postcured 24 hrs at 125°C)

Table H-2. Outgassing Specimen Description and Test Results

Material	Sheet Dimensions, in. Length	Width	Thickness	TWL Total Weight Loss, %	VCM Volatile Condensible Materials, %	RML Water Vapor Recovery, %
Soundcoat Dyad 606[1]	9.5	7.5	0.025	1.01	0.01	0.77
3M EC2216[2]	8	8	0.125	0.73	0.04	0.25
GE RTV 630[2]	8	5	0.125	0.49	0.20	0.02
MDAC L065-72A[3]	6	6	0.062	9.34	5.86	0.22
Hysol EA 9326[1]	9	9	0.125	17.13	11.56	0.40

NOTES:

1. Vacuum baked 44 hours at 170°F.
2. Vacuum baked 40 hours at 250°F.
3. Vacuum baked 96 hours at 200°F.

of how a constraining faceplate would improve outgassing. Additionally, encapsulation of the joint with a low outgassing sealant like GE's RTV 566 silicone could be employed as a control measure. Also, it is important to note that the rubber/plastic alloy developed by MDAC is a new material. Improvements in the fabrication process for this material, such as using liquid butyl rather than softening the solid butyl with oils, could result in reduced outgassing.

In summary, outgassing should not pose a problem for lap shear or constrained layer VEM joints, since improvements to the materials through further processing and the presence of faceplates will greatly reduce outgassing. If any problem does arise, encapsulation should eliminate it.

Creep Tests

Creep or compression set data are not available for most VEMs. Existing data for several of the stiffer VEMs available were previously reported in Ref. H-4. Materials, which are strong, cured rubbers with similar material properties to Dyad 606, demonstrated a 4.6 to 17.7% compression set when tested for 24 hours at room temperature. Materials such as ISD 110, which are soft gums, would probably show extremely high creep and compression set under a sustained high load, with resultant joint failure. A structurally redundant joint is needed for such soft materials.

References

H-1. Total Mass Loss and Collected Volatile Condensible Materials from Outgassing in a Vacuum Environment. American Society for Testing and Materials, ASTM E 595-77, 1977.

H-2. Anon. General Specification - Vacuum Stability Requirements for Polymeric Materials for Spacecraft Applications. JSC Specification SP-R-0022A, September 1974.

H-3. Anon. Compilation of VCM Data of Nonmetallic Materials. NASA-JSC report JSC 08962, Rev. U and Addendums 1-9, May 1979-August 1982.

H-4. R. W. Trudell. Passively Damped Joints for Advanced Space Structures - Annual Technical Report. McDonnell Douglas Astronautics Co. report MDC H1178, June 1984.

END

1-87

DTIC